THE CONVERGING FLOW OF DILUTE POLYMER SOLUTIONS

By

CHANDER BALAKRISHNAN

A DISSERTATION PRESENTED TO THE GRADUATE COUNCIL OF
THE UNIVERSITY OF FLORIDA
IN PARTIAL FULFILLMENT OF THE REQUIREMENTS FOR THE
DEGREE OF DOCTOR OF PHILOSOPHY

UNIVERSITY OF FLORIDA

1976

To

Baba and Mummy

ACKNOWLEDGMENTS

The author wishes to express his gratitude and appreciation to:

Dr. R. J. Gordon for suggesting the research topic and for his guidance.

Dr. H. E. Schweyer, Dr. J. C. Biery, Professor R. D. Walker and Dr. T. E. Hogen Esch for their helpful suggestions.

C. S. Chiou and M. C. Johnson for their help and suggestions.

P. M. Mathias, J. C. Noronha, J. V. Shah and E. Toko for keeping the author in good humor during difficult times.

Mr. Jack Kalway for building the experimental apparatus and being very patient with the author every time he broke it.

Mr. R. L. Baxley, Mr. M. R. Jones and Mr. T. Lambert for assistance in the laboratory.

Ms. Patricia Pfeifer for typing the first draft of the thesis.

Mrs. Jeanne Ojeda for typing the thesis in its final form.

The Chemical Engineering Department for financial support.

The National Science Foundation (Grant GK-31590) for partial support of this research.

Ms. Jean Slobe for helping the author in numerous ways.

TABLE OF CONTENTS

LIST OF FIGURES

Abstract of Dissertation Presented to the Graduate Council
of the University of Florida in Partial Fulfillment of the Requirements
for the Degree of Doctor of Philosophy

THE CONVERGING FLOW OF DILUTE POLYMER SOLUTIONS

By

Chander Balakrishnan

March, 1976

Chairman: Ronald J. Gordon
Major Department: Chemical Engineering

Many dilute polymer solutions exhibit what is commonly known as a wine glass stem shaped flow in flow through sudden contractions. For this situation, flow through the contraction occurs only within a narrow conical region, while the liquid external to this region moves in a slowly re-circulating pattern. The flow in the conical region is predominantly extensional in nature. In this work, flow behavior of very dilute polymer solutions was studied in such a geometry. Extensional viscosities were calculated from measurements of the pressure drop across the contraction and photographs of the angle defining the extent of the conical region. The dependence of extensional viscosity on molecular variables such as molecular weight, molecular weight distribution and polymer conformation was examined. The experimentally determined extensional stresses were compared with predictions of the Equations of Motion and constitutive theories of dilute polymer solutions. It was shown that previously measured values of extensional viscosities using the thrust technique were conservative due to the underestimation of tensile stresses by an amount equal to the entrance pressure drop.

The experimentally measured viscosities were extremely large. A 20 parts per million (by weight) solution of a high molecular weight polyacrylamide was found to have an extensional viscosity as high as 30 poise, while its viscosity in shear was nearly equal to that of water. Conformational studies carried out with polyelectrolytes showed that the extensional viscosity is maximum when the polymer molecules are in an expanded state.

The role of extensional viscosity in understanding the mechanism of turbulent drag reduction and vortex inhibition was closely examined. The results of this work offer considerable support to theories that explain these phenomena as manifestations of the large resistance of dilute polymer solutions to extensional motions.

CHAPTER I

1.1 Introduction

It is well known that the resistance of a liquid to turbulent flow can be considerably reduced by the addition of certain high molecular weight polymers. This phenomenon, commonly known as drag reduction (DR), has been observed with other substances as well, such as soaps and fibers (Patterson et al. (1969)). DR has found several applications both commercial and military. It has been successfully used in firefighting, sewage disposal, transportation of fluids through long pipelines and in reducing drag in the flow of liquids past submerged vessels.

DR is sometimes referred to as the "Toms Effect," after Toms (1949) who first reported it in the literature.* Following Toms, there was little interest shown in DR until the early sixties when, spurred by potential naval applications, a systematic investigation of the effect began. The extensive research of the last fifteen years has resulted in the elucidation of several important aspects of DR, such as its dependence on various flow and molecular variables, although the precise mechanism by which DR occurs is still being debated. Several hypotheses have been proposed, and of these, the most widely accepted explanation is that DR is a manifestation of the large viscosity of dilute polymer solutions in extensional motions

*Agoston (1954) observed DR in the turbulent flow of gasoline thickened by napalm during World War II but this was not reported until 1954.

such as those believed to occur in the wall region in turbulent flow.

The large resistance of dilute polymer solutions to extensional or "stretching motions" is predicted by many constitutive theories of dilute polymer solutions (Peterlin (1966), Denn and Marucci (1971), Everage and Gordon (1971)), and, in recent years, has been experimentally observed at polymer concentrations as low as 20 parts per million by weight (Balakrishnan and Gordon (1975a)). However, a detailed examination of the correlation between extensional viscosity and drag reducing ability under different conditions of polymer molecular weight, concentration, conformation and molecular weight distribution has yet to appear in literature and is the primary goal of this thesis. Extensional viscosities are obtained from a converging flow system and interpreted in light of the Simple Fluid Theory due to Noll (1958/1959). The converging flow of dilute polymer solutions is of interest not only as a means of measuring extensional viscosity but also due to the remarkable similarity in behavior between dilute polymer solutions and polymer melts and concentrated polymer solutions. Converging flows with polymer melts are commonly encountered in practical rheological operations such as fiber spinning and blow moulding (Petrie (1975)).

1.2 Summary of Thesis

The remainder of this chapter comprises a discussion of various theories of DR followed by a brief literature review of pertinent features of the phenomenon. In Chapter II, a review of extensional flows of polymeric systems is presented. The converging flow of

dilute polymer solutions is discussed in detail, and equations that are used later in the thesis developed.

The experimental techniques, procedures and apparatus used to measure extensional viscosity are described in Chapter III. Chapter IV summarizes the experimental results of this work. The implications of these results are discussed in Chapter V. It is shown that the sink flow kinematics proposed by Uebler (1966) can be used to describe the converging flow of dilute polymer solutions only under specific conditions. The correlation between extensional viscosity and DR and Vortex Inhibition (VI), a viscoelastic effect recently discovered by our group and believed to be closely related to DR, is discussed.

1.3 Theories of Drag Reduction

Ever since DR was discovered, the phenomenon has intrigued and baffled some of the keenest minds in science. An understanding of DR presents extreme difficulty because turbulence itself is not completely understood and coupled with this is the fact that a description of the behavior of dilute polymer solutions, at concentrations at which they are almost identical to the solvent, is extremely complex. However, some consistent explanations have been offered based on the current state of knowledge of turbulence and dilute polymer solution rheology.

The earliest explanation of DR was proposed by Oldroyd (1949), who suggested that the tube walls may cause preferred orientation of

polymer molecules in the wall region, thereby leading to, by some vague mechanism, a highly mobile viscous sublayer. This would effectively amount to slip at the wall which has not been experimentally verified for very dilute polymer solutions. In 1959, Shaver and Merrill proposed the shear-thinning viscosity theory to explain DR. In the light of the findings of Paterson (1969), that DR can be observed at very low polymer concentrations at which the solutions possess viscosity that is Newtonian and equal to that of the solvent, this theory is inadequate. Merrill et al. (1966) suggested that polymer molecules--due to the large shear rates near the wall region--could be elongated and oriented in the direction of flow, and thereby spatially hinder radial momentum transport. This theory is also inadequate in explaining DR because of the tremendous disparity between the dimensions of the macromolecules and the smallest eddies in turbulent flow in most pipes.* The polymer molecules are so much smaller than the eddies that they would be expected to be convected by the eddies rather than spatially hinder the processes of turbulence production and diffusion.

In 1965, Gadd pointed out that in seeking a mechanism for DR, one should focus on how polymer molecules affect turbulence generation rather than turbulence dissipation. Walsh (1967), using this concept, developed a theory that, according to a recent review by Hoyt (1972), is the most comprehensive theory of DR that has yet to appear in literature. In Walsh's theory, the fundamental idea is that in turbulent flow the large disturbances that produce the Reynolds

*A situation where the length scales of polymer molecules and turbulence are equal could conceivably arise in turbulent flow in capillaries.

stresses some distance downstream were, at an earlier time, small disturbances at the edge of the viscous sublayer some distance upstream. The production of turbulent energy (i.e., Reynolds stresses) can be considered as follows: if a small scale disturbance extracts more energy from the flow than it dissipates, it begins to grow. Such disturbances at the edge of the wall region move out from the wall and towards the core as they are convected downstream. After the elapse of some time, these small scale disturbances become large scale disturbances. They then become part of the large scale structure in the outer part of the boundary layer that produces the Reynolds stresses. Walsh hypothesized that polymer molecules alter this energy balance by absorbing energy from the small scale disturbances, and after being convected downstream and outwards from the wall, give up this energy by viscous dissipation. This would amount to an alteration of the turbulent energy balance, resulting in decreased production of Reynolds stresses. Walsh was able to correlate the data of several investigators quite successfully with this theory. However, he did not expound on how polymer molecules absorb energy from the disturbances that grow to generate turbulence.

In the late sixties and early seventies, another "wall effect" exhibited by drag reducing polymers began to attract the attention of scientists, viz., the tendency of polymers to adsorb on tube walls. This gave rise to the so-called "Adsorption Theory." In this theory, drag reduction is explained in terms of the interfacial properties of polymer solutions. Most polymer solutions are interfacially active, i.e., the polymers have a tendency to concentrate at interfaces. Bryson

was perhaps the first to use this observation in explaining drag reduction. Using a 30 ppm solution of Polyox WSR 301, Bryson et al. (1971) measured the concentration of the polymer at the wall in pipe flow and found it to be larger than in the bulk. It was then hypothesized that only the "active" sites in the polymer molecules adsorb on the wall leaving entangled loops of polymer chains protruding from the wall. Fluid is trapped and its motion retarded within this layer, thereby causing a thickening of the sublayer and consequently a smaller velocity gradient. Although Bryson's theory is capable of qualitatively explaining several phenomena exhibited by drag reducing systems, there is little conclusive experimental evidence in its support. Moreover, the observation of DR by Paterson (1969) at concentrations as low as 0.1 wppm suggests that the role of an adsorbed entangled layer of polymer chains at the wall is unlikely to be important. Several other investigators have reported the adsorption of drag reducing polymers on tube walls but they do not explain how this adsorbed layer acts to reduce friction. The adsorption theory has been challenged by a number of workers, including Little (1971,1975) and Gyr and Mueller (1974). Little measured the thickness of adsorbed layers of several drag reducing polymers and found that there is no correlation between the thickness of the adsorbed polymer layer and its drag reducing ability. Gyr and Mueller performed experiments with identical tubes of different materials and arrived at the conclusion that adsorption makes little or no contribution to drag reduction.

In 1970, Gordon offered an explanation of DR based on an analysis of the turbulence structure in the wall region proposed by Bakewell and

Lumley (1967). Bakewell and Lumley performed an extensive investigation of the viscous sublayer in turbulent flow and found that the dominant large scale structure of the wall region consisted of randomly distributed, counterrotating pairs of elongated eddies with their axes in the streamwise direction. This structure was theoretically predicted by Townsend (1956) and experimentally observed by the above mentioned authors. This large eddy structure is consistent with the experimental results on the so-called bursting phenomenon observed by Kline's group at Stanford (Runstadler et al. (1963)), and also reported by Corino and Brodkey (1969), and Brodkey et al. (1974).

The bursting phenomenon can be broken down into a sequence consisting of the following events:

(1) Local deceleration of flow over a large area near the wall. The region has very small velocity gradients and almost resembles plug flow except at the edges of the region where there are large velocity gradients. This corresponds to the initial formation of the eddy pair.

(2) An ejection of fluid outward from the wall from this decelerated region, occurring suddenly with a large normal velocity component. This was the most striking feature of Corino and Brodkey's observations. As noted by Bakewell and Lumley, this stage corresponds to a tilting of the plane of circulation of the counter-rotating pair of eddies more nearly normal to flow. The region between the eddies is characterized by a strong updraft of low momentum fluid moving away from the wall.

Figure 1-1 reproduces the streamlines of the large eddy structure described in Bakewell and Lumley's work.

(3) The sweep phenomenon in which, following the ejection sequence, a mass of fluid larger than the ejection scale and with velocity greater than the mean appears, moving nearly parallel to the wall or slightly towards it. This fluid swept the field of elements of retarded flow and reestablished a normal velocity profile.

Seyer (1969) analyzed the streamline pattern of the flow between the counterrotating pairs of eddies (Figure 1-1), and found that the fluid that is swept up and between the eddies undergoes a transient stretching motion. It was then proposed by Gordon (1970) that the large extensional viscosity of dilute polymer solutions would decrease the frequency and intensity of the "bursts" from the wall region into the bulk, thereby altering the fundamental step in the turbulence generation process. Thus a reduction in bursts would decrease turbulence and, therefore, drag. It is well known that constitutive theories of dilute polymer solutions predict extremely large resistances to stretching motions (Peterlin (1966), Gordon (1970), Denn and Marucci (1971), Everage and Gordon (1971)). Recent experimental studies have confirmed these predictions. Metzner and Metzner (1970) calculated the extensional viscosity of a 100 ppm solution of Separan AP 30 (a partially hydrolyzed polyacrylamide by Dow and an excellent drag reducer) to be as much as 6000 times the shear viscosity of the solution (1.44 cp). Similar results have been reported by the group headed by Oliver at the University of Birmingham (1973a), and by Balakrishnan and Gordon (1975a).

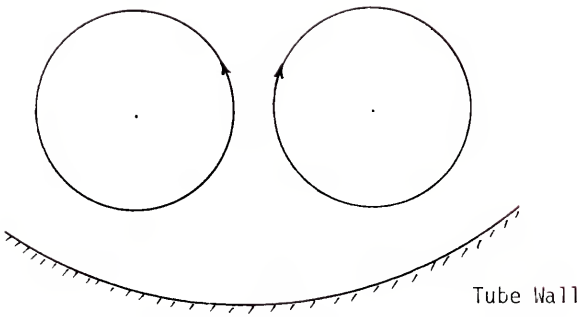

Figure 1-1. Representation of Counterrotating Eddy Pairs.

Recent experimental studies conducted by Donohue (1972) and Hanratty's group at the University of Illinois offer considerable support to the above mechanism. Donohue used a dye injection technique to study the bursting rate in a drag reducing fluid. This was found to be as much as 70% less than in water at equal mass flow rates. Also, there was a considerable decrease in the non-dimensionless streak spacing, indicating stabilization of the sublayer. Fortuna and Hanratty (1972), using an electrochemical technique (Mitchell and Hanratty (1966), Sirkar and Hanratty (1970a,1970b)), found an increase in width of longitudinally oriented eddies. As shown by Katsibas and Gordon (1974), this can be interpreted as a reduction in the frequency of ejection from the wall.

The mechanisms proposed by Peterlin (1970), and Lumley (1973) are similar to that proposed by Gordon in that they also attribute DR to the large extension (and, therefore, large intrinsic viscosity) of polymer molecules in extensional or irrotational flow fields.

1.4 Features of Drag Reduction

Some experimental aspects of DR that are pertinent to this work are briefly reviewed below.

1.4.1 Dependence of DR on polymer molecular weight and molecular weight distribution

The first detailed study of the effect of molecular weight on DR was performed by Pruitt and Crawford (1965). They concluded from their data that the reduction in friction shown by a homologous series of polymers increased with increasing molecular weight. However, Paterson (1969) showed that this general rule was true only if the

molecular weight distributions were similar. He found Polyox WSR 35, a poly(ethylene oxide) polymer, to be a better drag reducer than Polyox WSRN 750 even though the latter had a higher viscosity-average molecular weight. This immediately poses the question as to the effect of molecular weight distribution on DR. Paterson's study revealed that WSR 35 had a broad molecular weight distribution and that it possessed a high molecular weight "tail" which WSRN 750 did not. He also found that the intrinsic viscosity of polymer solutions did not correlate with either DR or shear degradation. Mechanical degradation affects the high molecular weight species more than the low molecular weight species of a polymer sample (Nakano and Minoura (1975)). Paterson found that large changes in DR due to degradation were accompanied by disproportionately small changes in intrinsic viscosity, and he concluded that DR depended predominantly on the high molecular weight species of a polymer. This has been further confirmed by Gordon and Balakrishnan (1972) and by Morgan and Pike (1972) who used fractionated samples of polyox.

1.4.2 The effect of solvent character and polymer conformation on DR

The early investigations of DR were mostly conducted using concentrated polymer solutions with pronounced shear-thinning behavior. In the studies of Pruitt and Crawford (1965) and Fabula (1965) it was shown that DR could also be observed with dilute polymer solutions with concentrations in the parts per million range. Later Paterson (1969) and Fabula (1966) measured DR at extremely low polymer concentrations--0.1 and 0.5 wppm respectively.

In such dilute polymer solutions, the polymer molecules are separated by large amounts of fluid, and hydrodynamic interaction is negligible. A measure of the separation between two polymer molecules is defined as

$$\xi = L_c/2R_g$$

where L_c is the center to center distance between two molecules and R_g is the radius of gyration. When ξ is equal to unity, the domains of the two molecules would be expected to interact each other, and smaller values of ξ would indicate overlapping domains. For the polymer solution that exhibited DR at 0.1 ppm, Paterson found $\xi = 8.5$, thereby indicating a large separation between polymer molecules. This is, of course, only an order of magnitude estimate because ξ is calculated using average quantities and so its value would be expected to change depending on the type of average used. Even so, it points out the importance of interaction between solvent and polymer molecules in turbulent DR.

Hershey (1965), using four polymers in three different solvents, found that the drag reducing ability of a polymer depended on the solvent used. For instance, it was found that poly(isobutylene) (PIB) is a better drag reducer in cyclohexane than in benzene. It is well known that polymer solvent interactions are favored in "good" solvents, and as a result the polymer molecules exist in an expanded state. On the other hand, "poor" solvents do not favor interaction with polymer molecules and the molecules therefore assume a compact structure.

In Hershey's work, benzene was at its θ temperature (thermodynamic interaction between PIB molecules and benzene was a minimum at this temperature and hence the macromolecules were of smaller dimensions in benzene than in cyclohexane). Hershey's work showed that DR increases with increasing molecular dimensions and his observations have been confirmed by several other investigators (Merrill et al. (1966), Liaw (1971), Pruitt and Crawford (1965), Kim et al. (1973), White and Gordon (1975)).

In 1966 Merrill et al. attempted to determine the effect of molecular parameters such as the rigidity and expansion factors on DR. They defined these factors as follows:

$$\varepsilon = \text{expansion factor} = \left(\frac{\bar{r}^2}{\bar{r}^2_\theta}\right)^{1/2}$$

$$s = \text{flexibility factor} = \left(\frac{\bar{r}^2}{\bar{r}^2_{\theta,f}}\right)^{1/2}$$

$\bar{r}^2$ = actual mean square end to end distance

$\bar{r}^2_\theta$ = (define) mean square end to end distance under θ conditions, and

$\bar{r}^2_{\theta,f}$ = calculated mean square end to end distance for a freely rotating chain.

It follows from the preceding discussion that ε is a measure of polymer solvent interaction with large values indicating favorable interactions. s on the other hand is a measure of steric and other such restrictions on rotation about the bonds on the chain backbone and small values of s indicate greater flexibility of the molecule. Comparing the values

of s for Polyox (PEO) in water and PIB in cyclohexane, and from experiments conducted with PEO in water (a good solvent), and in 0.4M potassium sulphate at 35°C (a theta solvent), Merrill et al. arrived at the tentative conclusion that for optimum drag reduction, ε must be maximized and s minimized. However, Lee (1966), from data obtained with a random coiling polymer, has pointed out that there is no simple relationship between s and effectiveness of a polymer in reducing turbulent friction. It is therefore seen that there is no clear agreement on the effect of rigidity on drag reduction.

With the exception of the carboxymethyl cellulose and polyacrylamide polymers used by Pruitt and Crawford (1965), almost all the work on solvent character and its effect on drag reduction that has been discussed so far was done with uncharged, random coiling polymers. In the past four years, intriguing results of several investigations have been reported in which charged polymers have been used.

Charged polymers are commonly known as polyelectrolytes and their behavior in solution is quite different from that of uncharged polymers. As the name suggests, polyelectrolytes have fixed charges on the backbone chain and this causes them to undergo dramatic changes in conformation with change in their ionic environment. Thus, poly (methacrylic acid) which has the repeating unit

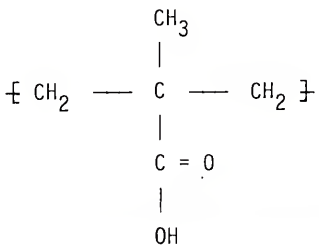

is known to be highly coiled in acidic environment, perhaps due to intramolecular hydrogen bonding, and has an extended conformation at high pH due to ionization. Similar behavior has been noticed with poly(acrylic acid) (PAA), partially hydrolyzed polyacrylamide (PAM), deoxyribonucleic acid (DNA), and other polyelectrolytes (Hand and Williams (1969,1970), Katchalsky and Eisenberg (1951), Mathieson and MacLaren (1965)). This tendency of polyelectrolytes to change in conformation with changes in their ionic environment makes them ideally suitable for studying the effect of polymer conformation on DR.

In 1969, Hand and Williams reported results obtained with a poly(acrylic acid) (PAA) polymer showing dramatic changes in DR with conformation. They arrived at the conclusion that PAA was most effective as a drag reducer when it was in a compact structure (pH between 2.8 and 3) believed to be helical. They also conducted experiments with calf thymus DNA and found that maximum drag reduction was obtained when the polymer was in the native state, in the form of a double helix (1970). Thus the results obtained by Hand and Williams seem to indicate that a helical structure is most suitable for drag reduction.

Parker and Hedley in 1972 reported results quite contrary to those reported by Hand and Williams. Using a very high molecular weight PAA, Parker and Hedley found that the polymer was most effective as a drag reducer when it was in the form of stretched rods, i.e., in neutral or alkaline medium. They also observed DR to decrease with decreasing pH. Kim et al. (1973), Banijamali et al.

(1974) and Balakrishnan and Gordon (1975b) have also obtained results similar to those of Parker and Hedley and it appears now that an extended conformation is indeed more suitable to drag reduction than a compact rigid structure (White and Gordon (1975), Banijamali et al. (1974), Frommer et al. (1974)).

There are many other important aspects of drag reduction besides those discussed here. Excellent summaries of these can be found in the review articles by Hoyt (1972) and by Virk (1975).

CHAPTER II

2.1 Extensional Flows: Qualitative Considerations

In Chapter I, the importance of extensional viscosity in explaining turbulent drag reduction, as well as in characterizing the extensional flow behavior of polymeric materials was discussed briefly. Before embarking on a discussion of the various geometries and techniques available for the measurement of extensional viscosity, it is important to qualitatively distinguish extensional flows from shearing flows.

Shearing flows are rotational in nature in the sense that the vorticity tensor is non-zero. For example, in the case of steady shearing flow (Lodge (1964)), the magnitudes of the second invariants of the strain rate and vorticity tensors are equal. In such flows, the particles in the fluid rotate about an axis that is normal to the direction of both the velocity and the velocity gradient. Polymer molecules in the fluid do not experience large extensions because the different segments of the coil are alternately stretched and compressed. This gives each segment an opportunity to relax.

Extensional flows, on the other hand, are primarily irrotational and are characterized by a strain rate tensor that is almost diagonal, and by negligible vorticity rates. In flow fields such as this, the polymer molecules tend to orient themselves in the direction of flow. Since the molecules do not rotate in extensional flows as they do in

shearing flows, molecular extension is considerably larger, and this causes large stresses to develop in the fluid.

2.2 Extensional Flows: Quantitative Considerations

Constitutive theories of viscoelastic materials such as polymer solutions in which the stress is entirely determined by the instantaneous rate of deformation, have frequently been found to be inadequate in predicting the stress response of these substances to imposed deformations. For example, consider the Reiner-Rivlin theory

$$\underline{\tau} = A_1(II_D, III_D)\underline{D} + A_2(II_D, III_D)\underline{D}^2 \tag{2-1}$$

where $\underline{\tau}$ is the extra stress tensor, $\underline{D}$ is the rate of strain tensor, II_D and III_D are the second and third invariants of $\underline{D}$ and A_1 and A_2 are scalar functions of the invariants of $\underline{D}$. For a simple shearing flow (in right cartesian coordinate system (RCCS)),

$$v^i = (Gx^2, 0, 0) \tag{2-2}$$

where G is the shear rate, the Reiner-Rivlin theory predicts the following results for the components of $\underline{\tau}$:

$$\tau_{12} = \tau_{21} = A_1 G/2 \tag{2-3a}$$

$$N_1 \equiv \tau_{11} - \tau_{22} = 0 \tag{2-3b}$$

$$N_2 \equiv \tau_{22} - \tau_{33} = A_2 G^2/4 \tag{2-3c}$$

The first normal stress difference N_1 is predicted to be zero, in contrast to the experimentally observed N_1 with viscoelastic fluids.

In order to accurately describe the behavior of viscoelastic fluids, the stress must be allowed to depend not only on the instantaneous value of the deformation rate but also the deformation history the fluid has experienced. For a fluid with a quickly fading memory, the stress at any particular instant is determined by the history of deformation only in the immediate past. When the fluid has been in the same deformation field for a sufficiently long time, such that it no longer remembers any other deformation it might have experienced at some earlier past time, the flow is said to be one of constant stretch history. To illustrate this point, consider the response of a viscoelastic fluid in a steady extensional flow. The constitutive equation chosen for this purpose is that due to Gordon, Schowalter and Everage. The GSE model was obtained from a continuum modification of the dumbbell theory of dilute polymer solutions and it predicts both a non-Newtonian viscosity and non-zero primary and secondary normal stress differences.

$$\tau^{ij} + \lambda \frac{\mathcal{D}}{\mathcal{D}t} \tau^{ij} = 2 \frac{N}{M} ckT\lambda(1-\varepsilon)D^{ij} \tag{2-4}$$

$$\frac{\mathcal{D}}{\mathcal{D}t} \tau^{ij} = \frac{\partial}{\partial t} \tau^{ij} + v^k \tau^{ij}_{,k} - \tau^{kj} v^i_{,k} - \tau^{ik} v^i_{,k} + \varepsilon\{D^i_m \tau^{mj} + \tau^i_m D^{mj}\} \tag{2-5}$$

The total stress tensor τ^{ij} is defined by

$$T^{ij} = - pg^{ij} + 2\mu_s D^{ij} + \tau^{ij} \tag{2-6}$$

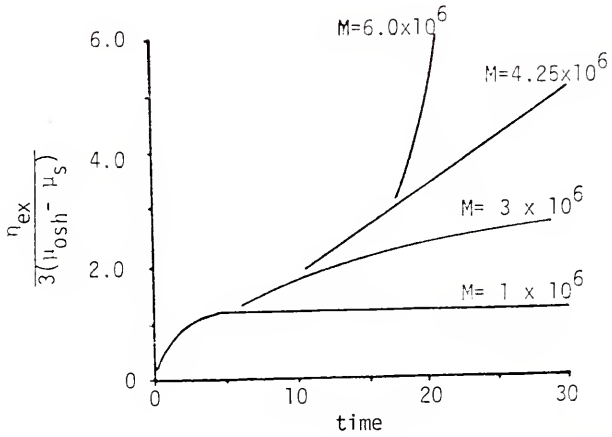

Figure 2-1. Predictions of the GSE model for steady extension.

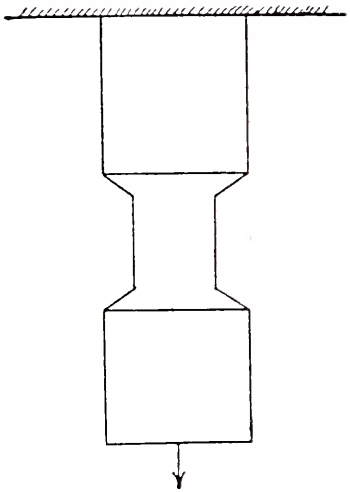

Figure 2-2. Ballman's Experiment.

In equations (2-4) to (2-6), ε is a phenomenological constant subject to the condition $0 \leq \varepsilon < 1$. λ, the relaxation time, is related to molecular parameters by the equation

$$\lambda = \frac{\mu_s \, kM^{1+a}}{NkT\,(1-\varepsilon)} \tag{2-7}$$

k and a are constants in the Mark-Houwink-Sakurada equation for zero shear intrinsic viscosity.

$$[\eta]_{G=0} = kM^a \tag{2-8}$$

M is the molecular weight of the polymer.

For the extensional flow field $v^i = [\Gamma(t)x^1, -\Gamma(t)x^2/2, -\Gamma(t)x^3/2]$, the predictions of the GSE model for the limiting case of constant stretch rate are (Everage and Gordon (1971)):

$$T^{11} = \tau^{11} - \tau^{22} + 3\mu_s\Gamma$$

$$= \frac{3NckT\lambda(1-\varepsilon)\Gamma}{M[\{1-2\lambda(1-\varepsilon)\Gamma\}\{1+\lambda(1-\varepsilon)\Gamma\}]} - \frac{2NckT\lambda(1-\varepsilon)\Gamma\, e^{-[1-2\lambda(1-\varepsilon)\Gamma]t/\lambda}}{M[1-2\lambda(1-\varepsilon)\Gamma]}$$

$$- \frac{NckT\lambda(1-\varepsilon)\Gamma\, e^{-[1+\lambda(1-\varepsilon)\Gamma]t/\lambda}}{M[1+\lambda(1-\varepsilon)\Gamma]} + 3\mu_s\Gamma \tag{2-9}$$

The extensional viscosity η_{ex} is defined by the equation,

$$\eta_{ex} \equiv (T^{11} - 3\mu_s\Gamma)/\Gamma \tag{2-10}$$

In Figure 2-1 η_{ex} is plotted versus time for different molecular weights

of a 200 wppm solution of poly(ethylene oxide), an excellent drag reducer with $\varepsilon = 0.4$ and stretch rate $G = 2000\ sec^{-1}$. It is seen that for low values of molecular weight (and, therefore, relaxation time, from equation (2-7)), the extensional viscosity reaches a constant value at large values of time. The flow is one of constant stretch history, and the extensional viscosity in the asymptotic region is a unique quantity for that material at the stretch rate $2000\ sec^{-1}$. In the transient region where the extensional viscosity is a function of time, the flow is not of constant stretch history because the stress in the fluid has not reached a steady value corresponding to the stretch rate. The extensional viscosity in this region is not uniquely determined by the stretch rate Γ.

In contrast to the predictions of a memory fluid, a fluid that has no memory at all (such as a Newtonian fluid), attains a steady value of stress as soon as the deformation is imposed, and the viscosity is constant at all times. For such fluids, the stress response is independent of the stretch history. However, in defining an extensional viscosity for a viscoelastic fluid, the history of deformation is extremely important, and η_{ex} is a unique quantity only when the stress in the fluid has reached a steady value corresponding to the deformation rate the fluid is experiencing.

In a flow field in which the deformation rate is spatially dependent (such as in converging flows (Section 2.4.2)), the material does not experience the same stretch rate as it flows from one point to another. For a viscoelastic fluid in such a flow field, the stresses vary with position, and the stress at any point in the

fluid may not attain the steady value associated with the local velocity field. This is illustrated by considering the predictions of the GSE model for spherical sink flow kinematics (Section 2.4.2) given by

$$v^r = - Q'/r^2 \qquad (2\text{-}11)$$

$$v^\phi = v^\phi = 0$$

Q' is the sink strength. The rate of strain tensor $\underline{D}$ is diagonal and is given by

$$D^{ij} = \begin{bmatrix} 2Q'/r^3 & 0 & 0 \\ 0 & - Q'/r^3 & 0 \\ 0 & 0 & - Q'/r^3 \end{bmatrix} \qquad (2\text{-}12)$$

The primary normal stress difference for the flow field defined by equations (2-11) and (2-12) is

$$N_E(\Gamma) = \frac{2NckT(1-\varepsilon)}{3M} \exp\left(\frac{2}{3\lambda\Gamma}\right) \left| \overline{(2)^{-\frac{5}{3}+\frac{8\varepsilon}{3}} \Gamma^{4(1-\varepsilon)} \int_0^\Gamma \xi^{(4\varepsilon-7)/3} \exp\left(\frac{2}{3\lambda\xi}\right) d\xi} \right.$$

$$\left. + (2)^{1-\frac{4\varepsilon}{3}} \Gamma^{-2(1-\varepsilon)} \int_0^\Gamma (3)^{\frac{4}{3}-\frac{4\varepsilon}{3}} \exp\left(\frac{+2}{3\lambda\xi}\right) d\xi \right| \qquad (2\text{-}13)$$

where Γ is the stretch rate at any point and is equal to $2Q'/r^3$.

The integration in equation (2-13) over all past stretch rates implies that the tensile stress ($N_E(\Gamma)$) depends not only on the stretch

rate at that point but also on all past values of $\dot{\varepsilon}$ that the fluid has experienced. Clearly, this is not a flow of constant stretch history and the extensional viscosity measured in such a flow will not generally be a unique quantity in the sense that it was in the case of steady extension. Thus the extensional viscosity measured at a particular stretch rate in a materially steady flow cannot, in general, be expected to be the same as that measured in an unsteady flow at the same value of stretch rate.

Ballman (1965) has pointed out that results of extensional flow experiments should be reported in terms of extensional viscosity only when the stress in the fluid has reached a steady value, a situation that can occur only in materially steady flows. In this work, however, results are reported in terms of extensional viscosities even though the flow field in which they are measured (converging flow) is materially unsteady. This, we believe, is acceptable so long as it is borne in mind that these values of extensional viscosities may not be equal to those measured in steady extension, and that they are used to give the reader only an indication of the large values of stresses that are developed in the fluid in such a flow.

2.3 Literature Review: Newtonian Fluids

The first measurement of extensional viscosity was by Trouton who, in 1906, measured the "coefficient of viscous traction" (i.e., extensional viscosity) of pitch and related it to its viscosity measured in shear. From his experiments he arrived at the relationship

$$\eta_{ex} = 3\mu_{sh} \tag{2-14}$$

where η_{ex} and μ_{sh} are the extensional and shear viscosities respectively. Equation (2-14) is known as Trouton's rule, and the ratio of extensional viscosity to shear viscosity, the Trouton ratio. Trouton's rule is known to be obeyed by Newtonian fluids, and by viscoelastic fluids at extremely low values of stretch rate. To illustrate this point, consider the predictions of the GSE model for the steady extension of an initially unstressed fluid (equation (2-9)). The extensional viscosity defined by equation (2-10) can be written as

$$\frac{\eta_{ex}}{3(\mu_{osh}-\mu_s)} = \frac{1}{[1-2\lambda(1-\varepsilon)\Gamma][1+\lambda(1-\varepsilon)\Gamma]} - \frac{2\exp-[1-2\lambda(1-\varepsilon)\Gamma]t/\lambda}{3[1-2\lambda(1-\varepsilon)\Gamma]}$$

$$- \frac{\exp[-\{1+\lambda(1-\varepsilon)\Gamma\}]t/\lambda}{3[1+\lambda(1-\varepsilon)\Gamma]} \qquad (2\text{-}15)$$

where $\mu_{osh} = \mu_s + \frac{Nc}{M} kT\lambda(1-\varepsilon)$ is the zero shear viscosity and μ_s is the solvent viscosity.

For large values of time, the GSE model predicts

$$\frac{\eta_{ex}}{3(\mu_{osh}-\mu_s)} = 1 \qquad (2\text{-}16)$$

Since $\mu_{osh} - \mu_s$ is the contribution to zero shear viscosity due to the presence of polymer molecules, equation (2-16) is equivalent to Trouton's rule.

Experiments performed at extremely low values of stretch rate have shown that viscoelastic materials approach Newtonian behavior in extension when the deformation rates are small enough (Spearot and Metzner (1972), Everage and Ballman (1975), Cogswell (1972)). At larger stretch rates,

the Trouton ratio for many polymeric materials such as melts and solutions is several orders of magnitude larger than that predicted by equation (2-14).

2.4 Literature Review: Non-Newtonian Fluids

As first discussed, extensional flows of polymeric materials can be conveniently divided into two categories--those which are materially steady and those which are materially unsteady--and the extensional viscosity measured in the two flows would not in general be expected to be equal.

2.4.1 Materially steady extensional flows

Materially steady flows are characterized by a constant stretch history. Mathematically, a materially steady extensional flow can be defined (Coleman and Noll (1962)) as a flow where there is a fixed cartesian coordinate system in which the following equations are obeyed:

$$v^i = \Gamma^i x^i \tag{2-17}$$

v^i are the components of velocity of a material point at x^i and Γ^i are constants subject to the condition

$$\sum_{i=1}^{3} \Gamma_i = 0 \tag{2-18}$$

There are several other definitions of materially steady extensional flows. A brief summary of these definitions can be found in Kanel (1972).

The steady extensional flows of polymeric materials has been experimentally investigated and theoretical analyses have also been made in order to compare theory with experiment. The typical experiment is that due to Ballman (1965) in which the material is clamped at one end and is extended in some programmed manner, usually to yield a constant stretch rate. This is schematically described in Figure 2-2. Most of the earlier extensional flow experiments at constant stretch rates were performed at low stretch rates, and in these experiments a constant value of extensional viscosity, independent of stretch rate was obtained. Using molten polystyrene, Ballman found extensional viscosity to vary only slightly from 9.975×10^3 poise at a stretch rate of 0.001 sec^{-1} to 9.5×10^3 poise at a stretch rate of 0.02 sec^{-1}. This value was nearly 160 times greater than the shear viscosity, and was found to be independent of the stretch rate.

The results of these experiments are consistent with the predictions of constitutive theories for low values of stretch rate. However, most of these theories, such as the convected Maxwell model and other rate models of this type, and also integral models such as the network theory of Lodge (1964), predict the growth of stress to very large values when the stretch rate exceeds a critical value. Experiments performed over a wide range of stretch rates have shown these predictions to be true. Specific examples of such observations are those of Meissner (1972), Spearot and Metzner (1972), Stevenson (1972), and Everage and Ballman (1975). Table 2.1 summarizes the results of some of the extensional viscosity measurements that have been discussed in this section.

TABLE 2-1

Summary of Extensional Investigations

Investigator	Material	Method	μ_{osh}, poise	Range of Γ, sec^{-1}	Remarks on η_{ex}
(a) High Viscosity Systems					
Trouton (1906)	Pitch	Constant Load	10^{10}	0.033-0.5	Constant Newtonian Value
Ballman (1965)	Polystyrene	Constant Γ	--	0.001-0.02	Constant value, $\eta_{ex}=160\mu_{sh}$
Lodge and Meissner (1972)	Low Density Polyethylene	Constant Γ	$5x10^{9}$	0.001-1	Newtonian value at low Γ Increased sharply with time at large Γ
Cogswell (1972a)	Polypropylene	Constant Stress	$5x10^{4}$	----	Constant Newtonian value
	Acrylic Acid	Constant Stress	$1.5x10^{5}$	----	Newtonian value at low Γ Decreased at large Γ
	Low Density Polyethylene	Constant Stress	$7.0x10^{4}$	----	Newtonian value at low Γ Increased at large Γ
Spearot and Metzner (1972)	Polyethylene	Spinning	$2.5x10^{5}$	0.05-0.125	Did not reach steady value at low Γ. Increased sharply with time at large Γ.
Everage and Ballman (1975)	Polystyrene	Constant Γ	$1.4x10^{6}$	0.026-0.413	Reached steady Newtonian value at low Γ. Increased very sharply with time at large Γ.
Denson and Gallo (1971)	Polyisobutylene	Bubble Blow	--	10^{-4}-10^{-3}	Decreased with Γ

TABLE 2-1 (continued)

Summary of Extensional Investigations

Investigator	Material	Method	μ_{osh}, poise	Range of Γ, sec^{-1}	Remarks on η_{ex}
(b) Moderate Viscosity Systems					
Astarita (1970)	Polyacrylamide in Glycerine	Fano Flow	--	On the order of 0.1	Not Clear
Pickup (1970)	Polyacrylamide in water 0.3%	Converging Flow	--	20-40	Large values, increased with Γ
Murch (1970)	Polyacrylamide in water	Converging Flow	--	Assumed values 6-20	Large values, constant
Baid (1973)	Polyacrylamide in Glycerine water solution Concentration 100 to 300 wppm	Spinning	1 to 6	4-15	Not Clear
Hudson (1974)	Polybutadiene in decalin 7.9%	Spinning	25	5-100	Large values, decreased with Γ
(c) Low Viscosity Systems					
Balakrishnan & Gordon (1975a)	Polyacrylamide in water	Converging Flow	1-10 cp	10^3-10^4	Very large values, increased slightly with Γ
Oliver & Bragg (1973a)	,,	Thruster	--	Kinematics unknown	Not Clear
Metzner and Metzner (1970)	,,	Thruster	Nearly equal to water	Kinematics unknown	Not Clear

A common feature of all these experiments is the low deformation rates that can be attained and their limitation to high viscosity systems. For low viscosity systems, the techniques that are available for measuring extensional viscosity are different and they come under the category of materially unsteady flows.

2.4.2 Materially unsteady flows

In materially unsteady flows, the history of deformation is not constant (Section 2.2) and therefore the stress and other dependent variables depend on the instant of observation. Materially unsteady flows commonly occur in accelerative flows--flows that are steady from an Eulerian sense but not steady from a Lagrangian sense.

As pointed out by Kanel (1972), there are several frame indifferent criteria that can be used to characterize the nature of a flow--whether it is predominantly shearing or extensional--when it is materially steady. For materially unsteady flows, however, it is difficult to find a frame indifferent quantity that can serve as a measure of the character of the flow. In view of the fact that extensional flows are characterized by a rate of strain tensor that is almost diagonal, and by negligible vorticity, it is convenient to use the magnitude of the ratio of the second invariants of the vorticity tensor $\underline{W}$ and the strain rate tensor $\underline{D}$ to determine the nature of an unsteady flow.

$$\zeta \equiv \left| \frac{II_{\underline{W}}}{II_{\underline{D}}} \right| \qquad (2\text{-}19)$$

For a shearing flow defined by equation (2-2), $\zeta = 1$, and for the extensional flow defined by $v^i = (\Gamma x^1, -\frac{\Gamma x^2}{2}, -\frac{\Gamma x^3}{3})$, $\zeta = 0$. For spherical sink flow kinematics which is of interest to this work (Section 2.5), and is described by equation (2-11),

$$\underline{D} = \begin{pmatrix} 2Q'/r^3 & 0 & 0 \\ 0 & -Q'/r^3 & 0 \\ 0 & 0 & -Q'/r^3 \end{pmatrix} \qquad (2\text{-}12)$$

$$\underline{W} = \begin{pmatrix} 0 & 0 & 0 \\ 0 & 0 & 0 \\ 0 & 0 & 0 \end{pmatrix} \qquad (2\text{-}20)$$

and $$\zeta = 0 \qquad (2\text{-}21)$$

The flow is therefore purely extensional, by the above criterion.

Detailed investigations of two materially unsteady flows--FANO FLOW AND CONVERGING FLOW--have appeared in the literature.

FANO FLOW: The Fano flow (also known as the tubeless siphon or self-siphon) experiments utilize the ability of some viscoelastic fluids to maintain a siphon even when the liquid surface is below the siphoning tube. This is pictorially described in Figure 2-3. In a flow such as this, the material is subjected to extensional modes of deformation (Astarita (1970)). From photographs of the liquid column (to measure stretch rates in the liquid) and measurement of the force required to support the siphoning tube (to determine the tensile stress in the

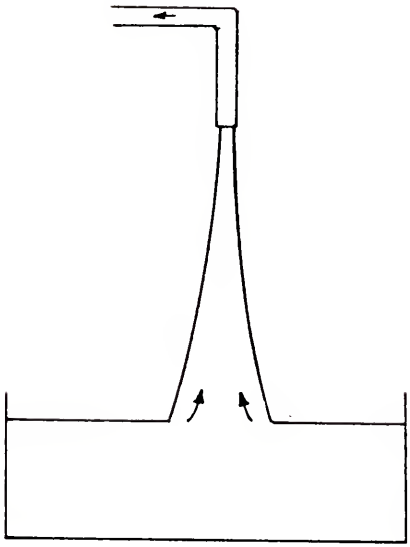

Figure 2-3. Fano Flow

liquid at the tube entrance), one can calculate an extensional viscosity.

Pickup (1970), using aqueous solutions of Separan AP 30, a partially hydrolyzed polyacrylamide made by Dow, measured Trouton ratios as large as 160. Similar results were reported by Astarita (1970) who also used aqueous solutions of the same polymer.

In a very detailed investigation of Fano flow, Kanel (1972) found that the kinematics of the flow are described by the equation

$$\frac{1}{D^m} = c_1 x + c_2 \qquad (2\text{-}22)$$

D is the diameter of the liquid column at any height x from the free surface of the liquid (Figure 2-4). c_1, c_2 and m are constants that depend on the liquid. For a flow with kinematics described by equation (2-22), it can be easily shown that the rate of change of stretch rate experienced by the fluid depends only on the instantaneous value of Γ and the value of m.

$$\frac{D\Gamma}{Dt} = v^1 \frac{dv^1}{dx^1} = [(2-m)/2]^2 \Gamma^2 \qquad (2\text{-}23)$$

Thus two fluids having the same value of m have identical stretch histories when the stretch rates overlap. Kanel's observations on Fano flow are important in that the kinematics of the flow as described by equation (2-22) have been found to describe the thread profile in many fiber spinning operations (Kanel (1972), Baid (1973)). Equation (2-23) implies that the deformation histories of fluids in km flow

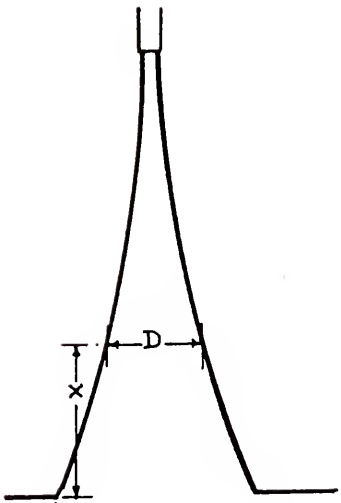

Figure 2-4. Coordinate System in Fano Flow

(i.e., flow described by equation 2-22) are identical when they have the same values of m and Γ, regardless of the value of c_1 and c_2. When m, the history parameter, is equal to 2, the stretch rate does not change with time in a Lagrangian sense, and the flow is materially steady.

CONVERGING FLOW: The term converging flow is commonly used to describe the flow of a fluid through a sudden contraction. The dramatic difference between the converging flow of Newtonian and viscoelastic fluids was noticed as early as 1956 by Tordella. Clegg (1957) and Bagley and Birks (1960) have described this difference in detail. In the case of a Newtonian fluid, the flow entering the contraction does so from all locations upstream of the contraction, and the secondary eddy flow at the 90° corner of the contraction occupies a minor portion of the flow. In the case of some viscoelastic fluids, however, the flow through the contraction is restricted to a narrow conical region upstream, and the liquid surrounding this region slowly recirculates, resembling a large vortex (Figure 2-5). This phenomenon is commonly referred to as Wine Glass Stem Shaped Flow (or simply WGS flow) and has been observed with some polymer melts. It is to be noted that not all polymer melts show this behavior. Thus, low density polyethylene has been known to exhibit WGS flow whereas high density polyethylene has not. Though it is believed that WGS flow occurs due to the elasticity of the polymer under consideration, the precise reason for its occurrence is not well understood.

In recent years, WGS flow has also been observed with relatively dilute polymer solutions (Giesekus (1968), Uebler (1966), Pickup (1970)).

Figure 2-5. Wine Glass Stem Flow

This observation has now been extended to extremely dilute polymer solutions of concentrations in the ppm range (Oliver and Bragg (1973a,1973b), Balakrishnan and Gordon (1975a).

Uebler found that WGS flow can be modeled as a spherical sink flow towards a point sink on the axis of the contraction, with velocity field

$$v^r = - Q'/r^2 \qquad (2\text{-}11)$$

$$v^\theta = v^\phi = 0$$

v^r is the velocity measured at any distance r from the sink, and Q', the sink strength, is proportional to the flow rate Q. For a flow such as this the rate of strain tensor is diagonal (equation (2-12)), and the material is therefore subjected to extensional deformation. Thus η_{ex}, the extensional viscosity, can be measured for polymer melts and solutions that exhibit WGS flow if the stretch rate and the normal stress difference arising from such deformations can be measured. For the case of extremely dilute polymer solutions, this is in fact the most widely used method to determine η_{ex} (Metzner and Metzner (1969), Oliver and Bragg (1973a), Balakrishnan and Gordon (1975a)).

In a very detailed analysis of WGS flow, Murch (1970), using 0.5% solutions of Separan AP 30, determined the extensional normal stress difference by using measurements of $T^{\theta\theta}$ in conjunction with the r component equation of motion in spherical coordinates.

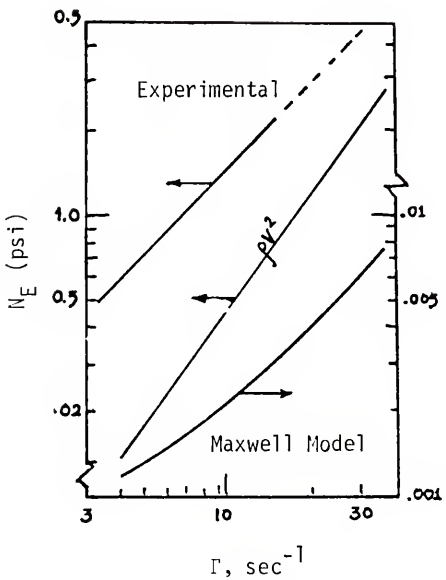

Figure 2-6. Predictions of the Maxwell Model

$$N_E(r) = \rho v^2(r) + \frac{1}{r^2}\int_r^\infty (\bar{r})^2 \frac{dT^{\theta\theta}}{d\bar{r}}\, d\bar{r} \qquad (2\text{-}24)$$

From measurements of $T^{\theta\theta}$ as a function of r, Murch was able to calculate the integral in equation (2-24), and thereby obtain N_E. The extensional viscosities obtained from this procedure were constant, indicating Newtonian behavior, and were roughly three orders of magnitude greater than the shear viscosity! Comparison of these values with those predicted by the White-Metzner model for sink flow kinematics showed vast disagreement (Figure 2-6). It is premature to attribute this to any inadequacy on the part of the model because of experimental difficulties associated with Murch's techniques as well as invalid assumptions made in calculating stretch rates. A detailed discussion of sources of error in Murch's work is presented in Section 5.3.

Metzner and Metzner used the jet thrust technique to measure normal stress differences in WGS flow. In this method, the thrust exerted by a jet of dilute polymer solution issuing from a reservoir through a sharp-edged orifice was measured and was related to the tensile stress N_E in the liquid by the equation

$$N_E = \rho v_o^2 - T/A_o \qquad (2\text{-}25)$$

where v_o is the orifice velocity and T/A_o is the thrust per unit area of the orifice. Metzner and Metzner used a Separan AP 30 solution that was identical to that used by Murch and they obtained very large values of extensional viscosity. Metzner and Metzner made the same assumptions

in calculating stretch rates as Murch--that the stretch rate at the orifice was a linear function of orifice velocity.

$$\Gamma_o = kv_o \qquad (2\text{-}26)$$

The results of the present work show that equation (2-26) is not generally true (Section 5.1). Furthermore, the thrust technique used by Metzner and Metzner actually yields die swell and not tensile stress at the orifice (Section 5.3).

Despite all the uncertainties in these methods, the results obtained by Metzner and Metzner and by Murch clearly demonstrate the enormous resistance exhibited by dilute polymer solutions to extensional motions. For a 100 wppm solution of Separan AP 30 the former group of authors estimated a conservative value of η_{ex} that was 500 times larger than the shear viscosity (1.44 cp).

2.5 Kinematics of WGS Flow

Extensional viscosities were measured in the present work in WGS flow. A detailed description of the kinematics of WGS flow is presented in this section.

A WGS flow can be conveniently divided into four sections (Figure 2-7).

(1) The section upstream of the actual WGS flow. In this region, velocities are extremely small as compared to the region close to the contraction. Pickup (1970) observed simple laminar shearing flow in this region.

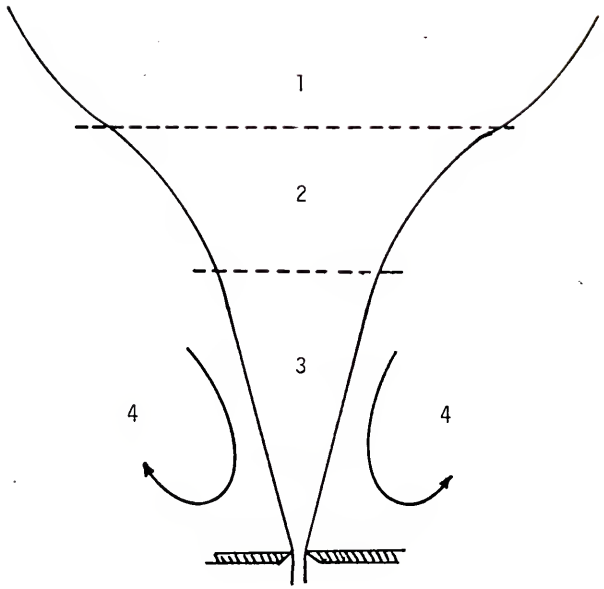

Figure 2-7. Division of WGS Flow into Different Regions.

(2) As one travels downstream with the flow in region (1), one observes a transition from shearing flow to WGS flow. The liquid begins to accelerate in the direction of flow, and converges towards the centerline. The distance from the contraction where this transition occurs would be the distance to which the large toroidal vortices surrounding the central flow penetrate into the experimental apparatus.

(3) Following region (2), the flow is more or less well defined and resembles flow through a "cone" with a liquid wall. As described by Pickup (1970), and Uebler (1966), the velocity vector at any point in this region is directed towards the contraction, and the fluid accelerates rapidly as it approaches the apex of the cone. There is little or no shear in the major portion of this region. At the interface between region (3) and the liquid surrounding it (region (4)), there is intense shearing. The deformation levels in region (3) are extremely large compared to the rest of the liquid.

(4) Region (4) surrounds region (3). Here the liquid simply recirculates slowly, and the deformation levels in this region are extremely small compared to those in region (3) (Uebler (1966)).

Several velocity profiles have been proposed to approximate the kinematics of WGS flow. Notable among these are those of Uebler (1966), Pickup (1970), and Kanel (1972).

Uebler conducted experiments with concentrated solutions of Separan AP 30 in water. Using air bubbles in the viscous solution as tracer particles, he studied the kinematics of WGS flow. The results obtained by Uebler suggested that the flow in the region upstream of the contraction was radially directed toward the origin of a spherical coordinate system located at the apex of the liquid cone. This yielded the velocity profile described by the equations (2-11):

$$v^r = - Q'/r^2 \qquad (2\text{-}11a)$$

$$v^\theta = v^\phi = 0 \qquad (2\text{-}11b)$$

$$Q' = Q'(\theta) \qquad (2\text{-}11c)$$

where θ is the half angle of the liquid cone. Uebler also found that $Q'(\theta)$ was approximately constant and equal to $\frac{Q}{2\pi r^2 (1-\cos\theta)}$, where Q is the volumetric flow rate, r is the position at which the velocity is measured. Thus the velocity profile becomes

$$v^r = \frac{- Q}{2\pi r^2 (1-\cos\theta)} \qquad (2\text{-}27a)$$

$$v^\theta = v^\phi = 0 \qquad (2\text{-}27b)$$

The above equations are good for about 70% of the flow that enters the contraction (Uebler (1966)).

Uebler's measurements were carried out at values of generalized Reynolds number ranging from moderate to high, and the radial flow kinematics described by equations (2-27) are therefore a good approximation to the actual kinematics of the flow under these conditions.

The kinematic measurements of Pickup (1970) yielded results very similar to those of Uebler. Pickup found the velocity in the central region to be approximated by the following equation:

$$v_x = v_o \, e^{\beta x} \tag{2-28}$$

where v_x is the velocity at any point x, v_o is the velocity in the region upstream of the WGS flow and x is the distance measured from the origin of a cartesian coordinate system located at the point where the flow enters WGS flow (Figure 2-8).

Yet another velocity field that has been used to describe the kinematics of WGS flow is that due to Kanel (1972). In many fiber spinning operations and Fano flows, the diameter of the column of the liquid is given by equation (2-22). The shape of the central region in WGS flow resembles the shape of liquid column in Fano flow. However, attempts made in this work to fit an equation of the form of (2-22) showed that (1) an equation with single values for c_1, c_2 and m does not describe the entire flow and (2) that the flow is best described by using equation (2-22) for a minor part of the flow, at the beginning of WGS flow (i.e., to describe regions (2) and part of

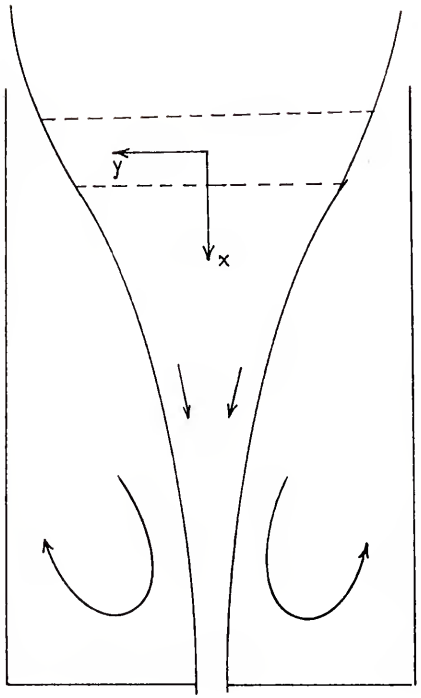

Figure 2-8. Coordinates Used in Pickup's Kinematics

(3)), and sink flow kinematics to describe the major part of the flow in region (3).

In this work, the sink flow kinematics of Uebler have been used to arrive at relationships for stretch rates and normal stress differences at the orifice. This is only an approximation to the actual flow because equations (2-27) are not valid in region (2) (Figure 2-7), where the flow field resembles the mouth of a trumpet. However, they are applicable for the most part of region (3) where the fluid rapidly accelerates and deformation levels are their largest. The extensional behavior of a material in WGS flow would be expected to depend largely on the kinematics of this region.

2.6 Analysis of Stress Field in WGS Flow

In order to analyze the stress field in a flow described by equation (2-27), one can adopt the following techniques:

(i) Point measurement of stresses by the use of probes. This technique is now known to be inaccurate in the case of viscoelastic fluids. As pointed out by Astarita and Metzner (1967), the fluid approaching a probe introduced to measure the stress at a point in the flow experiences large changes in the deformation rate with position from an Eulerian sense and with time from a Lagrangian sense. Such deformational processes are characterized by large values of the Deborah Number

$$N_{De} = \lambda \sqrt{\frac{D}{Dt}} \sqrt{II_D} \qquad (2\text{-}29)$$

where λ = relaxation time of the fluid and II_D = second invariant of the rate of strain tensor. Large values of N_{De} imply a solidlike response of the liquid immediately adjacent to the surface of the probe (Astarita and Metzner (1967)), leading to inaccurate and sluggish response of the probe. Also, the use of a probe with a hole in it fails in the case of viscoelastic fluids due to hole error (Kaye et al. (1968)).

Murch used solid probes and probes with holes in them to measure $T^{\theta\theta}$ in the central region (region 3) of WGS flow, and from $T^{\theta\theta}$ vs. r profiles was able to calculate $N_E(r)$. It is obvious from the factors stated above that Murch's results could be considerably in error.

(ii) Stress birefringence technique: Adams et al. (1965) have used the birefringent properties of viscoelastic fluids to analyze stresses in a converging flow. By using stress-optical relations derived for slow flows, they obtained estimates of shear stresses and normal stress differences in converging and diverging flows. The weakness in this approach is the extension of equations derived for slow flows to accelerative flows such as those encountered in converging flow, with no justification for this assumption.

(iii) Momentum balances. In the absence of techniques to explicitly measure stresses at different points in WGS flow, one can resort to the use of natural laws as continuity and momentum balance equations to yield expressions relating pressure drop to flow rate, both of which are easily measurable quantities.

Bagley in 1957 noticed that the converging flow of certain polymer melts gave rise to large entrance pressure losses, in excess of those predicted for a purely viscous material. This excess pressure drop is commonly attributed to the elasticity of the melt and is determined from the Bagley plot. In the typical experiment that is performed in the capillary viscometry of polymer melts, the melt is placed in a reservoir and forced through an attached capillary tube. The pressure drop in the reservoir is commonly neglected in comparison with that in the capillary. Thus the pressure drop across the length of the capillary is simply the pressure in the reservoir minus the loss in pressure at the entrance of the capillary due to rearrangement of the velocity profile and viscous and elastic effects. This loss in pressure at the entrance to the capillary ΔP_e is determined by measuring the pressure in the reservoir P at a fixed value of the apparent shear rate $\frac{8v}{D}$ for different values of L/D, the length to diameter ratio of the capillary. ΔP_e is then obtained by plotting P vs. L/D and extrapolating the plot to zero L/D (Figure 2-9). Attempts have been made to separate the entrance pressure drop into viscous and elastic parts (Bagley (1961)), and it is generally believed that the entrance pressure drop is closely related to the elasticity of the material. In particular, large entrance pressure drops are believed to be due to extensional viscosity effects (Metzner et al. (1969), Balakrishnan and Gordon (1975a)).

The converging flows of polymer melts and concentrated solutions have received a fair amount of attention due to their common occurrence in polymer processing applications. In recent years, certain anomalies have been reported in association with these flow fields for dilute

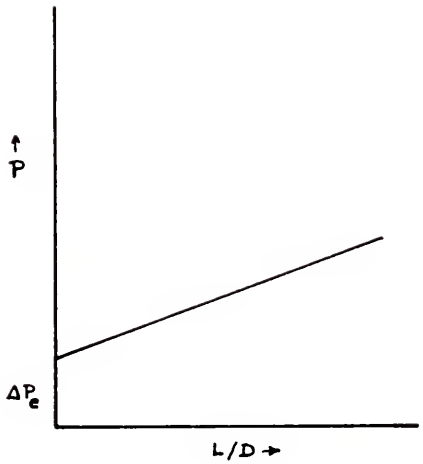

Figure 2-9. The Bagley Plot.

polymer solutions. Pruitt and Crawford (1965) observed in their experiments on turbulent drag reduction that dilute polymer solutions exhibit pressure drops across contractions in flow much greater than water alone. Giles (1969) found orifice discharge coefficients to be much lower for a 300 wppm solution of Polyox WSR 301 than for water, indicating an increase in pressure drop across the orifice. In a novel experiment in which a liquid was made to flow out of an orifice located on the wall of a tube (this was done in order to reproduce a feature that is characteristic of turbulence--motion normal to the wall), Morgan (1971) found the addition of small amounts of polymer to water to reduce flow rates through the orifice. This again indicates larger pressure drops across the orifice for the polymer solution than for water alone. Bilgen (1973), using an orifice of diameter 0.1 mm, found significant increase in pressure drop across the orifice due to the addition of as little as 10 wppm of Polyox FRA (a higher molecular weight homolog of WSR 301). This pressure loss was found to increase with increasing molecular weight of the polymer. Similar results have been reported by several other investigators (Sylvester and Rosen (1970), Oliver et al. (1970), Balakrishnan and Gordon (1975a)). Since the viscosities of the solutions used in most of these studies were nearly equal to the viscosity of water, the increased pressure loss cannot be attributed to viscous effects, and is presumably due to elastic effects at the entrance region to the orifice. It will be shown presently from a momentum balance that in the case of WGS flow the entrance pressure drop is explicitly related to the primary normal stress difference

at the orifice. The control surfaces used in making the momentum balance are shown in Figure 2-9.

The apparatus is a large reservoir fitted with a sharp-edged orifice. Section 1 is taken far upstream of the orifice so that it is located in region 1 described in Section 2.5. Section 0 is located in the plane of contraction. Section 2 is taken at the free surface of the jet emerging from the orifice. In writing momentum balances, the following assumptions are utilized (these are mostly identical to the observations made in describing WGS flow):

(1) At section 1, the velocities and stresses arising from deformations are very small. This would be a fair approximation for a large reservoir fitted with a small orifice.

(2) The velocities and deformation levels in the recirculating region (region 4 of Figure 2-7) are also very small (Murch (1970)). Therefore, the stresses in this region would not be expected to vary much with position.

(3) Viscous drag in the reservoir is negligible. In view of the magnitude of velocities near the walls, this is a valid assumption.

Let the area of the reservoir perpendicular to the direction of flow be A_1, and those of the orifice and the free jet A_o and A_2 respectively. The subscripts o, 1 and 2 identify locations at which various quantities are measured. A momentum balance between sections 1 and 0 yields

$$\int_0^{R_o} 2\pi\rho v_z^2 \, r\,dr - \rho v_1^2 A_1 = \int_0^{R_o} 2\pi T_{zz}^{11} \, r\,dr - p_R(A_1 - A_o) + p_1 A_1 \qquad (2\text{-}30)$$

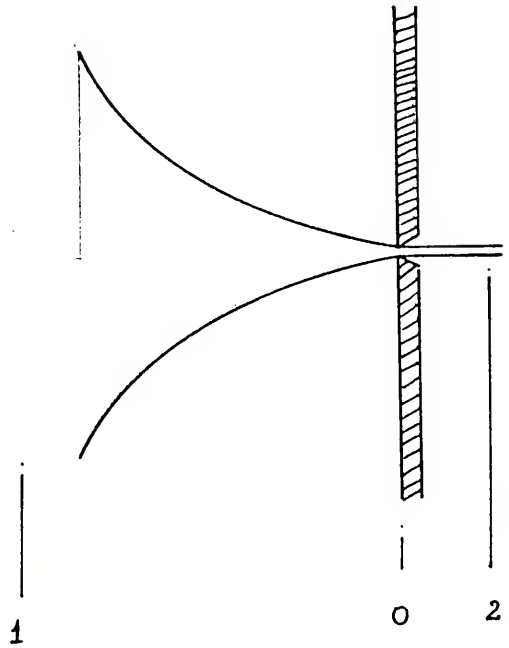

Figure 2-10. Momentum Balance Sections

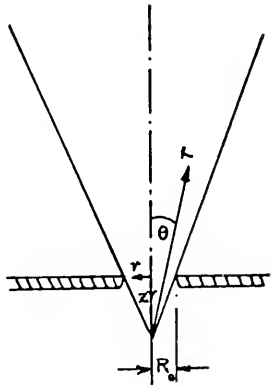

Figure 2-11. Coordinate Systems used in Sink Flow Kinematics

T^{ll} is the total stress in the l direction at the orifice (this would coincide with the z direction of a cylindrical coordinate system with its origin located at the orifice (Figure 2-10)). p_l and p_R are the isotropic pressures at section l and in the recirculating region respectively. For small values of θ, the half angle of convergence, the velocity is fairly uniform across the diameter of the orifice and v_z is nearly equal to v^r (in the spherical coordinate system with origin located at the sink). Also v_l, the velocity in the reservoir upstream of the WGS flow, is very small compared to velocities near the orifice. Equation (2-30) then becomes

$$\rho v_o^2 A_o = T_{zz} A_o - p_R(A_l - A_o) + p_l A_l \tag{2-31}$$

Resolving T_{zz} into isotropic and deviatoric components,

$$T_{zz} = - p + \tau_{zz} \tag{2-32}$$

Now T_{rr} (in cylindrical coordinates) is nearly equal to $T^{\theta\theta}$ (in spherical coordinates) which, following Metzner et al. (1969), can be assumed equal to $- p_R$, the isotropic pressure in the recirculating region.

$$T_{rr} = T^{\theta\theta} = - p_R = - p + \tau_{rr} \tag{2-33}$$

Eliminating the unknown isotropic pressure term from equations (2-32) and (2-33), we obtain the following relationship:

$$N_{E_o} \frac{A_o}{A_l} - \rho v_o^2 \frac{A_o}{A_l} = p_R - p_l \tag{2-34}$$

where $N_E = (\tau_{zz} - \tau_{rr})$. In the case where inertial terms are negligible as would occur with polymer melts, equation (2-34) predicts an adverse pressure gradient. Metzner et al. have suggested that the upstream flow near the walls of the reservoir might be due to this pressure gradient.

A momentum balance between sections 0 and 2 yields

$$\rho v_2^2 A_2 - 2\pi \int_0^{R_o} \rho v_z^2 \, r dr = - 2\pi \int_0^{R_o} T_{zz} \, r dr \qquad (2\text{-}35)$$

Once again for small values of θ, the half angle of convergence, equation (2-35) becomes

$$\rho v_2^2 A_2 - \rho v_o^2 A_o = - T_{zz_o} A_o \qquad (2\text{-}36)$$

In the absence of vena contracta or die swell effects,* the diameters of the jet at section 2 would be the same as the orifice diameter, and equation (2-36) becomes

$$T_{zz_o} = 0 \qquad (2\text{-}37)$$

Once again, using equations (2-32) and (2-33), the above equation can be rewritten as

$$N_{E_o} = (\tau_{zz} - \tau_{rr})_o = p_R \qquad (2\text{-}38)$$

*A situation such as this would be expected for dilute polymer solutions with small values of θ.

Thus the normal stress difference at the orifice is simply equal to the pressure in the recirculating region, which is actually the entrance pressure drop as would be measured by a transducer located on the wall of the reservoir in the recirculating region. Designating this as ΔP_e,

$$N_{E_o} = \Delta P_e \tag{2-39}$$

For the case where the half angle of convergence is not small, and the velocity profile is therefore not uniform across the diameter of the orifice, the integrals in equation (2-35) have to be explicitly evaluated. This can be done as follows:

Let v_z be the velocity in the direction of flow at any point across the diameter of the orifice. Referring to Figure 2-11 it is clear that v_z is related to v^r (in spherical coordinates) by the relationship

$$v_z = v^r \cos \Phi \tag{2-40}$$

where Φ is the angle from the orifice axis at which v_z is measured.

It can be easily shown that the momentum influx into the orifice is given by

$$2\pi\rho \int_0^{R_o} r v_z^2 \, dr = 2\pi\rho \int_0^{\theta} \frac{v_o^2}{4} \frac{(1 + \cos\theta)^2}{\cos^4\theta} \frac{R_o^2}{\tan^2\theta} \cos^6\phi \tan\phi \sec^2\phi \, d\phi \tag{2-41}$$

Carrying out the integration gives the following result

$$2\pi\rho \int_0^{R_o} r v_z^2 \, dr = \frac{\rho A_o v_o^2}{8} \frac{(1 + \cos\theta)^2 (1 + \cos^2\theta)}{\cos^2\theta} \qquad (2\text{-}42)$$

Following a similar procedure for integrating the term on the right hand side of equation (2-35), and neglecting die swell or vena contracta occurrences, we obtain

$$\rho v_o^2 A_o - \frac{\rho v_o^2 A_o}{8\cos^2\theta}(1 + \cos^2\theta)(1 + \cos\theta)^2 = 2A_o T^{rr} \frac{\cos\theta}{(1 + \cos\theta)} \qquad (2\text{-}43)$$

Resolving T^{rr} into isotropic and deviatoric components

$$T^{rr} = (-p + \tau^{rr}) \qquad (2\text{-}44)$$

and eliminating the isotropic pressure term using equations (2-33) and (2-38) we obtain

$$N_{E_o} = \Delta P_e + \frac{\rho v_o^2}{2\cos\theta}(1 + \cos\theta)\left\{1 - \frac{(1 + \cos\theta)^2(1 + \cos^2\theta)}{8\cos^2\theta}\right\} \qquad (2\text{-}45)$$

Equations (2-45) and (2-39) give a simple means of measuring N_{E_o} from measurements of entrance pressure drops and angles of convergence.

Pickup (1970) has performed a similar analysis to determine the normal stress difference at the orifice in the two-dimensional converging flow of polymer solutions. The final result obtained by Pickup was

$$N_{E_o} = \Delta P_e - \Delta p_{sh} \tag{2-46}$$

where Δp_{sh} is pressure drop due to shear in flow through the slit die.

CHAPTER III
EXPERIMENTAL

3.1 Test Solutions

The polymers used in this study are listed in Table 3.1. Separans AP 273 and AP 30 are very high molecular weight synthetic water soluble polymers made from the polymerization of acrylamide

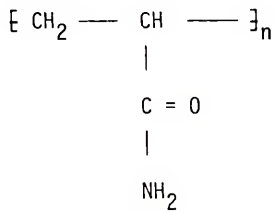

For both AP 273 and AP 30, a small portion (about 20%) of the amide units are hydrolyzed to COOH (Burkholder (1971)). The Separans may be classified as anionic in neutral and alkaline solutions. Under acidic conditions, the ionization of the carboxyl groups is suppressed and the molecules assume a non-ionic character (Ref. Technical Service Report (1969)). Due to the anionic character of these two polymers, their solution viscosity is extremely sensitive to changes in ionic environment. The ionic charge of the carboxylate group disappears at pH = 3 and gradually increases to a maximum at pH = 8. Viscosity is likewise maximum at pH = 8 and a minimum at pH = 3. Of the two Separans the AP 273 grade is of a higher molecular weight grade than AP 30 but both polymers are believed to have similarly shaped molecular weight distributions (Penzenstadler (1975)).

Table 3.1

Polymers Used in this Work

Polymer Designation	Polymer Type	Manufacturer	Nominal Molecular Weight
Separan AP 273	Polyacrylamide	Dow	8-10 x 10^6
Separan AP 30	Polyacrylamide	Dow	4-5 x 10^6
Percol 155	Polyacrylamide	Allied Colloids	10 x 10^6
Polyhall 295	Polyacrylamide	Stein Hall	Not available
Versicol S25	Polyacrylic acid	Allied Colloids	20 x 10^6
Polyox WSR 301	Poly(ethylene oxide)	Union Carbide	4 x 10^6

Percol 155 and Polyhall 295 are also non-ionic polyacrylamides that dissolve readily in water, and are very similar to the Separans in their properties.

Versicol S25 is a very high molecular weight partially neutralized poly(acrylic acid) (PAA). It dissolves readily in water yielding a white translucent solution of pH 5-6. Due to the presence of carboxyl groups along its chain, Versicol shows dramatic changes in its solution properties with change in pH, much the same as the polyacrylamides do. The viscosity of Versicol solutions is fairly stable in the range of pH 5.5-12.5 (Ref. Versicol Catalog). Addition of electrolytes to Versicol solutions suppresses the viscosity of the solutions.

The only non-ionic polymer used in this work was Polyox WSR 301 (PEO), a poly(ethylene oxide) polymer. Due to the ether groups present along its chain, the polymer has the potential of forming hydrogen bonds with water. Its viscosity is very stable over a wide range of pH (Gordon et al. (1973)). PEO is extremely susceptible to shear degradation, much more so than the other polymers used in this study.

The range of polymer concentrations used was 10 to 200 wppm, and all solutions were made in deionized water. Conformational studies were carried out with Separan AP 273 and the pH of these solutions was varied by using HCl and dilute NaOH solutions.

3.2 Polymer Solution Preparation

All the polymers used in this study have a tendency to form gel-like agglomerates when they come in contact with water. To avoid the formation of these agglomerates and the consequent increase in dissolution time, the following procedure was adopted in making polymer solutions:

The required amount of polymer was weighed and placed in a dry 4 1/2 gallon Nalgene jar. To this, about 50 ml of isopropanol was added. The isopropanol served as a non-solvent medium in which the polymer formed a dispersion, and in the case of Polyox FRA, it also acted to prevent chemical degradation. Demineralized water was then added to the dispersion in the jar and the resulting solution allowed to sit for about 8 hours before it was used. In order to expedite the dissolution process, the solution was mixed periodically by hand with a glass rod.

The procedure described above yielded polymer solutions that were clear and free of undissolved polymer or agglomerates and was ideally suited for dissolving small amounts of polymer (less than 10 gms.). For the case where larger amounts of polymer were required, the dissolution process was slightly different. Once again the required amount of polymer was weighed and was placed in a beaker and about 50 ml of isopropanol added to it. The Nalgene jar was filled with some water and a vortex created in it by the use of a low speed mixer.* The polymer-isopropanol mixture was then poured into the vortex, resulting in immediate dispersion of the polymer in water, and the mixer was turned off. Periodical mixing by hand (with a glass rod) and keeping the solution for about 8 hours yielded a clear solution that was ready for use. In all the cases the concentration of the solution made in the Nalgene jar was about 1000 wppm. This solution was then diluted in the storage tank of the converging flow apparatus (Section 3.3), or the DR apparatus (Section 3.6) to yield solutions of the desired concentration level.

*The use of a mechanical mixer was kept to a minimum in order to avoid shear degradation of the polymer solutions.

3.3 Converging Flow Apparatus

The apparatus used to study the converging flow of dilute polymer solutions is shown in Figure 3-1. It consisted of four major components--the storage tank, the pressure tank, the flow (visualizing) tank, and the dye reservoir. The dimensions of the first three are given in Figure 3-1. The storage and flow tanks were made of Plexiglas while the pressure tank was made of stainless steel. The flow tank had the capability of having orifices of different sizes fitted to it. It also had two baffles in it to prevent channeling of the test liquid (i.e., to ensure uniform distribution of the liquid before it entered the converging flow field). Dye from a reservoir could be injected into the flow tank by means of small holes drilled into a 3 mm stainless steel tube that spanned the width of the tank. The dye injection tube could be positioned at different distances from the orifice. Details of the dimensions and arrangement of the various fittings on the flow tank are given in Figure 3-2. During a run, the flow tank was set up in such a way that the jet emerging from the orifice was in a horizontal plane (in other words, the flow tank was laid on its back with its face up, facing the camera that was used to take photographs of the flow pattern in the tank). The positioning of the flow tank and camera during a run is shown in Figure 3-3.

3.3.1 Details of orifices used

All the orifices used in this study were made of Plexiglas. Their dimensions are given in Table 3.2, and the details of their construction in Figure 3-4. There were three major components

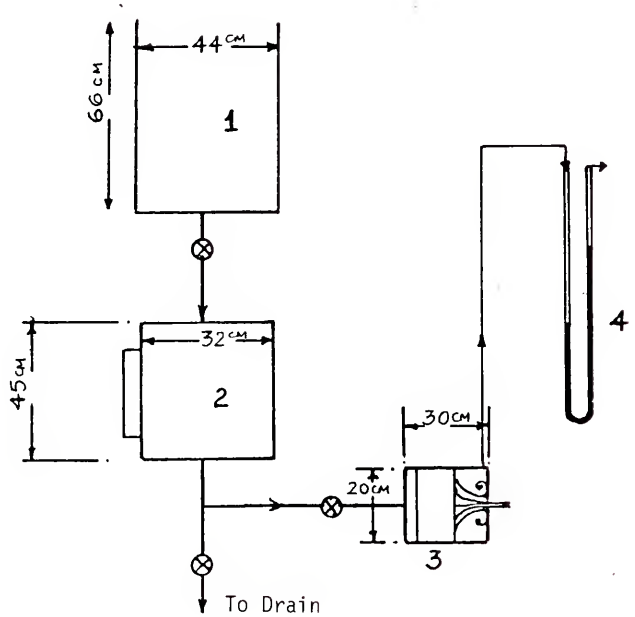

1. Storage Tank
2. Pressure Tank
3. Flow Tank
4. Manometer

Figure 3-1. Converging Flow Loop

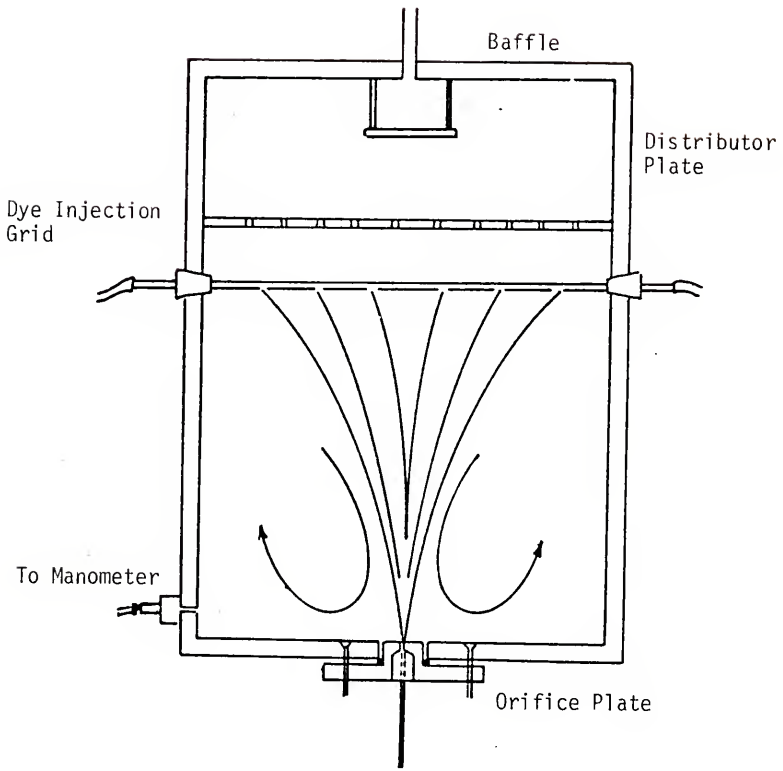

Figure 3-2. Details of Flow Tank

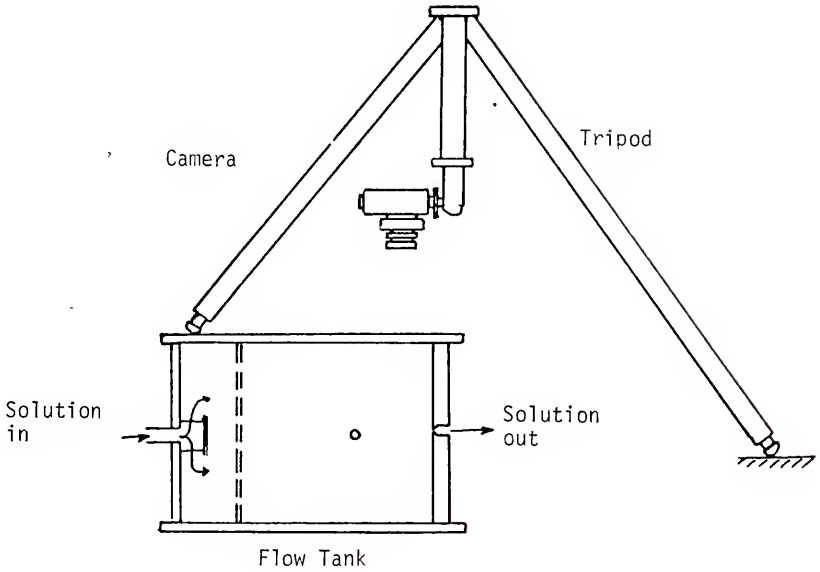

Figure 3-3. Positioning of Camera During a Run.

TABLE 3-2

Dimensions of Orifices

Orifice diameter cms	Orifice Length cms	L/D ratio
0.040	0.150	3.75
0.051	0.150	2.94
0.109	0.347	3.18
0.132	0.284	2.15
0.178	0.347	1.96
0.244	0.400	1.64

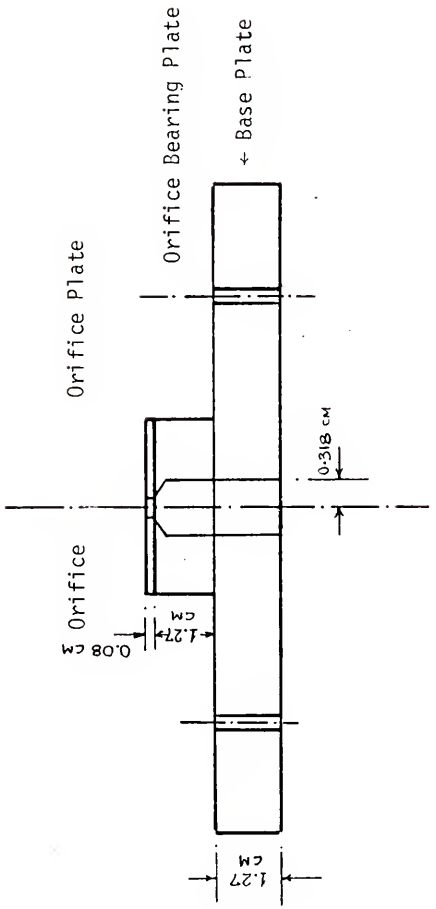

.Figure 3-4. Details of Orifice Construction.

constituting the orifice plates--(i) the base plate made of 1.27 cm thick Plexiglas, (ii) the orifice bearing plate which was a 1.27 cm thick, 2.54 cm dia Plexiglas plate glued to the base plate, and (iii) the orifice disk that was a 0.16 cm thick, 2.54 cm dia Plexiglas plate that was mounted on the orifice bearing plate. The orifice hole was drilled into the orifice disk. This hole then flared into a 0.62 cm hole that went through part of the disk and through the orifice bearing and base plates. All drilling processes were carried out extremely slowly in order to avoid distortion of the hole surfaces due to heat generation.

3.4 Photographic Equipment

As mentioned earlier in Chapter II, the angle defined by the streamlines converging into the orifice is required for the calculation of stretch rates at the orifice. These angles were measured by taking photographs of the streamlines and projecting the developed film on tracing paper through an enlarger. The camera used was a Bell and Howell FD 35 single lens reflex camera equipped with a 50 mm lens and close-up lenses. The film used was Kodak Tri-X rated at 400 ASA. The camera was mounted on a tripod and positioned over the flow tank of the converging flow apparatus such that the field of view covered all of the flow from the dye injection grid to the orifice.

3.5 Making of a Run

The concentrated polymer solution made in the Nalgene jar was first poured into the storage tank of the converging flow apparatus and water added to it to bring the polymer concentration to the

desired level. Following slow mixing of the solution with a paddle (to ensure uniformity of the solution), the pressure tank and the flow tanks were filled with the polymer solution. Some polymer solution was also taken in the dye reservoir and a few drops of dye (food color) added to it. The pressure tank was then pressurized with compressed air in order to force the polymer solution through the orifice. Dye was injected into the flow through the dye injection grid and photographs of the streamlines were taken. Flow rates were measured by collecting the liquid issuing out of the orifice and weighing it. Entrance pressure drops were measured by a mercury manometer connected to the flow tank (Figure 3-2). Several photographs were taken at each flow setting to make sure that the flow was steady, and fully developed.

3.6 Thrust Measurements

A jet thrust apparatus similar to that used by Oliver (1966) was built to measure normal stress differences at the orifice. A photograph of the apparatus is given in Figure 3-5. The jet issuing from the orifice was made to strike a small Plexiglas plate attached to one end of a brass rod that was vertically suspended by bearings. The other end of the brass rod was kept in contact with a Statham force transducer (Model UC3 Gold Cell) that was connected to a recorder through a Sanborn (Model 311A) transducer-indicator-amplifier. The force exerted by the jet on the Plexiglas plate was transmitted to the transducer by the brass rod, and by calibrating the system by suspending weights from the Plexiglas plate (Figure 3-6), these forces could be measured.

Figure 3-5. The Thrust Apparatus

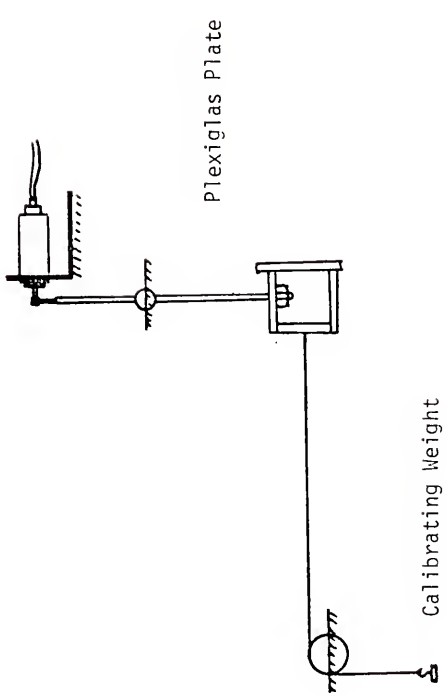

Figure 3-6. Calibration of Thrust Apparatus

3.7 Drag Reduction Measurements

Drag reduction measurements were made in two kinds of apparatus--a flow loop and a gravity flow setup. The flow loop (Figure 3-7) consisted of (i) a Moyno pump (Model 2L6) with a Carter variable speed drive, and (ii) four stainless steel tubes of inside diameters 0.457 cm, 1.092 cm, 1.656 cm, and 2.146 cm. Details of entrance length, exit length and location of pressure drop taps are given in Figure 3-7. Flow rates were measured by collecting the liquid and weighing it and pressure drops by using manometers containing mercury, Meriam Red Fluid (sp. gr. 2.95) and Meriam Blue Fluid (sp. gr. 1.75).

The gravity flow apparatus was identical to that described in the author's master's thesis. It consisted of a 100 liter 44 cm dia 68.5 cm tall Plexiglas tank to the bottom of which a 0.45 cm i.d., 185 cm long stainless steel tube was attached. A schematic representation of the apparatus can be found in Figure 3-7. The tank was filled with water and the water allowed to drain. The times for the water level to drop from 92ℓ to 87ℓ and 91ℓ to 86ℓ were measured and averaged. Similar measurements were then made for the polymer solutions and percent drag reduction was defined as

$$\% \text{ DR} = 100(t_w - t_p)/t_w \qquad (3\text{-}1)$$

where t_w = average efflux time for water, and

t_p = average efflux time for polymer solution.

By measuring t_p at different polymer concentrations DR was determined as a function of concentration. Successive lowering of concentration

A 0.457 cm I.D. Stainless Steel Tube
B 1.092 cm I.D. Stainless Steel Tube
C 2.146 cm I.D. Stainless Steel Tube

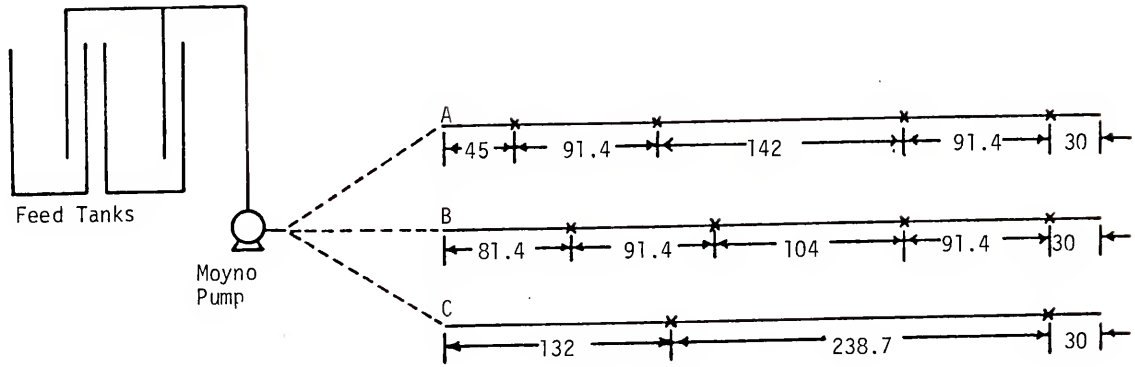

Figure 3-7. Flow Loop Description

was achieved by diluting the polymer solution in situ.

3.8 Vortex Inhibition (VI)

Vortex Inhibition, a viscoelastic phenomenon believed to be related to DR was discovered during the course of some experiments on DR, and is discussed in detail in Balakrishnan (1972). The effect and its measurement are briefly described here:

When a square Plexiglas tank was filled with water and the plug at the bottom of the tank was removed after stirring the water, a vortex was found to form immediately. The vortex was quite stable to perturbations and it remained intact until all the water in the tank had drained. In the presence of drag reducing polymers above a critical concentration (that depended on the polymer in question), this was not the case--the vortex was not complete in that the air core did not reach the drain hole at the bottom of the tank. The appearances of the vortex with water and with polymer solution are shown in Figures 3-8 and 3-9. At polymer concentrations slightly below the critical, the vortex reached the bottom of the tank intermittently and with further reduction in concentration the liquid became indistinguishable from water. When the polymer concentration was increased above the critical, the vortex became progressively smaller until at very high concentrations only a very small dip formed at the surface of the liquid. At polymer concentrations equal to or very near the critical the vortex was extremely unstable in that its

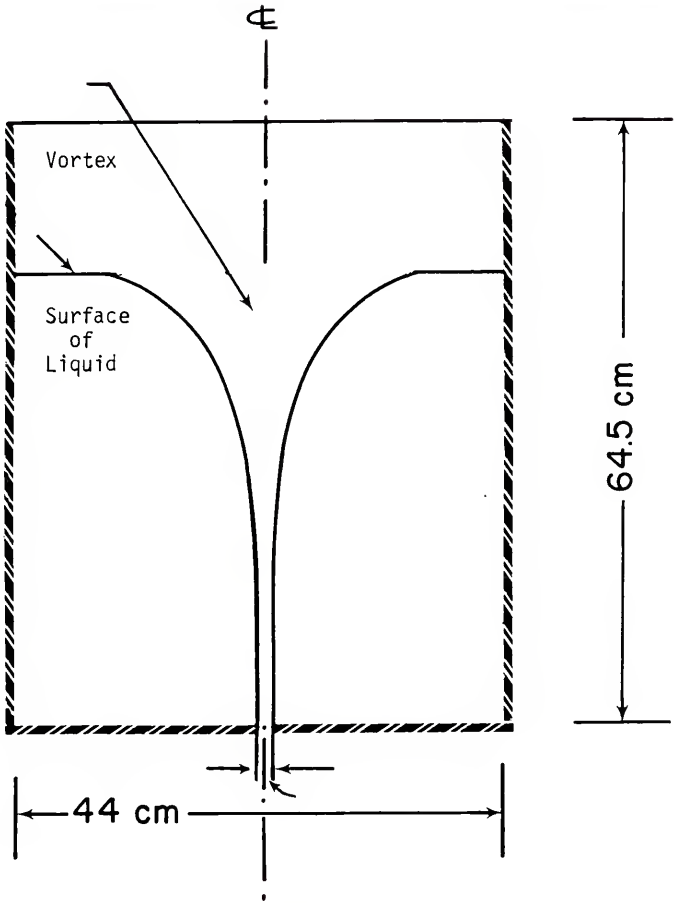

Figure 3-8. Vortex Formation

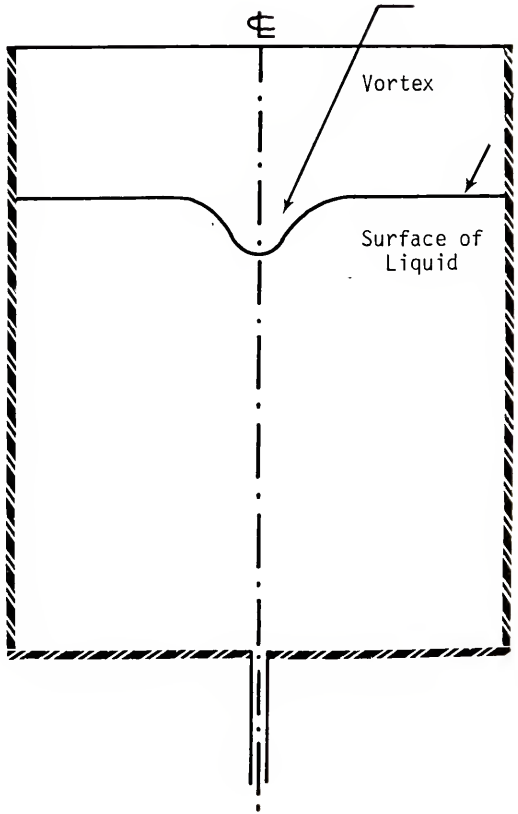

Figure 3-9. Vortex Inhibition

length fluctuated (the tip of the vortex kept moving up and down). Experimental investigation of VI showed that it correlated extremely well with the drag reducing ability of polymers and that it was a sensitive measure of polymer degradation at concentrations less than 10 wppm. Table 4.1 summarizes the vortex inhibiting ability of the polymers used in this study. In the table C_{VI} is the critical polymer concentration below which vortex formation occurs, and it was determined as follows:

The square Plexiglas tank illustrated in Figures 3-9 and 3-10 was filled with the polymer solution to a level of 65 liters, the solution stirred vigorously and allowed to drain. The liquid level was allowed to drop to 58 liters before the vortex was inspected for completion. This drop in level from 65 to 58 liters was arbitrarily chosen to remove the effects of initial stirring. If the vortex completed when the liquid level was between 58 and 53 liters C_{VI} was taken as the next highest concentration in the dilution sequence.* Even though the procedure was arbitrary, the results were extremely reproducible.

*The dilution sequence used was (in wppm): 3000, 2000, 1500, 1000, 800, 600, 400, 300, 200, 150, 100, 75, 50, 40, 30, 20, 15, 10, 7.5, 5, 4, 3, 2, 1. For most polymers the starting concentration was well below 500 wppm.

CHAPTER IV
EXPERIMENTAL RESULTS

All experimental data are summarized in this chapter.

4.1 Drag Reduction

Drag reducing ability was determined by using the flow loop described in Chapter III. The polymer concentration chosen for DR runs was 5 wppm. Data obtained in the 1.09 cm tube are given in Figure 4-1 in which the friction factor f is plotted versus Reynolds Number, N_{Re}, based on solvent viscosity.

4.2 Vortex Inhibition

The vortex inhibition of the polymers used in this study is listed in Table 4.1.

4.3 Extensional Viscosity

As discussed in Chapter II, values of entrance pressure drop and the angle of convergence are required for an extensional viscosity to be calculated.

Angle of Convergence Measurements

Stretch rates at the orifice are calculated from measurements of θ, the half angle of convergence in WGS flow, using equations (2-12) and (2-27). In this section, results are presented for the polyacrylamide solutions (PAMS), followed by those for PAA (Versicol S25), and

Table 4.1

Summary of VI Data

Polymer	C_{VI}, wppm
Separan AP 273	2
Separan AP 30	10
Percol 155	2
Polyhall 295	15
Versicol S25	3
Polyox WSR 301	3

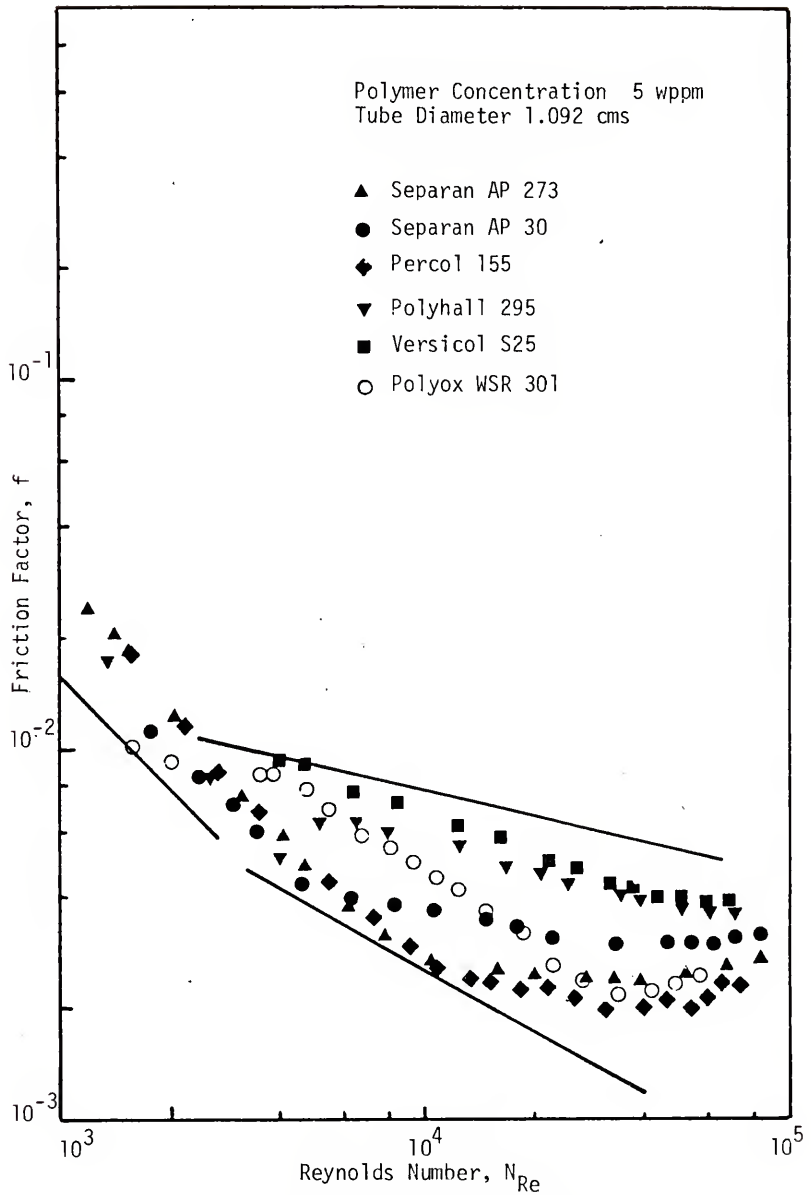

Figure 4-1. Summary of Drag Reduction Data

PEO (Polyox WSR 301). Values of θ for all the runs are tabulated in Appendix A.

PAM: As mentioned in Chapter III, the polyacrylamides used in this study were Separan AP 273, Separan AP 30, Percol 155 and Polyhall 295. All of these exhibit pronounced WGS flow that extends far upstream from the orifice. In the case of Separan AP 273, WGS flow was observed at concentrations as low as 10 wppm. At polymer concentrations below 10 wppm, traces of WGS flow were still visible but were not clear enough for the angle of convergence to be accurately defined.

The angle of convergence θ was found to depend on orifice velocity v_o, orifice radius R_o, and polymer concentration. With most polymer solutions, θ was found to decrease slightly with increasing v_o at low flow rates, increase slightly with increasing v_o at moderate to high flow rates, and, in some cases, decrease slightly with increasing v_o at very high flow rates. This trend was observed with polymer solutions that were of moderate or high concentrations (e.g., 20 wppm or above for Separan AP 273) and is illustrated in Figure 4-2a in which θ is plotted versus v_o for a 20 wppm solution of Separan AP 273. The limits on the data points in the figure correspond to $\pm$ 2% error in measurement of θ from photographs. The orifice diameter was 0.132 cm. At concentrations lower than 20 wppm, θ did not decrease with increasing v_o at very large flow rates.

Considering next the influence of orifice radius, it was observed that θ tended to increase slightly with increasing R_o. This trend is illustrated in Figure 4-2b in which θ is plotted against R_o for a 40 wppm solution of Separan AP 273. θ also showed some dependence

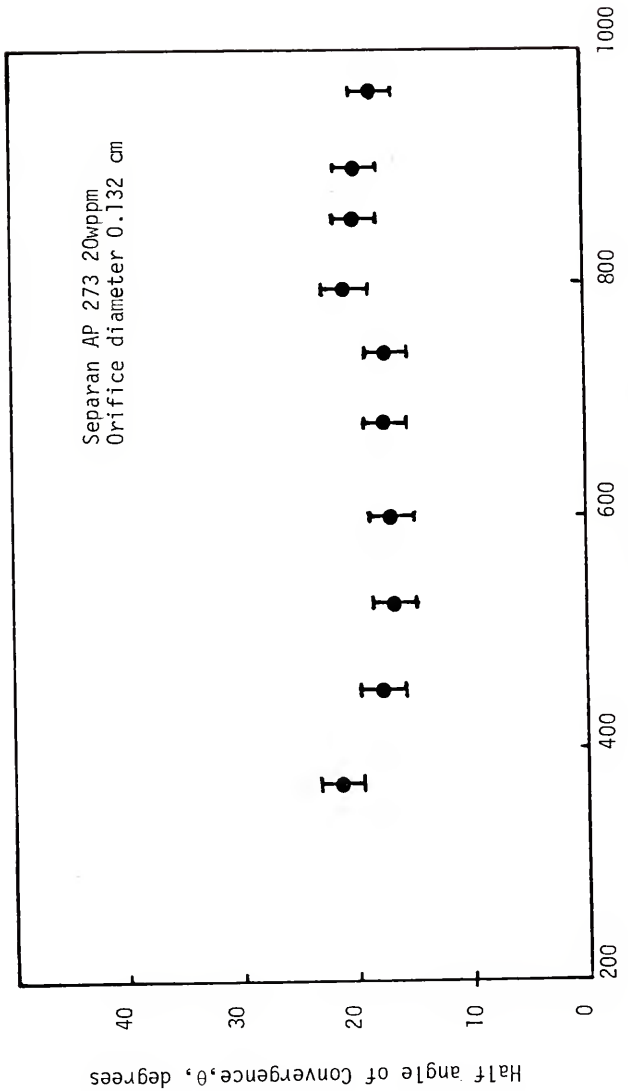

Figure 4-2a. Dependence of θ on Orifice Velocity

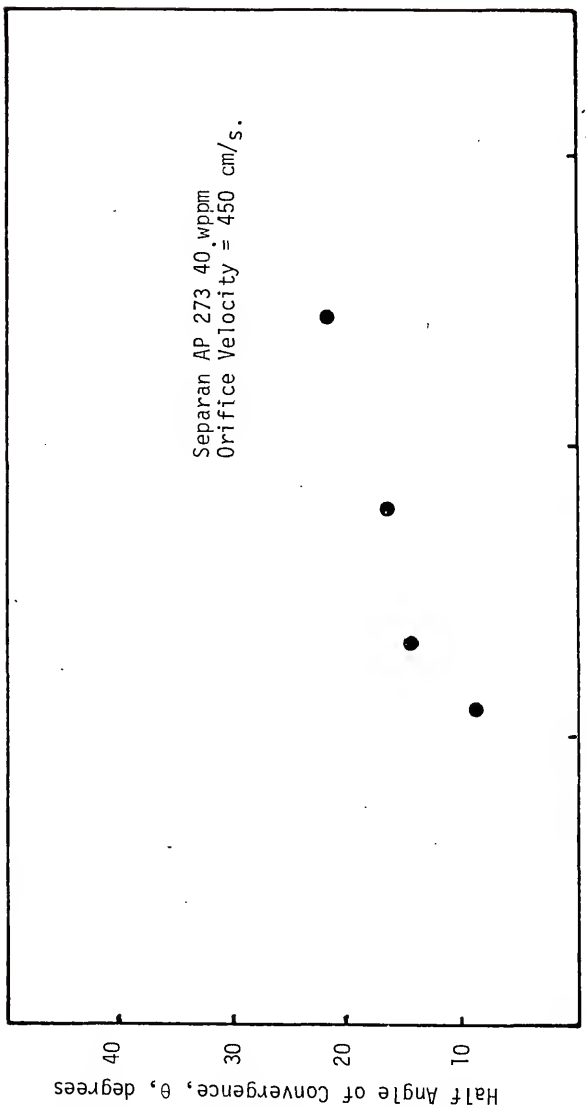

Figure 4-2b. Dependence of θ on Orifice Radius

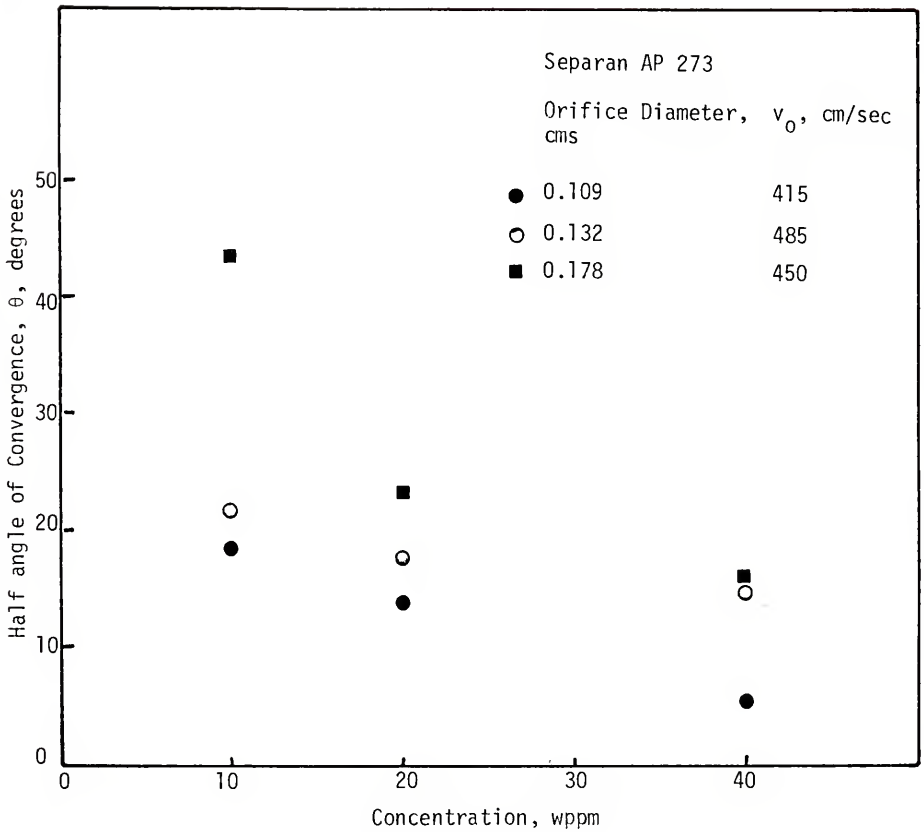

Figure 4-2c. Dependence of θ on Polymer Concentration

on polymer concentration. For a fixed orifice radius and velocity, it decreased with increasing polymer concentration. Figure 4-2c illustrates this trend.

Most of the data presented here were taken in the flow region where θ was a slightly increasing function of v_0. In making measurements of stretch rates at the orifice, problems were encountered with the determination of θ. The most important of these are listed below.

(a) Nature of the flow field and flow visualization technique:

Accurate measurement of θ was difficult due to the nature of the flow field as well as the flow visualization technique used. As described in Section 2.5, WGS flow is characterized by a central converging region shaped like a cone, surrounded by slowly recirculating fluid. The fluid in the space that borders these two regions experiences shear rates nearly equal to the stretch rates in the central flow and is dragged down towards the orifice with the fluid in the central region. Close to the orifice, the liquid in this thin shearing region bounces away from the orifice while the fluid in the central converging region goes through it. It is extremely difficult to delineate the boundary between these two regions. Moreover, dye in the thin shearing region had a tendency to diffuse into a broad band (due to shear) instead of forming well-defined streamlines and this obscured the border between the shearing region and the central converging flow. Figure 4-3 illustrates these effects for a 40 wppm solution of Separan AP 273.

Γ_0, the stretch rate at the orifice, was calculated from the equation

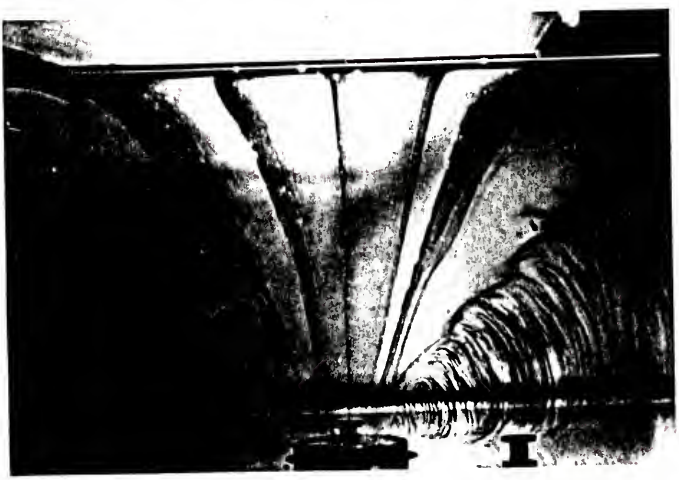

Figure 4-3. WGS Flow with 40 wppm Separan AP 273
Orifice Diameter 0.096 cm

$$\Gamma_o = \frac{v_o}{R_o} \sin\theta\,(1 + \cos\theta) \qquad (4\text{-}1)$$

Equation (4-1) follows from equations (2-12) and (2-27) and the value of r at the orifice.

$$\Gamma(r) = \frac{dv^r}{dr} \qquad (2\text{-}12)$$

$$v^r = \frac{-Q}{2\pi r^2(1-\cos\theta)} \qquad (2\text{-}27)$$

$$r\Big|_{\text{orifice}} = \frac{R_o}{\sin\theta} \qquad (4\text{-}2)$$

Plots of Γ_o vs. v_o for various polyacrylamide solutions are given in Figures 4-4 to 4-9. Figures 4-4 to 4-6 are for Separan AP 273 in deionized water at concentrations of 10, 20, and 40 wppm and Figures 4-7 to 4-9 are for solutions of Separan AP 30 (20 wppm), Percol 155 (40 wppm) and Polyhall 295 (100 wppm), respectively in deionized water.

It is important to note that the flow field observed with the lowest polymer concentration studied (Separan AP 273 at 10 wppm) in the largest orifice (0.178 cm) was quite different from the WGS flow described earlier. At large velocities, the streamlines entering the orifice resembled the bottom of a wine glass rather than a wine glass stem. The appearance of the flow field at low and high velocities is illustrated by photographs in Figures 4-10a and b. At large velocities, the flow angle became quite large and with the exception of a small recirculating region, the flow field bore little resemblance to WGS flow.

In the case of Percol 155, large gel-like particles were noticed in the solution which did not disappear even when the solution was kept

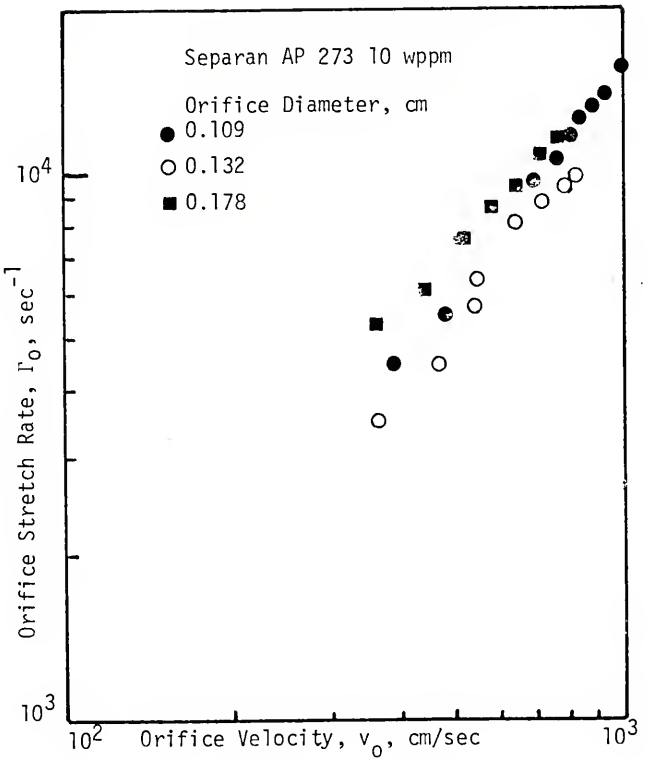

Figure 4-4. Dependence of Stretch Rate on Orifice Velocity

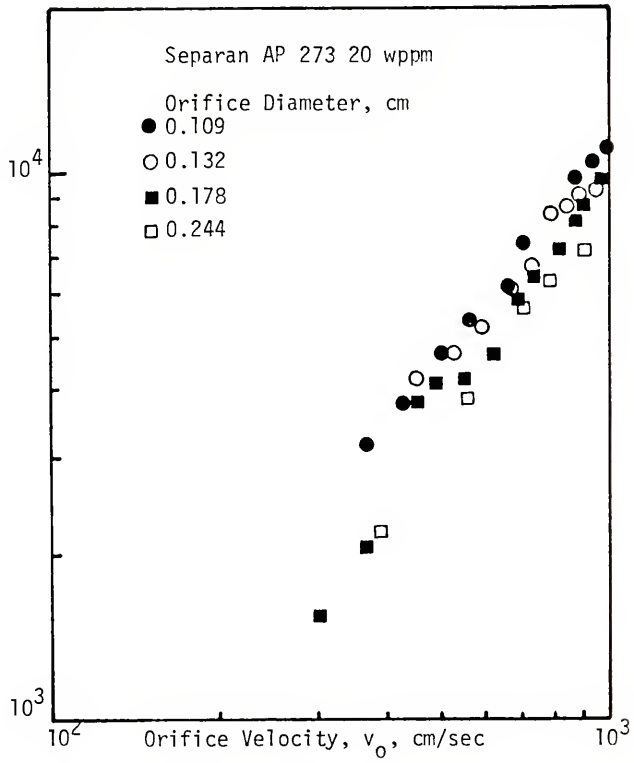

Figure 4-5. Dependence of Stretch Rate on Orifice Velocity

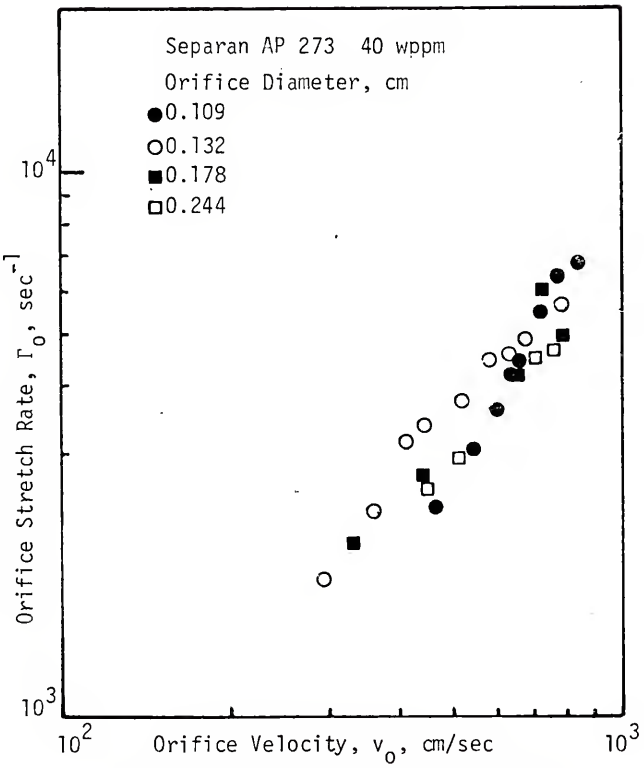

Figure 4-6. Dependence of Stretch Rate on Orifice Velocity

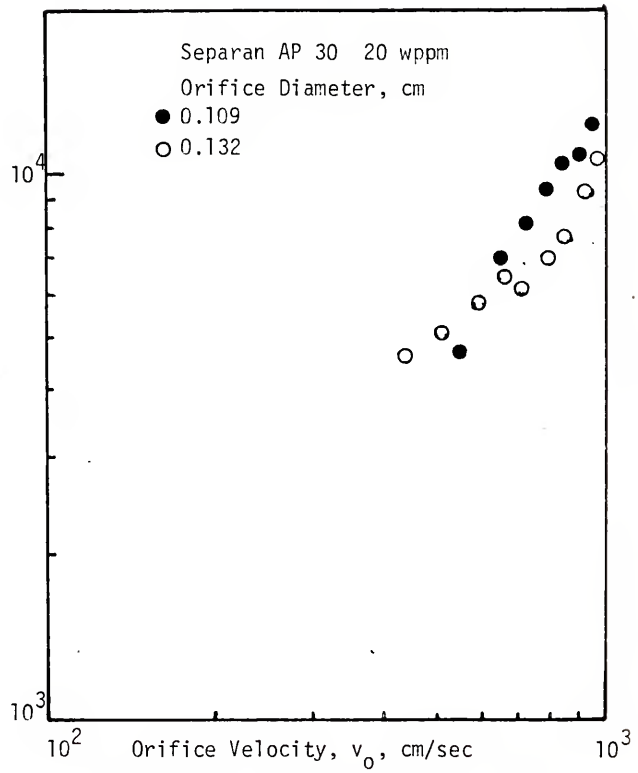

Figure 4-7. Dependence of Stretch Rate on Orifice Velocity

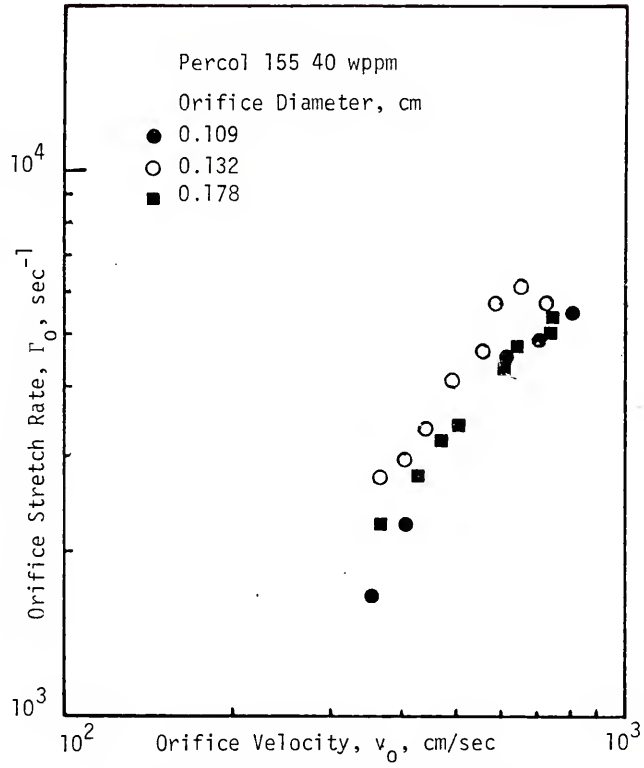

Figure 4-8. Dependence of Stretch Rate on Orifice Velocity

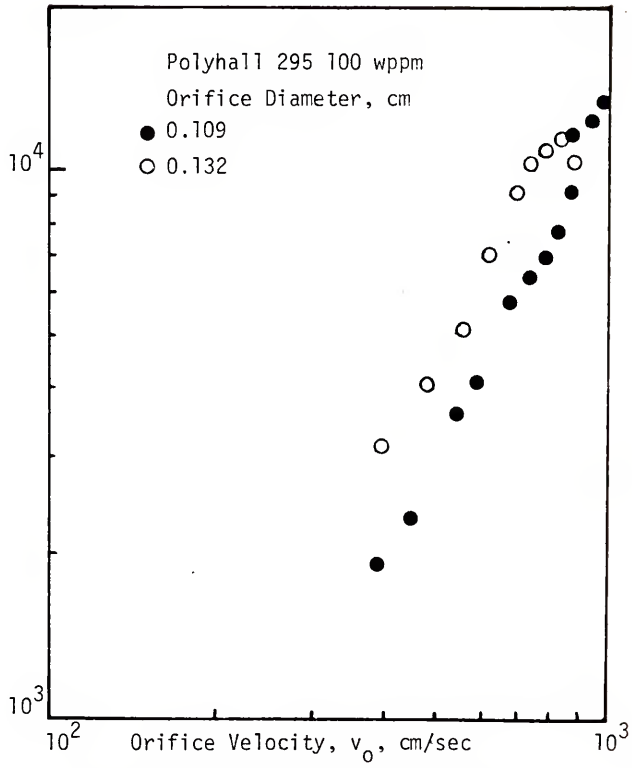

Figure 4-9. Dependence of Stretch Rate on Orifice Velocity

for several days. These particles were so large that at times they blocked the flow in the 0.109 cm orifice. Fortunately, this problem did not occur frequently and was not encountered with the larger orifices.

Separan AP 30 and Polyhall 295 were very similar to Separan AP 273 and Percol 155 in that they exhibited pronounced WGS flow.

PAA: The results obtained with Versicol S25 were similar to those obtained with the PAMs except that the WGS flow pattern did not extend as far upstream. At 100 wppm, WGS flow was clearly visible and the angle of convergence could be measured. At lower concentrations (40 wppm), however, traces of WGS flow could be seen only at low velocities. As the velocity increased the cone angle increased considerably until at high velocities the flow field appeared Newtonian (i.e., the flow entered the orifice from a 180° solid angle). As mentioned earlier, in the case of Separan AP 273 at extremely low concentrations, it was not possible to calculate stretch rates under such conditions. Figure 4-11 shows the dependence of stretch rate on orifice velocity for a 100 wppm solution of PAA. The orifice diameter was 0.109 cms. It is interesting to note in Figure 4-11 that between orifice velocities (v_0) of 300 and 500 cm/sec, the stretch rate varies with v_0 quite randomly. This is primarily due to problems associated with the measurement of θ, and is discussed in detail in Section 5.1.

PEO: The poly(ethylene oxide) used in this work was Polyox WSR 301. The converging flow behavior of PEO was quite different from those of

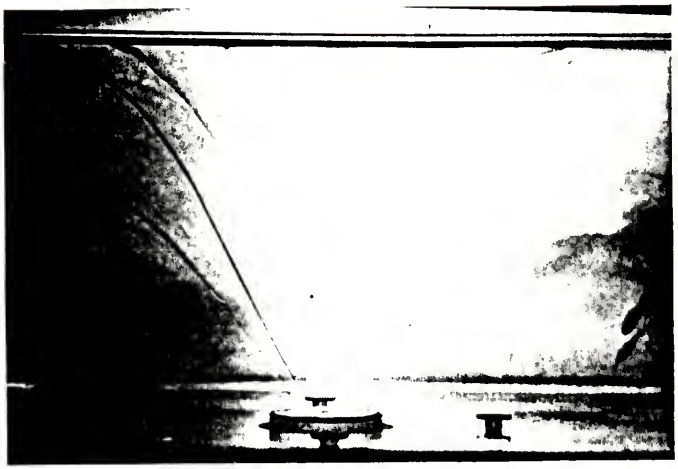

Figure 4-10a. WGS flow with Separan AP 273 10 wppm
Orifice Velocity = 400 cm/sec

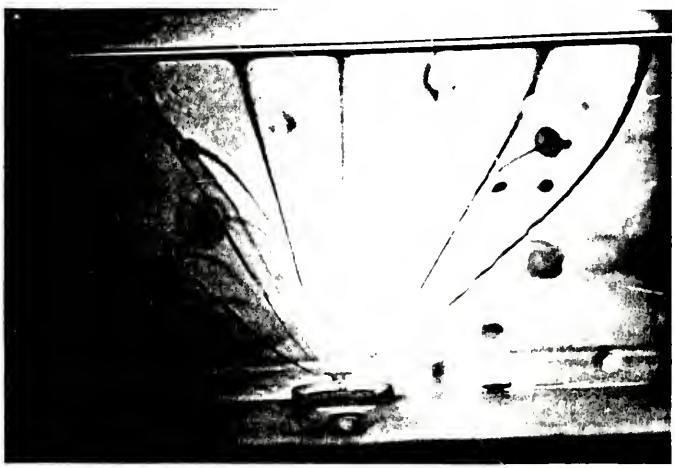

Figure 4-10b. WGS flow with Separan AP 273 10 wppm
Orifice Velocity = 900 cm/sec

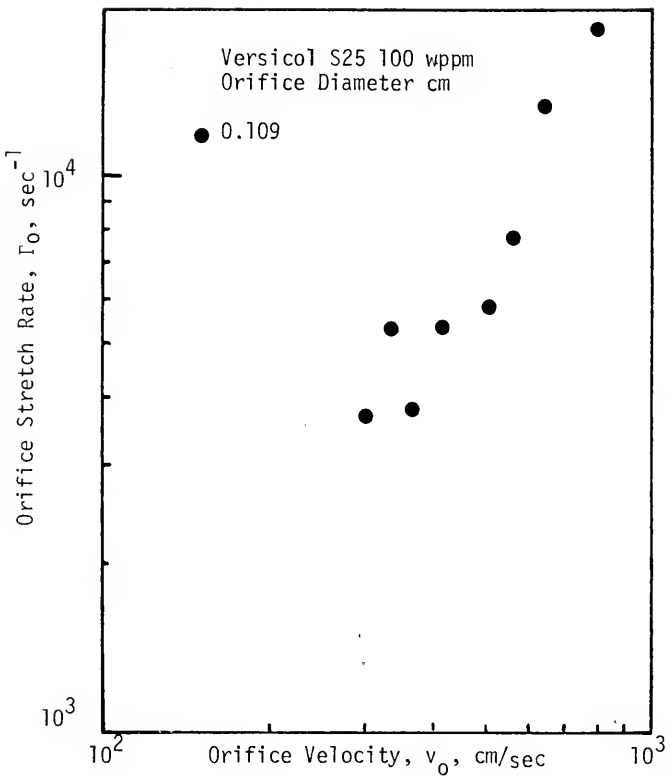

Figure 4-11. Dependence of Stretch Rate on Orifice Velocity

the PAMs and PAA. In experiments conducted with PEO solutions with orifices larger than 0.109 cm, the flow field appeared Newtonian. Furthermore, the entrance pressure drop exhibited by PEO was considerably lower than those observed with the PAMs and PAA at equal concentrations. When the orifice diameter was extremely small (0.04 cm), traces of WGS flow could be seen but the flow pattern was not clear enough for measurement of θ, and, therefore, calculation of the stretch rates.

Entrance Pressure Drop Measurements

PAM: Plots of entrance pressure drop, ΔP_e, vs. v_o for the PAMs are given in Figures 4-12 to 4-17. Comparison of these plots with the entrance pressure drop data for water (Figure 4-18) shows the PAMs to exhibit much larger entrance pressure drops. It is also seen from Figures 4-12 to 4-17 that ΔP_e is a function of only the orifice velocity, independent of orifice diameter. The normal stress difference at the orifice (N_{Eo}) can be calculated from measurements of ΔP_e and θ by using equation (2-45). For orifice velocities less than 1000 cm/sec and values of θ less than 40°, equation (2-45) is nearly identical to equation (2-39) in which N_{Eo} is equated with ΔP_e. Almost all data taken in this work had orifice velocities and values of θ within 1000 cm/sec and 40° respectively and N_{Eo} is therefore, to a good approximation, equal to ΔP_e. Thus Figures 4-12 to 4-17 can be treated as plots of N_{Eo} vs. v_o. It is important to note that equations (2-39) and (2-45) are both applicable only for the case where WGS flow is present. Thus, in the case of the 10 wppm solution of

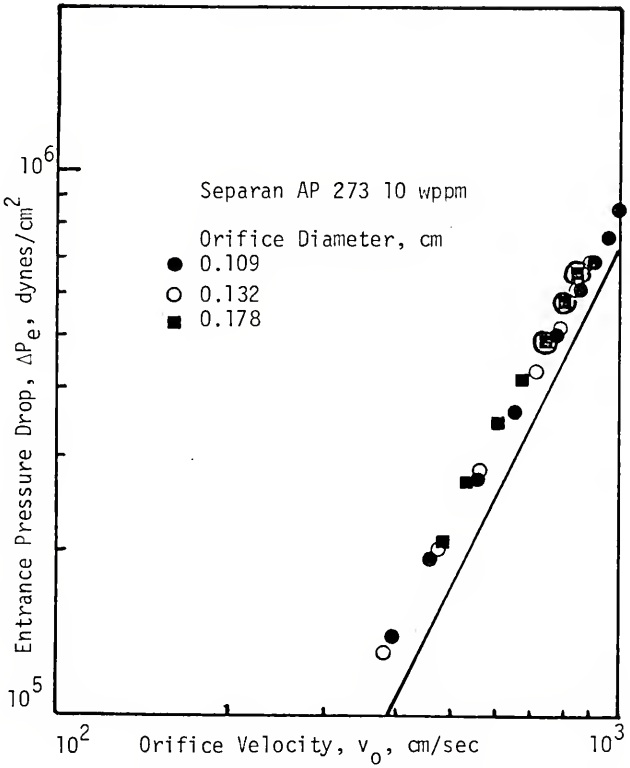

Figure 4-12. Dependence of Entrance Pressure Drop on Orifice Velocity

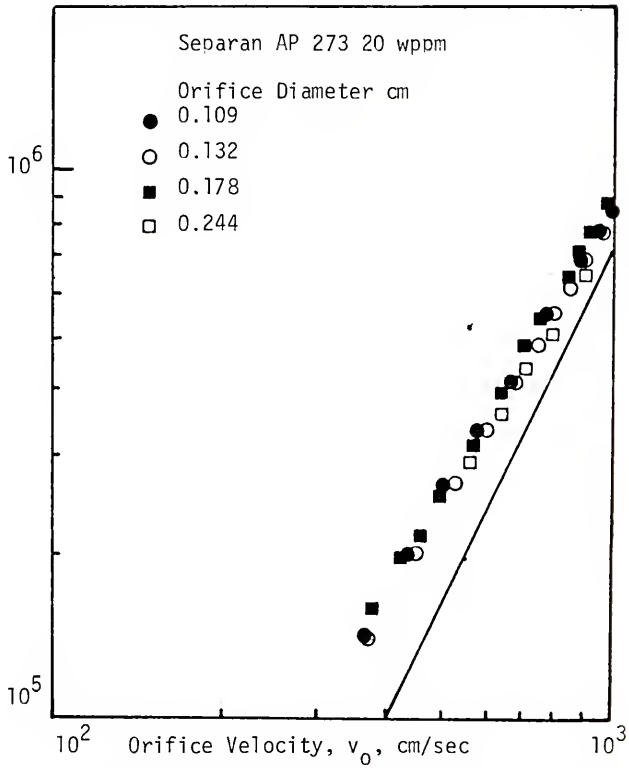

Figure 4-13. Dependence of Entrance Pressure Drop on Orifice Velocity

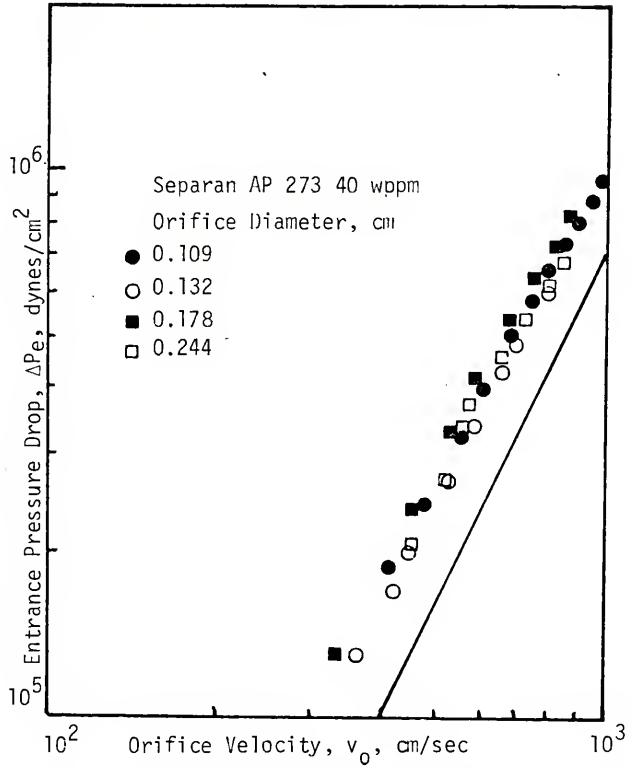

Figure 4-14. Dependence of Entrance Pressure Drop on Orifice Velocity

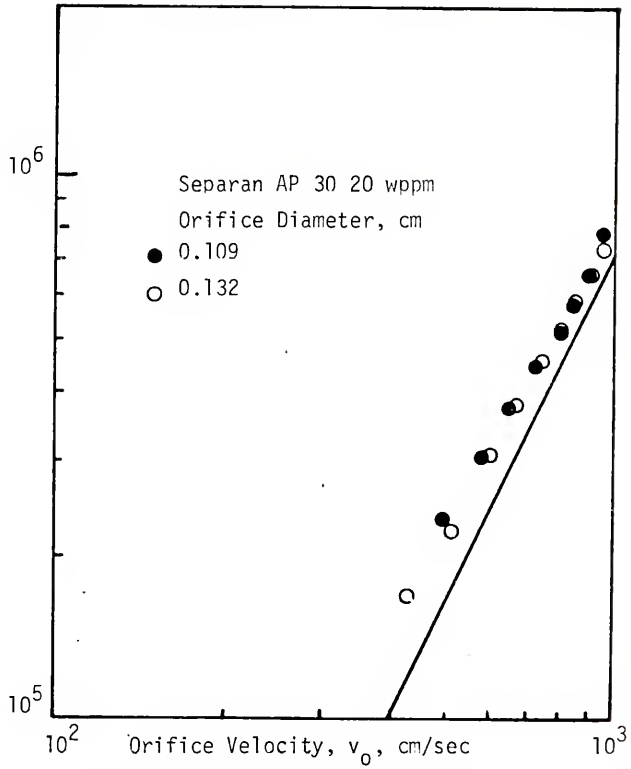

Figure 4-15. Dependence of Entrance Pressure Drop on Orifice Velocity

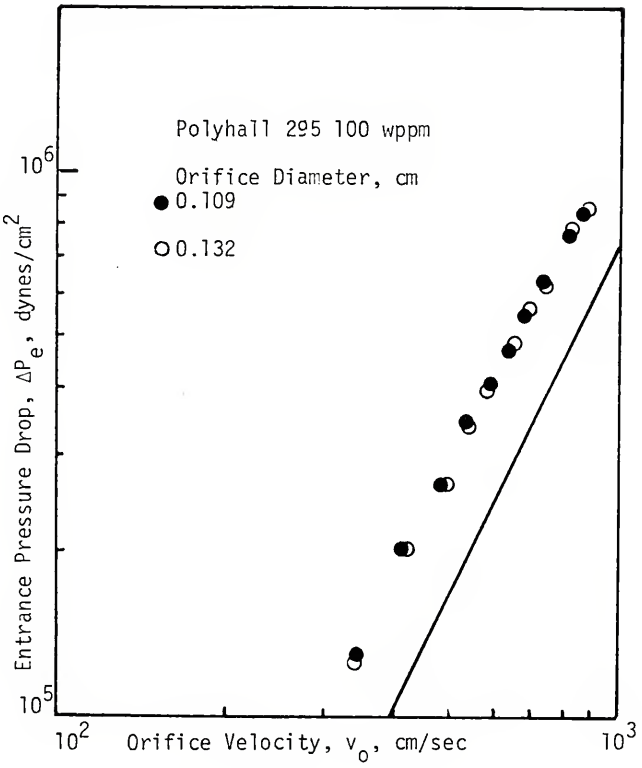

Figure 4-16. Dependence of Entrance Pressure Drop on Orifice Velocity

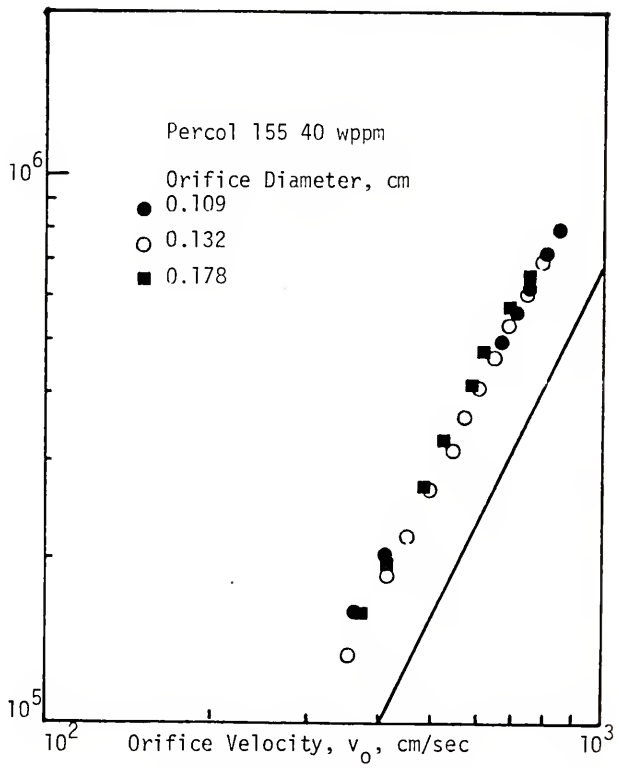

Figure 4-17. Dependence of Entrance Pressure Drop on Orifice Velocity

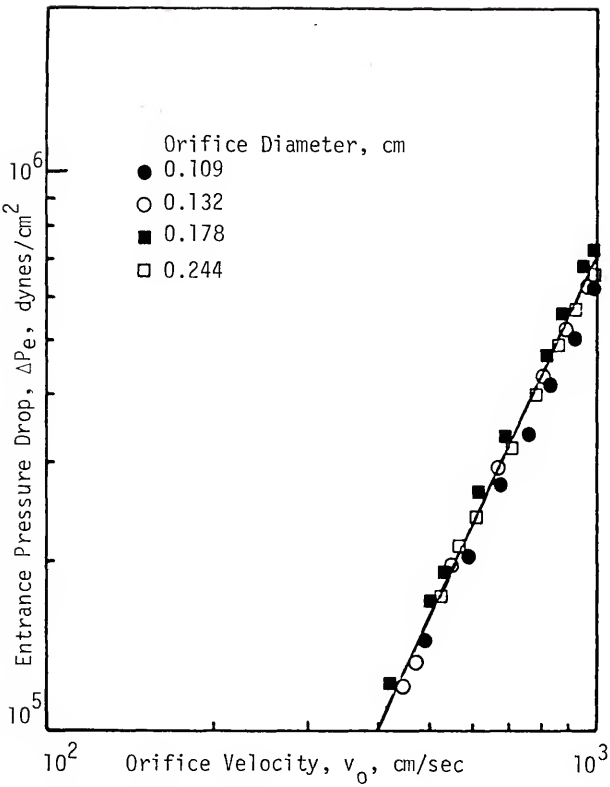

Figure 4-18. Entrance Pressure Drop Data for Water

Separan AP 273 in the 0.178 cm orifice, the flow field did not resemble WGS flow at large velocities and N_{Eo} could not be calculated under these conditions. The data points at which N_{Eo} could not be calculated are marked by circles around them in Figure 4-12.

Entrance pressure drops were also measured for a 200 wppm solution of Separan AP 273 (Figure 4-27).* This was done in order to compare N_{Eo} calculated from ΔP_e measurements with those calculated from thrust measurements (Section 4.4).

PAA: PAA, like the PAMs, exhibited large entrance pressure drops but the angle of convergence was not clear below 100 wppm. The entrance pressure drops exhibited by PAA were similar in magnitude to those exhibited by Separan AP 273 at equal concentrations. Plots of ΔP_e vs. v_o for PAA at 40, 80 and 100 wppm are given in Figure 4-19. The orifice diameter was 0.109 cm.

PEO: The entrance pressure drops exhibited by PEO were much less than those exhibited by the PAMs or PAA. At 40 wppm, PEO was indistinguishable from water when the orifice diameter was greater than 0.109 cm. With smaller orifices (0.04 and 0.051 cm), the 40 wppm solution exhibited entrance pressure drops that were significantly greater than those exhibited by water (Figures 4-20 and 4-21). In addition, the polymer solution exhibited WGS flow that was clearly visible to the naked eye but could not be readily photographed because the recirculating regions and the central converging region were extremely small.

---

*A concentration of 200 wppm was chosen for two reasons: (i) die swell was clearly noticeable at this concentration and could be measured from photographs of the emerging jet, and (ii) significant reduction in thrust could be measured at this concentration. This point is discussed in detail in Chapter V.

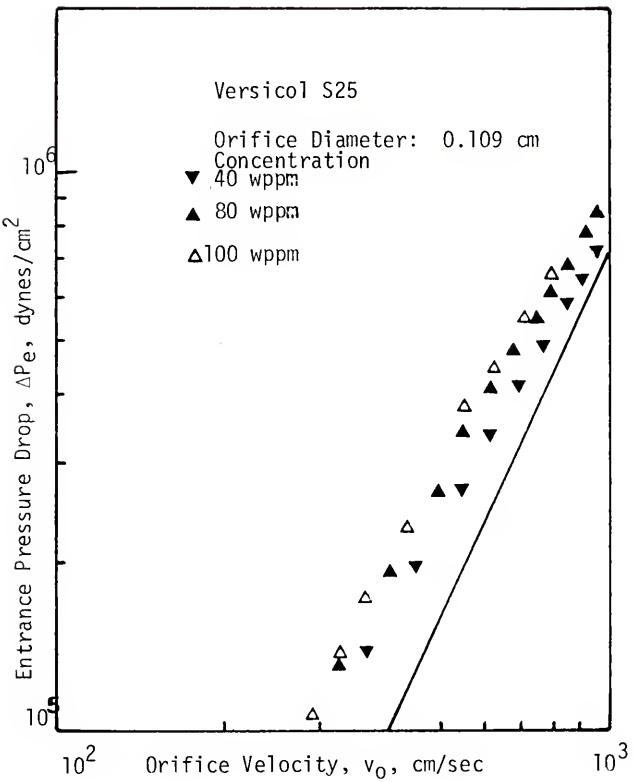

Figure 4-19. Dependence of Entrance Pressure Drop on Orifice Velocity

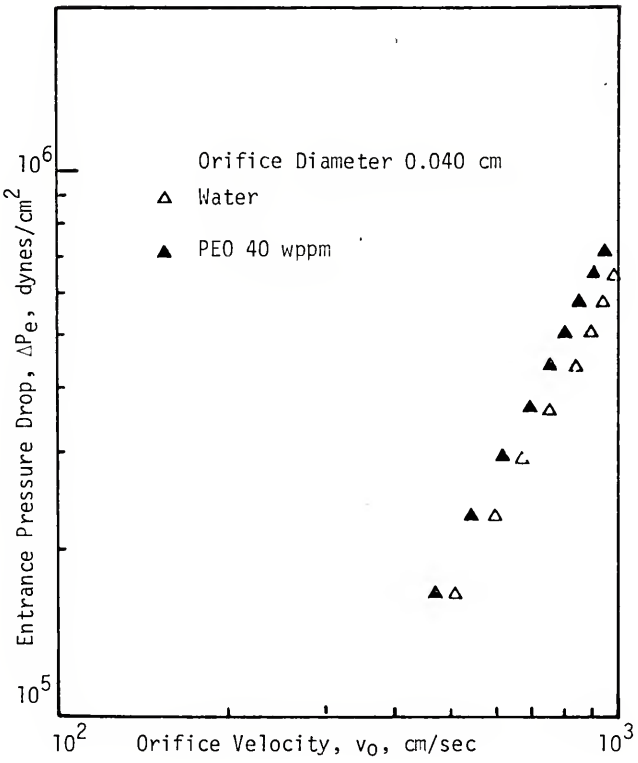

Figure 4-20. Dependence of Entrance Pressure Drop on Orifice Velocity

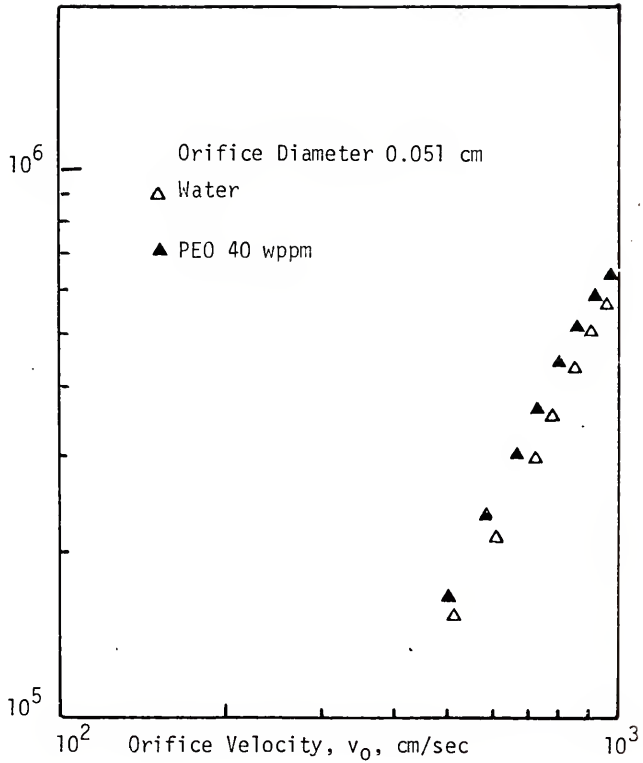

Figure 4-21. Dependence of Entrance Pressure Drop on Orifice Velocity

At 100 wppm, PEO exhibited entrance pressure drops greater than those of water in the orifices used with the PAMs and PAA (greater than 0.109 cm). However, the ΔP_e was, unlike the PAMs, dependent on orifice diameter. Thus, PEO at 100 wppm exhibited significantly larger ΔP_e than water in the 0.109 cm orifice but was indistinguishable from water in the 0.178 cm orifice. This effect is illustrated in Figures 4-22 to 4-24. The implications of this somewhat anomalous behavior is discussed in Chapter V.

Effect of Solution Viscosity on ΔP_e

The polymer solutions used in this study all had viscosities slightly greater than that of water. This factor could have an effect on ΔP_e. The influence of viscosity was estimated by measuring the entrance pressure drop for several glycerine-water solutions of viscosities ranging from 0.094 to 57 cps. The results of these experiments are shown in Figure 4-25. The orifice diameter was 0.109 cm. It is seen that the solutions of viscosities 4.9 to 9 cps exhibit entrance pressure drops slightly greater than water at low velocities, and become indistinguishable from water at large velocities.

Effect of L/D Ratio on ΔP_e

In the normal stress difference data presented above, N_{Eo} was calculated using equation (2-39), which is applicable only in the presence of a WGS flow. In making the momentum balance to derive equation (2-39), it was assumed that the flow was through a sharp

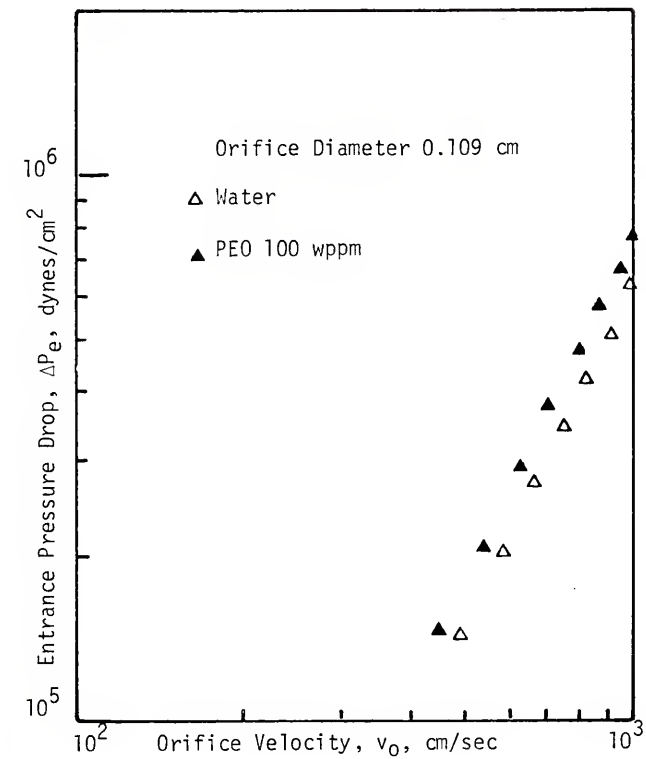

Figure 4-22. Dependence of Entrance Pressure Drop on Orifice Velocity

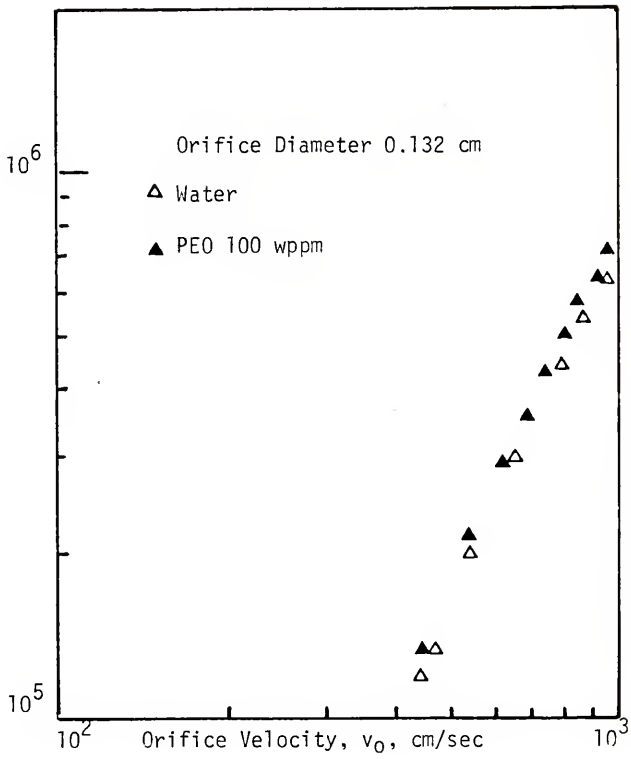

Figure 4-23. Dependence of Entrance Pressure Drop on Orifice Velocity

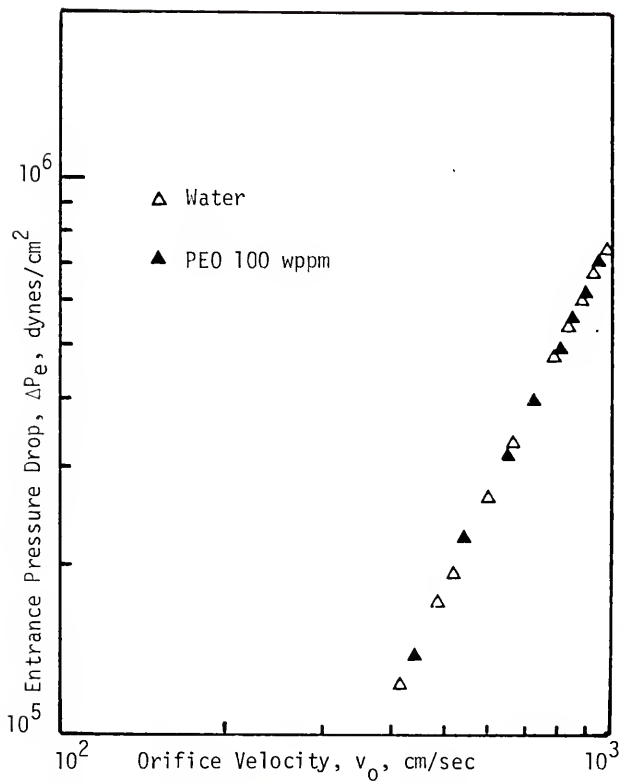

Figure 4-24. Dependence of Entrance Pressure Drop on Orifice Velocity

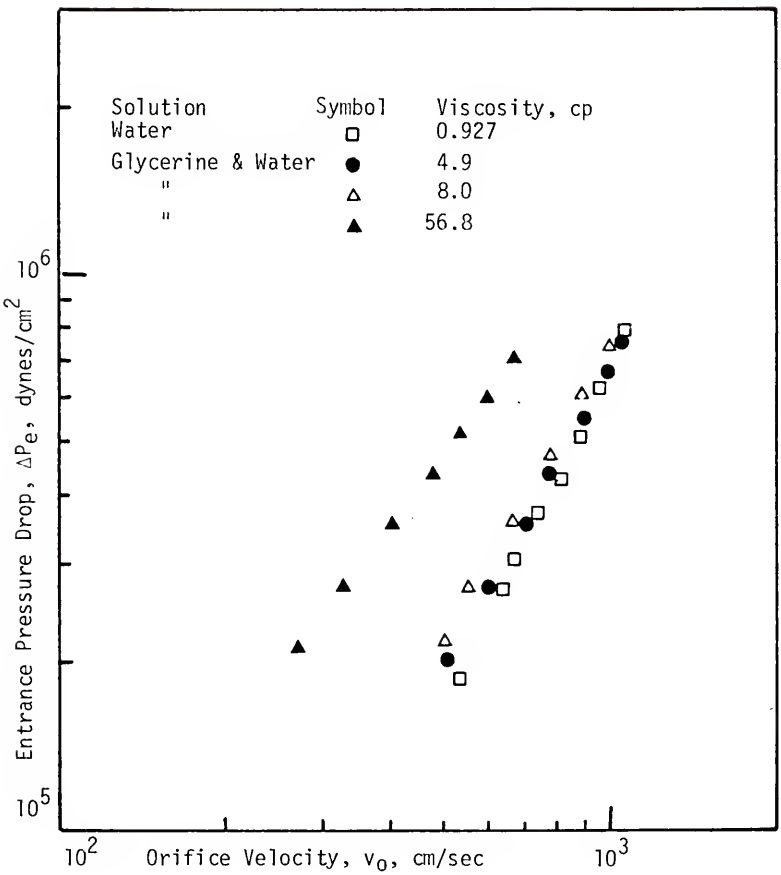

Figure 4-25. The Effect of Shear Viscosity on Entrance Pressure Drop

edged orifice in which losses in pressure due to shear in the orifice are negligible. The orifices used in this work were all square edged and, therefore, contribution to ΔP_e from shear in these orifices may not be negligible. Such losses were estimated by measuring the entrance pressure drop for water in flow through a 0.109 cm "orifice" of different lengths, 0.675 cm (L/D = 6), 0.349 cm (L/D = 3.2), and 0.237 cm (L/D = 2.17), to see if there was a significant increase in the entrance pressure drop with increase in L/D ratio. Plots of ΔP_e vs. v_o for the three "orifices" are given in Figure 4-26.

4.4 Thrust Measurements

As mentioned in Chapter III, thrust measurements were carried out in order to measure N_{Eo} and compare these values with those measured using the entrance pressure drop method (Section 4.3.2).

Thrust measurements carried out with Separan AP 273 solutions at 40 and 200 wppm are shown in Figure 4-27. It is seen that Separan AP 273 at 40 wppm does not show a dependence of thrust on orifice diameter and the thrust is indistinguishable from water. The solid line on the figure corresponds to ρv_o^2. Its coincidence with the points obtained with water indicates the absence of vena contracta formation in the flow of water through the square edged orifices used in this work.

At 200 wppm, a significant reduction in thrust is observed. It will be shown in Chapter V that this is a measure of die swell rather than N_{Eo}.

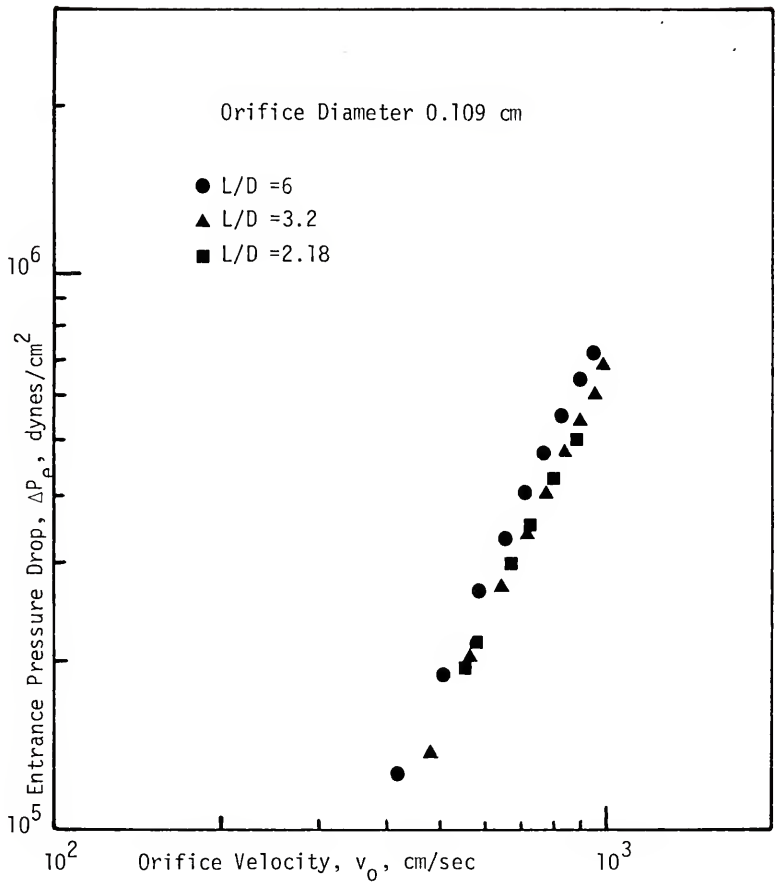

Figure 4-26. The Effect of L/D ratio on Entrance Pressure Drop

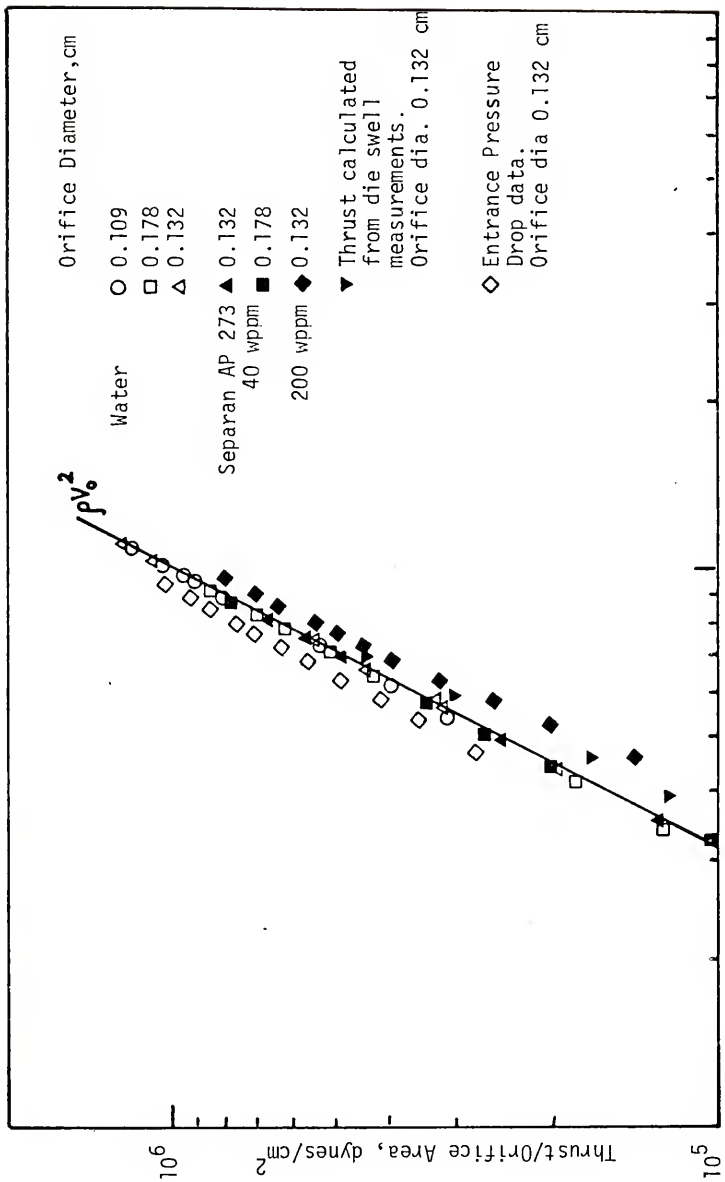

Figure 4-27. Summary of Thrust Measurements

4.5 Conformational Studies

As mentioned in the introduction to Chapter IV, conformational studies were carried out with solutions of Separan AP 273 at 10 wppm in different ionic media. The macromolecular dimensions of Separan, a partially hydrolyzed polyacrylamide, are extremely sensitive to its ionic environment. Changes in polymer conformation can be conveniently followed by measuring the viscosity of the polymer solution in different ionic media.

Viscosity Measurements

Figure 4-28 shows the variation in viscosity of a 200 wppm solution of Separan AP 273 with pH at a shear rate of 115 sec^{-1}. The maximum viscosity occurs in the deionized water solution (pH = 9.4) and an increase or decrease of pH results in a reduction of viscosity, the effect being more pronounced at low pH. Macromolecular conformation can also be changed by the addition of salts to polyelectrolyte solutions. The effect of 0.5% NaCl on the viscosity of the 200 wppm solution is shown by the dark point in Figure 4-28.

Drag Reduction Measurements

The effect of polymer conformation on DR is illustrated in Figure 4-29a in which friction factor, f, is plotted versus solvent based Reynolds Number for a 10 wppm solution of Separan AP 273 in deionized water at high and low pH, and in 0.5% NaCl solution. The inside diameter of the tube was 1.09 cms. As discussed in Section 4.1, in the case of the 5 wppm solution of Separan, there is a significant

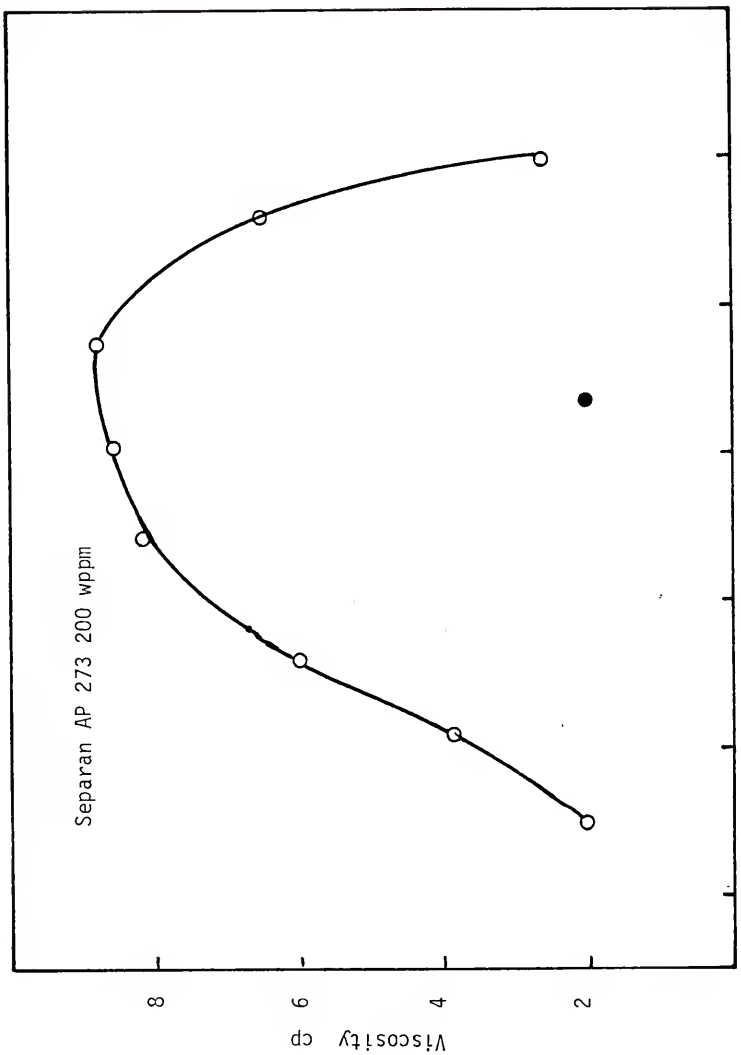

Figure 4-28. Effect of pH on Solution Viscosity

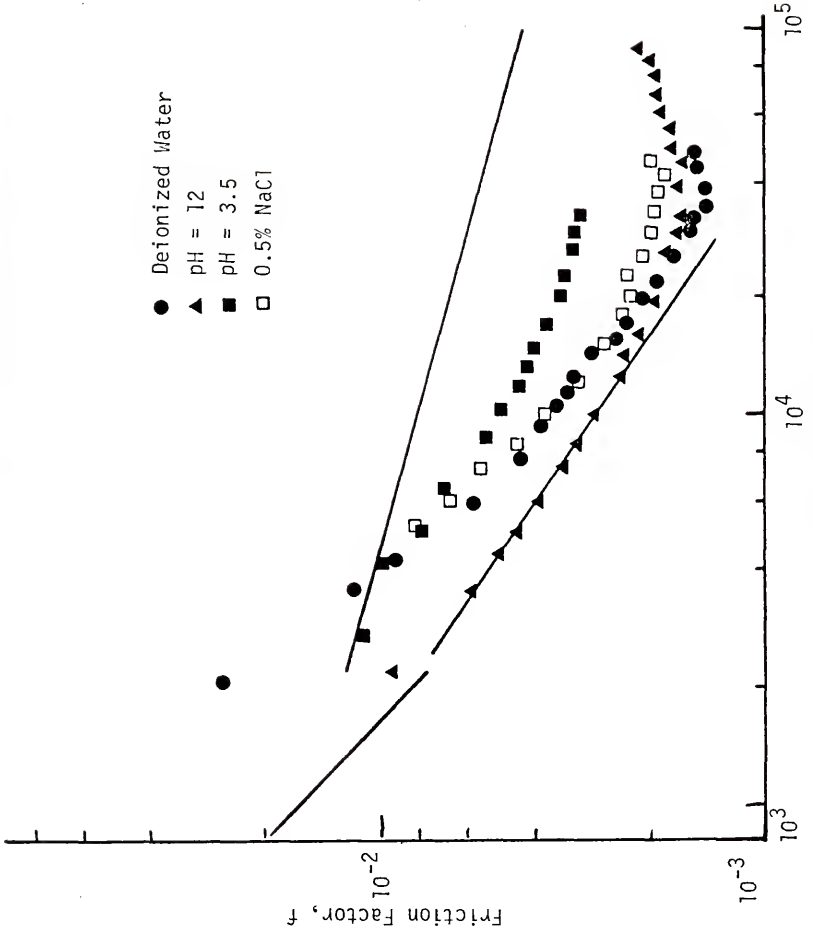

Figure 4-29a. Effect of Polymer Conformation on Drag Reduction

non-Newtonian viscosity effect at low N_{Re}. In order to portray the true drag reducing ability of the polymer solutions, Reynolds Numbers were calculated using solvent viscosity.

Experiments performed with the gravity flow apparatus are summarized in Figure 4-29b in which percent DR is plotted versus concentration for Separan AP 273 at different pH.

Vortex Inhibition Measurements

The vortex inhibiting ability of Separan AP 273 was determined by measuring C_{VI} at different pH, and in 0.5% salt solution. The results are summarized in Table 4.2. It is clear from the table that the vortex inhibiting ability is not changed by the addition of salt or increase in pH while it is considerably reduced by a decrease in pH. Thus, changes in polymer conformation seem to have the same effect on DR and VI.

Extensional Viscosity

The effect of polymer conformation on extensional viscosity was investigated using a 10 wppm solution of Separan AP 273. The orifice diameter was 0.109 cm.

Angle of convergence (stretch rate) measurements. Stretch rate data for Separan AP 273 in deionized water have already been presented in Section 4.3.1. As mentioned in that section, WGS flow could be clearly seen at 10 wppm and stretch rates could be calculated at different orifice velocities from photographs of the cone angle (Figure 4-30). When NaOH or HCl was added to the solution to alter

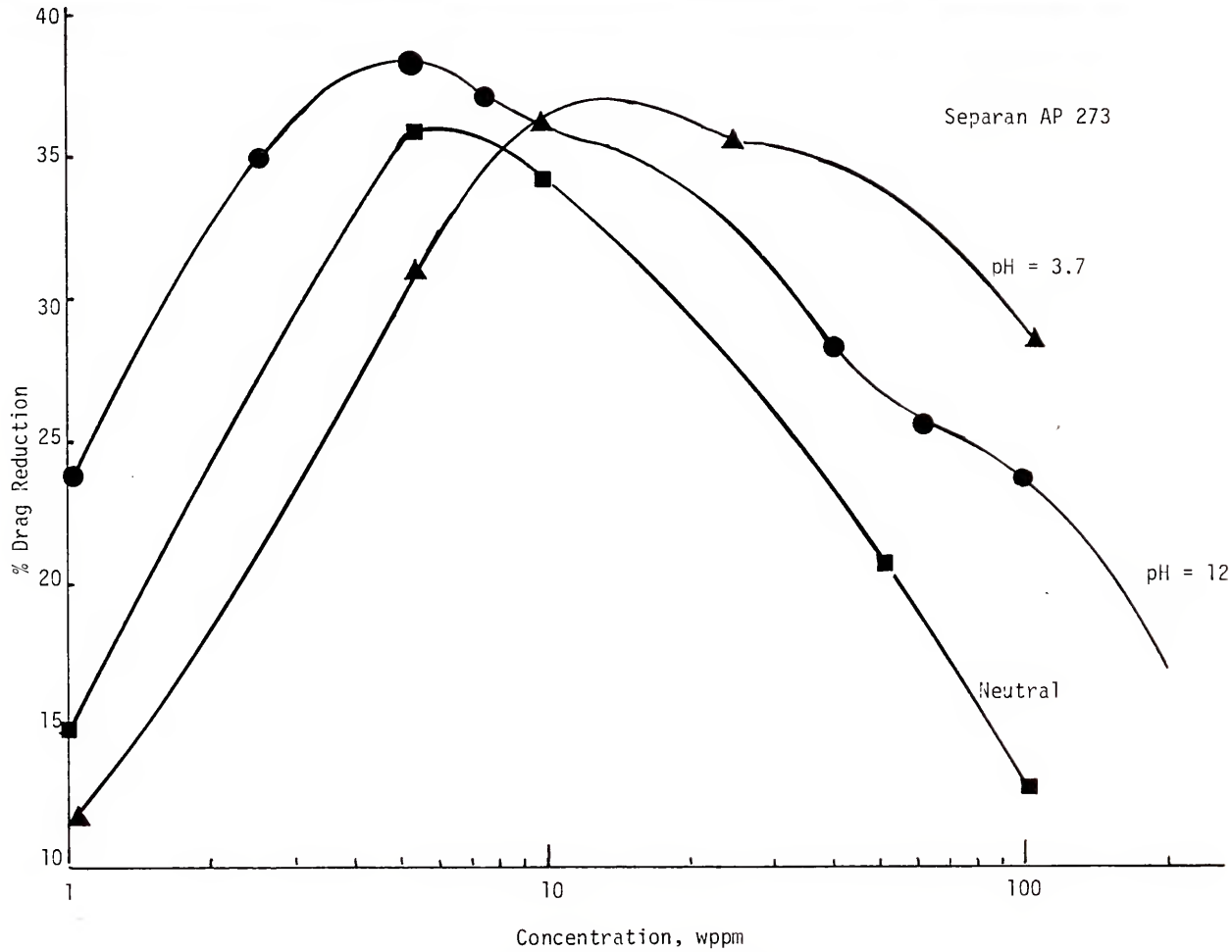

Figure 4-29b. Effect of pH on Drag Reduction

Table 4.2

Vortex Inhibition Versus pH for Separan AP 273

pH	C_{VI}, wppm
2.1	40
3.75	5
5	3
7	3
12	1.5
0.5% NaCl	3

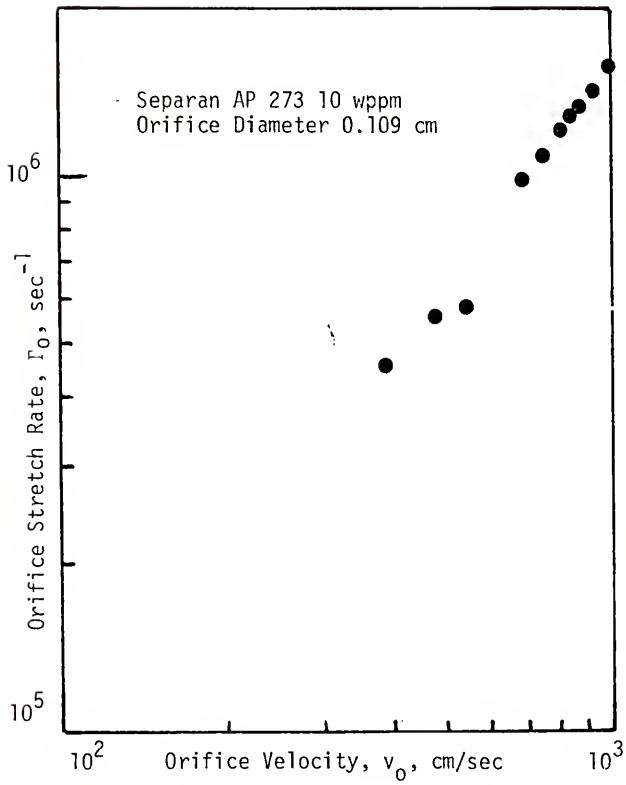

Figure 4-30. Stretch Rate data for Fresh Separan AP 273 10 wppm

its pH the fluid no longer exhibited WGS flow and the flow field was Newtonian in appearance. Therefore, stretch rates at the orifice could not be calculated for these solutions.

Normal stress difference measurements. Figure 4-31 summarizes the results of entrance pressure drop measurements made with 10 wppm solutions of Separan AP 273 in deionized water, at high and low pH, and in 0.5% NaCl solution. It is interesting to note that the plots for the high pH and deionized water solutions are identical while the solutions at low pH are indistinguishable from water. As mentioned earlier, it is not possible to relate the entrance pressure drop to N_{Eo} when the flow field is not of the WGS type. Thus, N_{Eo} could not be calculated for the polymer solutions in salt solution and at high pH. Plots of N_{Eo} versus v_o for the 10 wppm solution in deionized water have already been given in Figure 4-12.

4.6 Polymer Degradation

As discussed briefly in Chapter I, the drag reducing ability of a polymer depends predominantly on the high molecular weight species of the molecular weight distribution of the polymer. Moreover, these high molecular species are extremely susceptible to shear degradation and DR is therefore very sensitive to polymer degradation. The results of polymer degradation experiments performed to determine its effect on DR, VI and extensional viscosity are summarized in this section. The polymer used was Separan AP 273 at 10 wppm.

A fresh polymer solution was degraded by passing it through the 0.45 cm tube of the flow loop at Reynolds Numbers of 20,000 and

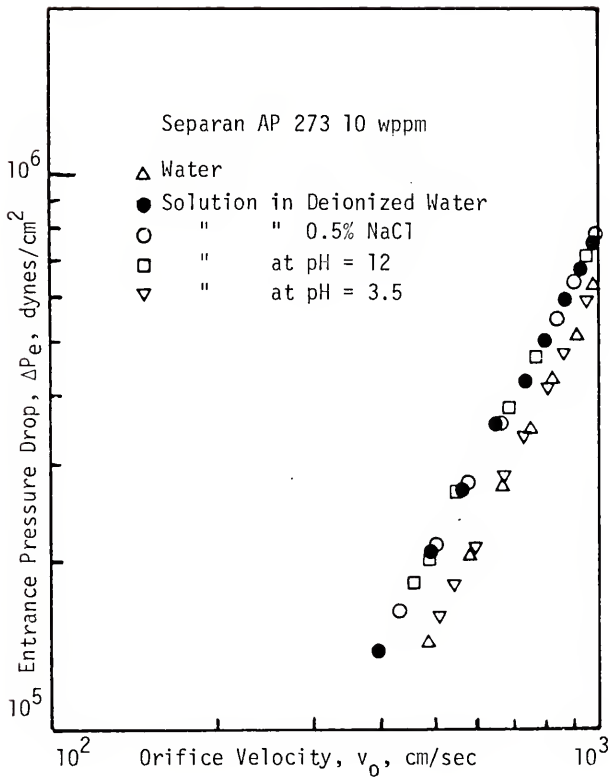

Figure 4-31. Effect of Polymer Conformation on Entrance Pressure Drop

40,000. The degraded solutions were collected and their drag reduction, vortex inhibition and extensional viscosity were measured and compared with the fresh solution properties.

Drag Reduction

Plots of f versus N_{Re} for the fresh polymer solution, and the solutions degraded at N_{Re} = 20,000 and 40,000, are given in Figure 4-32. It is clear from the figure that shear degradation at N_{Re} = 20,000 causes almost no change in the drag reducing ability of the solution, while at N_{Re} = 40,000, there is a significant reduction in the DR exhibited by the solution.

Vortex Inhibition

The results of vortex inhibition experiments are given in Figure 4-33 in which $\frac{C_{VIo}}{C_{VI}}$ is plotted versus Reynolds Number. C_{VIo} is the value of C_{VI} for the fresh solution. The figure reveals that C_{VI} for the solution degraded at N_{Re} = 20,000 is unchanged from its value for the fresh solution, and that at N_{Re} = 40,000 there is a significant increase in C_{VI}. This trend in change of C_{VI} with polymer degradation is consistent with that of DR. This has been demonstrated in previous studies also (Gordon and Balakrishnan (1972)).

Extensional Viscosity

The extensional viscosity of the fresh polymer solution, and the solutions degraded at N_{Re} = 20,000 and 40,000, were measured in the converging flow apparatus.

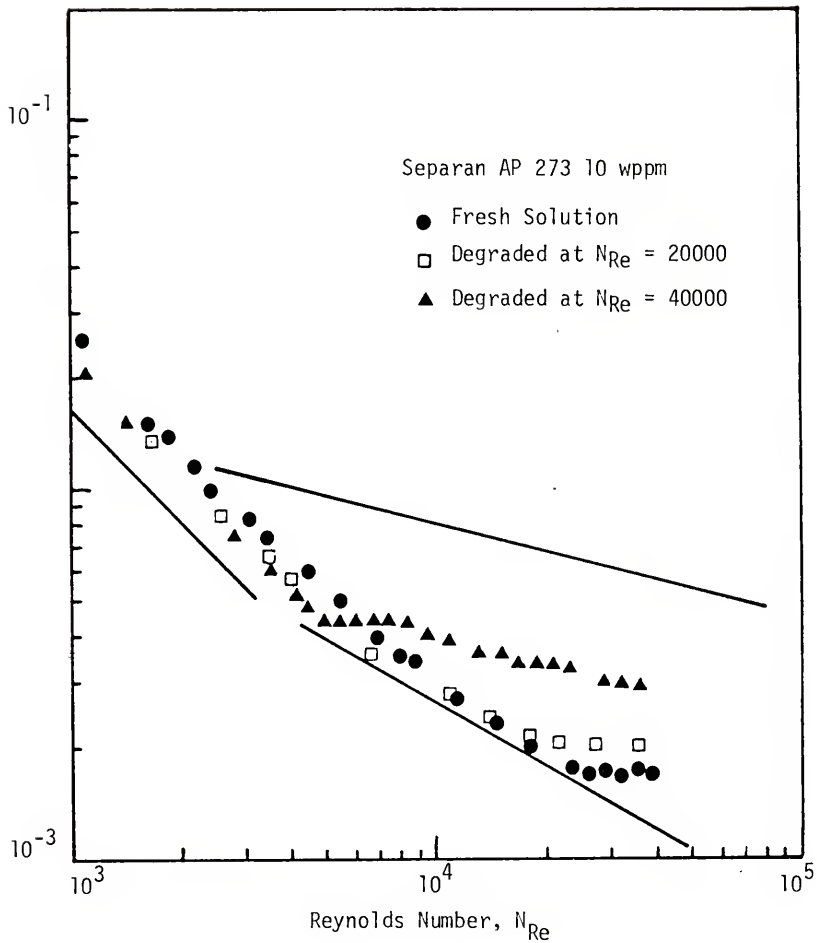

Figure 4-32. Effect of Shear Degradation on Drag Reduction

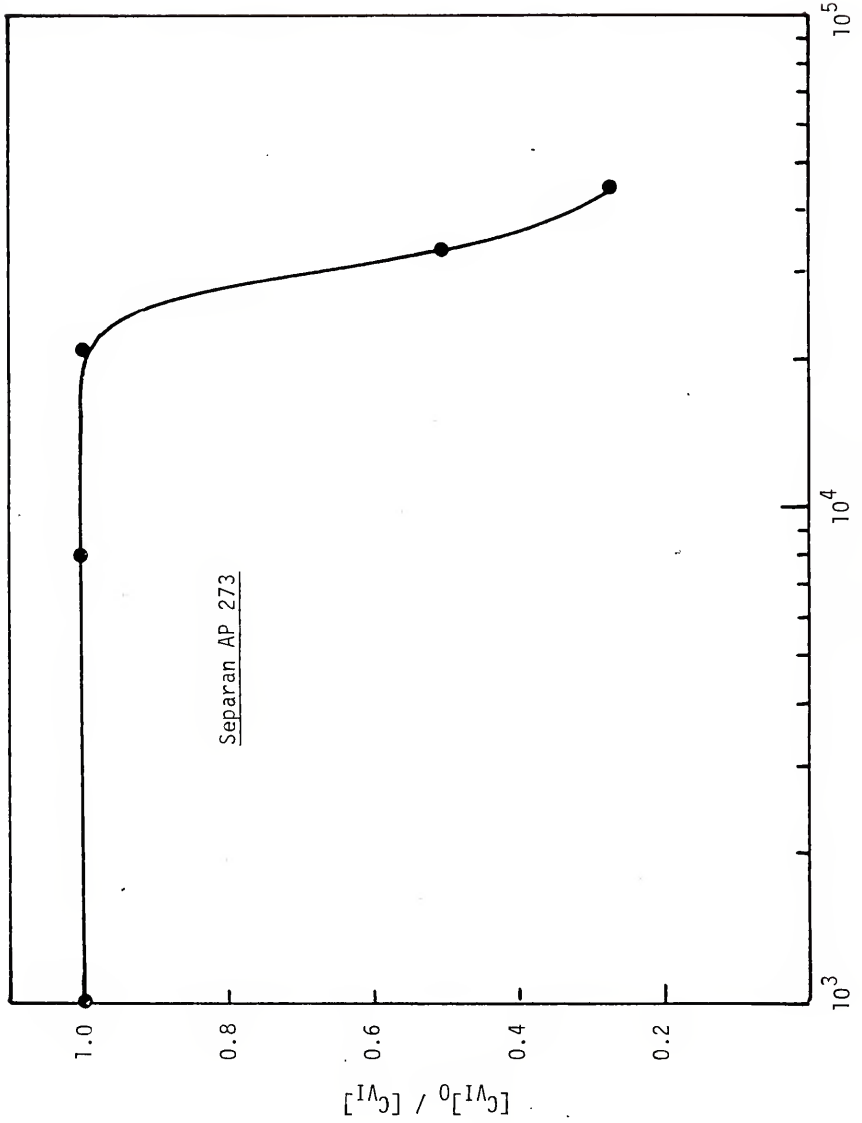

Figure 4-33. Effect of Shear Degradation on Vortex Inhibition

Stretch rate measurements. Stretch rate data for the fresh 10 wppm solution of Separan AP 273 have already been presented in Section 4.3.1. In the case of the polymer solution degraded at N_{Re} = 20,000, flow visualization revealed that the flow field was of the WGS type only at low velocities. At high velocities the flow entered the orifice from a 180° solid angle close to the orifice. This is illustrated in Figure 4-34. The solution degraded at N_{Re} = 40,000 appeared nearly Newtonian at all flow rates. Stretch rates could not therefore be calculated for the degraded solutions over a wide range of flow rates. Thus, shear degradation seemed to destroy the flow pattern exhibited by the fresh solution.

Normal stress difference measurements. Plots of ΔP_e versus v_o for the three solutions are given in Figure 4-35. It is interesting to note that there is no change due to degradation in the ΔP_e exhibited by the polymer solutions. This, of course, does not imply invariance of N_{Eo}, the normal stress difference at the orifice, with polymer degradation. As discussed in earlier sections, ΔP_e can be related to N_{Eo} by equation (2-39) only when the polymer solution exhibits WGS flow. Figure 4-12 shows the dependence of N_{Eo} for the fresh polymer solution on v_o. For the degraded polymer solutions, N_{Eo} could not be calculated when WGS flow was not observed. The implications of these findings will be discussed at length in Chapter V.

4.7 Flow Instability

It was mentioned in Section 4.3 that instabilities were observed in the WGS flow pattern exhibited by the PAM solutions, the instabilities being particularly pronounced at the larger polymer concentrations

Figure 4-34a. Flow Visualization with Fresh Separan AP 273 Solution, 10 wppm

Figure 4-34b. Flow Visualization with Solution Degraded at N_{Re} = 20000

Figure 4-34c. Flow Visualization with Solution Degraded at N_{Re} = 40000

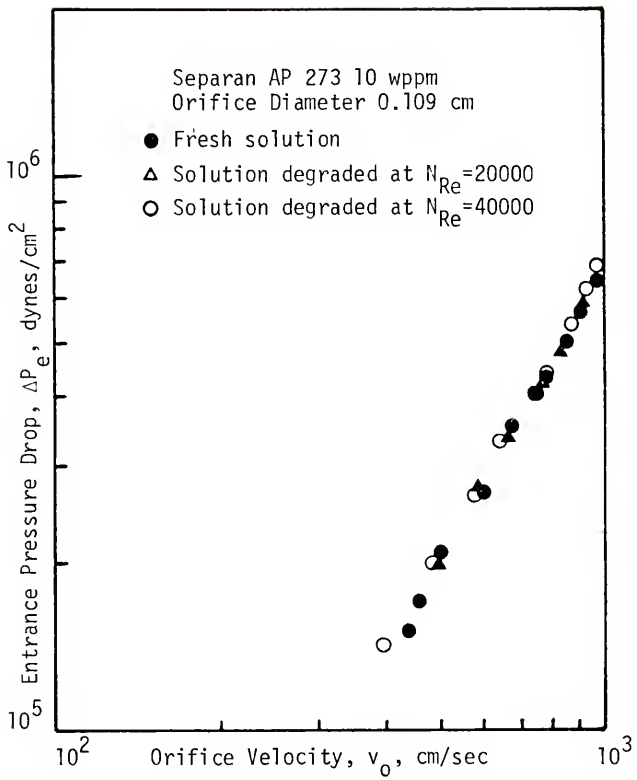

Figure 4-35. Effect of Shear Degradation on Entrance Pressure Drop

studied (40 wppm and above). These are briefly described in this section.

The instabilities observed in this work were very similar to those seen with polymer melts (Tordella (1969), Bagley and Birks (1960), Ballenger et al. (1971)) and concentrated polymer solutions (Bagley (1961), Giesekus (1968,1969), Pickup (1970), Murch (1970) and Rama Murthy (1974)). They occurred mostly with the polymer solutions that had the largest extensional viscosities, such as Separan AP 273 and Percol 155 at 40 wppm and above. With these polymer solutions, the flow was quite stable at very low velocities and no fluctuations were observed in the streamlines defining the central converging region of WGS flow. As the flow was increased, the half angle of convergence (θ) decreased slightly but the flow remained quite stable. A decrease in θ was accompanied by an increase in the distance which the recirculating region penetrated into the reservoir. As the flow rate was further increased, the onset of flow instability was observed. The instability consisted mainly of the central converging region whipping from side to side as shown schematically in Figures 4-36a and 4-36b.* The periodicity of this motion was about 15 to 20 seconds. The swirling motion of the central region was accompanied by a fluctuation in the size of the recirculating region. Thus, when the central region leaned to the left, the recirculating region on the right hand side was larger and vice versa. Increasing the orifice velocity was found to increase the intensity of the swirling motion until, at a particular velocity, the flow through the orifice from the central region became intermittent, with liquid

*The lateral motion of the central region actually corresponds to a swirling motion because flow visualization in this work was in two dimensions.

Figure 4-36. Instability in WGS Flow: Stage 1

from the recirculating region beginning to periodically enter the orifice. The appearance of the flow field under such flow conditions is illustrated in Figure 4-37. Fluid in the central region would flow towards the orifice, stop momentarily and snap back while fluid from the recirculating region entered the orifice. After a while, the flow became stable and remained so for a few moments before the fluid in the central region stopped and snapped back and fluid from the recirculating region once again entered the orifice.

During this stage of instability, increase of flow rates to yield still higher orifice velocities often resulted in a sharp increase in θ, accompanied by very stable WGS flow. This flow regime presumably corresponds to the second stage stability described by Rama Murthy (1974). As the velocity was further increased, θ decreased slightly, with the flow remaining quite stable.

The remarkable feature of these instabilities is that they were observed with polymer solutions with concentrations in the parts per million range, and that they are qualitatively similar to those observed with polymer melts and concentrated solutions. This shows the marked similarity between the WGS flow of dilute polymer solutions and concentrated polymer systems, and suggests the possibility of understanding polymer melt instability in WGS flow (which is widely believed to be responsible for melt fracture) by studying polymer solutions that are much easier to characterize rheologically, and handle experimentally.

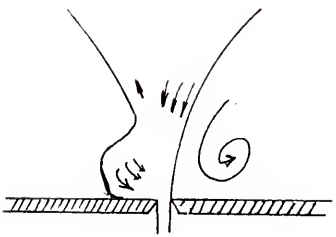

Figure 4-37. Instability in WGS Flow: Stage 2

CHAPTER V
DISCUSSION OF RESULTS

In this chapter, the various experimental results presented in Chapter IV are discussed. In Section 5.1, the dependence of extensional viscosity on stretch rates is analyzed. This is followed by a comparison of experimental results with predictions of the equations of motion (Section 5.2) and with those of previous investigations (Section 5.3). In Section 5.4, the correlation between DR, VI, and extensional viscosity is examined, and in Section 5.5 some observations are made on the converging flow behavior of Polyox WSR 301. The experimental results are compared with predictions of constitutive theories in Section 5.6 and, finally, in Section 5.7, the conclusions of this work are listed, and recommendations made on possible extensions of the present work.

5.1 Extensional Viscosity

It was briefly mentioned in Chapter IV that problems were encountered with the accurate measurement of θ, the half angle of convergence, due to instability of flow and haziness of streamlines separating the recirculating and central converging regions. This was particularly severe in the case of Separan AP 273 at 40 wppm and Percol 155 at 40 wppm for which the cone angles were extremely small.

The stretch rate at the orifice in WGS flow is given by the equation

$$\Gamma_o = \frac{v_o}{R_o} \sin\theta\ (1 + \cos\theta) \qquad (4\text{-}1)$$

Both v_o, the orifice velocity, and R_o, the orifice radius can be measured quite accurately. Inaccuracies in the determination of Γ_o arise primarily from errors in measurement of θ. When θ is less than about 40°, Γ_o is very sensitive to small changes in angle as illustrated in Figure 5-1. Here, the group $\sin\theta\ (1 + \cos\theta)$ is plotted against θ. When $\theta = 15°$, an error of 3° in measurement changes the value of $\sin\theta\ (1 + \cos\theta)$ by as much as 19%. Scatter in stretch rate data is also due, in part, to abrupt changes in θ that were noticed during flow instabilities (Section 4.7). This could lead to the same value of Γ_o for multiple values of v_o. In addition to problems associated with the measurement of θ (which would be expected to decrease with decreasing polymer concentration), scatter in stretch rate data can also arise from the fact that the kinematic equations used to derive the expression for stretch rate do not apply to all the fluid that exits from the orifice. As pointed out by Metzner et al. (1969) and by Pickup (1970), these equations are good for only about 70% of the flow.

With these qualifications in mind, inspection of stretch rate data for the PAM solutions (Figures 4-4 to 4-9) suggests that Γ_o is a unique function of orifice velocity for a given solution. Γ_o and v_o are related by an equation of the form

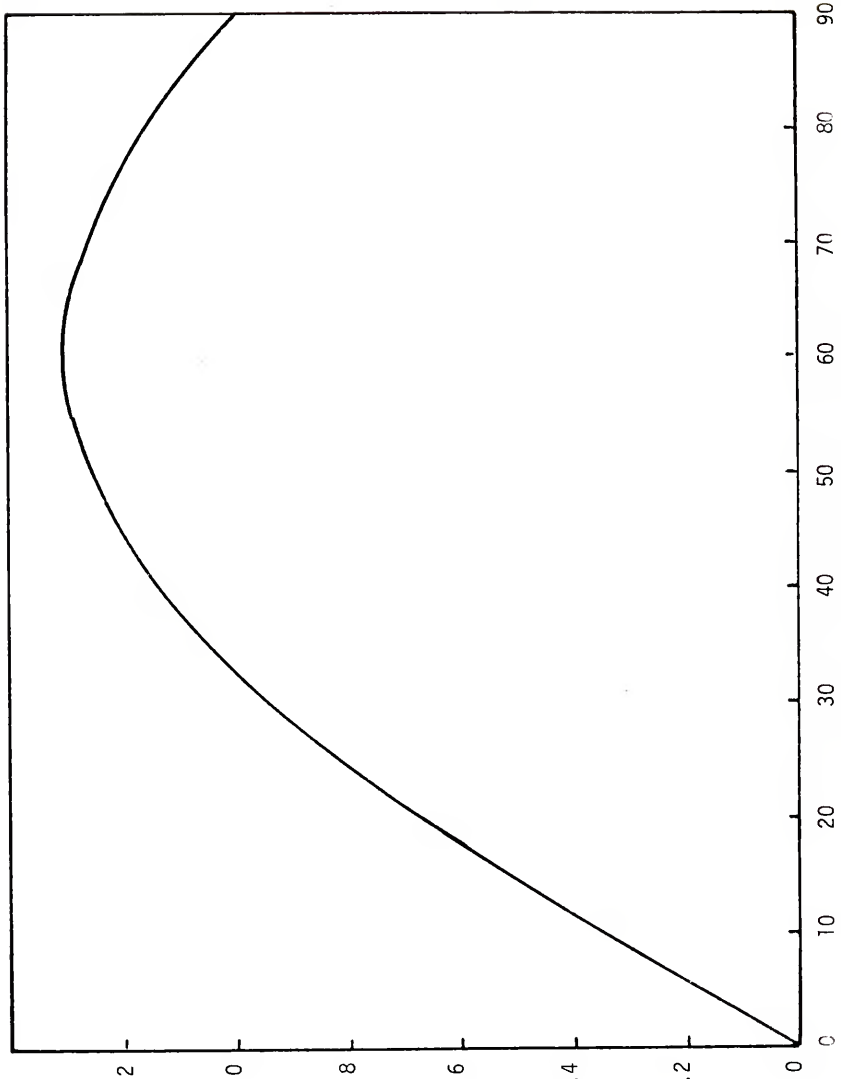

Figure 5-1. Variation of $\sin\theta(1+\cos\theta)$ with θ

$$\Gamma_o = \alpha\, v_o^{\beta} \qquad (5\text{-}1)$$

where α and β are constants that depend on polymer type and concentration. Values of α and β were determined for the three Separan AP 273 solutions by a least squares analysis and are given in Table 5.1.

We consider next the dependence of N_{Eo}, the normal stress difference at the orifice, on v_o. It was mentioned in Chapter IV that for the polymer solutions that exhibit WGS flow, N_{Eo} can be approximated by ΔP_e, the entrance pressure drop. In arriving at this result, contributions to ΔP_e from viscous losses were neglected. In order to show that these losses are negligible, we refer to Figure 4-25 in which the entrance pressure drops exhibited by glycerine-water solutions of viscosities ranging from 0.094 to 57 cps are plotted against v_o. It is seen that the solutions of viscosities 4.9 and 9 cps exhibit ΔP_e's greater than water (0.094 cps) at low velocities but become indistinguishable from water at high velocities. The polymer solutions used in this work were more viscous than water at low shear rates but they would be expected to have viscosities nearly equal to that of water at the shear rates that exist in the orifice (on the order of 10^4 sec^{-1}). The contribution to ΔP_e from the marginally larger shear viscosity of these solutions would therefore be negligible. Viscous losses can also be estimated from the work of Collins and Schowalter (1963) on the entrance region flow of power law and Newtonian fluids. Using Figure 8 of their paper, it can be shown that pressure losses due to shear in the orifice are negligible (Balakrishnan and Gordon (1975)).

Inspection of Figures 4-12 to 4-17 in which ΔP_e (= N_{Eo}) is plotted against v_o for the PAM solutions shows that N_{Eo}, like Γ_o, is a function of v_o only. N_{Eo} can be expressed in terms of v_o by the equation

$$N_{Eo} = Av_o^B \tag{5-2}$$

Values of A and B for the three Separan AP 273 solutions are given in Table 5.1.

Table 5.1

Values of Constants in Equations 5-1 and 5-2

Polymer	Concentration wppm	α	β	A	B
Separan AP 273	10	0.595	1.468	1.985	1.855
	20	0.345	1.494	3.986	1.778
	40	0.117	1.621	0.903	2.025

Combining equations (5-1) and (5-2) we obtain the following expressions for N_{Eo} and η_{ex} (the extensional viscosity at the orifice), in terms of Γ_o:

$$N_{Eo} = K\Gamma_o^m \tag{5-3}$$

$$\eta_{ex} \equiv \frac{N_{Eo}}{\Gamma_o} = K\Gamma_o^{m-1} \tag{5-4}$$

$$K = \frac{A}{(\alpha)^m}, \quad m = \frac{B}{\beta} \tag{5-5}$$

Plots of N_{Eo} versus Γ_o for the three Separan AP 273 solutions are given in Figures 5-2 to 5-4. Scatter in the data, which is seen to be considerable in the case of the 40 wppm solution, is much less at 20 and 10 wppm solution. As mentioned earlier, this is primarily due to the small angles of convergence observed with the 40 wppm solution. Furthermore, the flow was very unstable at 40 wppm while the 10 and 20 wppm solutions exhibited very stable WGS flow patterns.

The experimental results obtained with the Separan AP 273 solutions therefore show that the normal stress difference at the orifice depends only on the stretch rate at the orifice. This is an important conclusion because WGS flow is a flow in which the stretch rate is spatially dependent and the flow is not of constant stretch history. The unique dependence of N_{Eo} on Γ_o implies that N_{Eo} is independent of the history of deformation of the fluid. This is predicted by simple fluid theory for spherical sink flow where the fluid no longer remembers its stress state prior to its entering the sink flow (Section 5.6 and Murch (1970)). In the case of the PAM solutions at the concentrations studied, WGS flow was found to extend very far upstream from the orifice. For Separan AP 273 and Percol 155 at 40 wppm in the 0.109 cm orifice, WGS flow began at a distance of about 180 orifice diameters away from the orifice. In cases such as these, it would be reasonable to expect the fluid close to the orifice to have no memory of its stress state before it entered the WGS flow.

5.2 Comparison of Results with Predictions of Equations of Motion

In this section, the predictions of the equations of motion for spherical sink flow kinematics are compared with experimental results obtained with the PAMs.

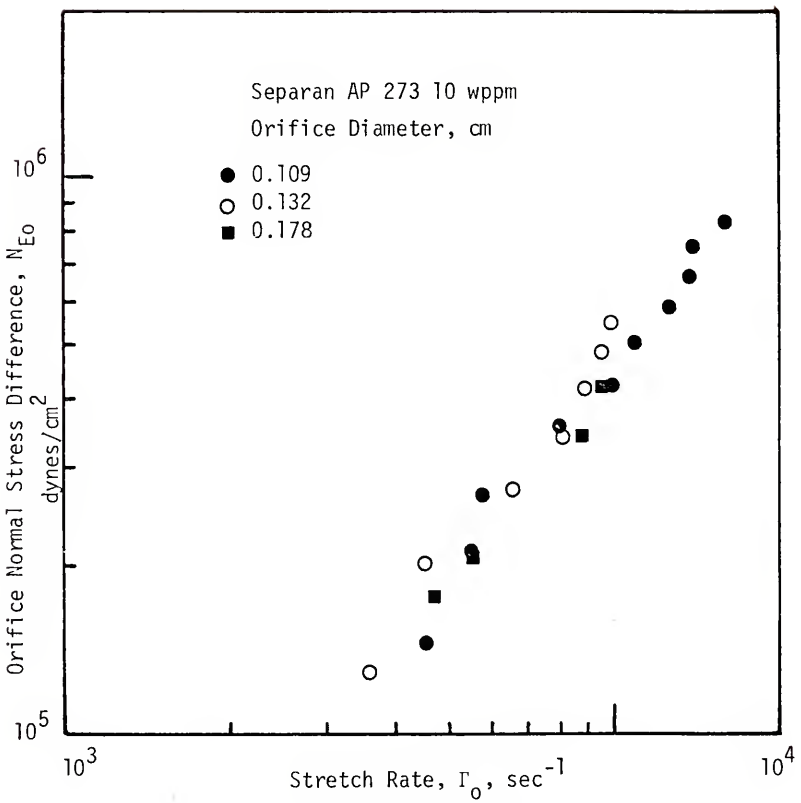

Figure 5-2. Dependence of Normal Stress Difference on Stretch Rate

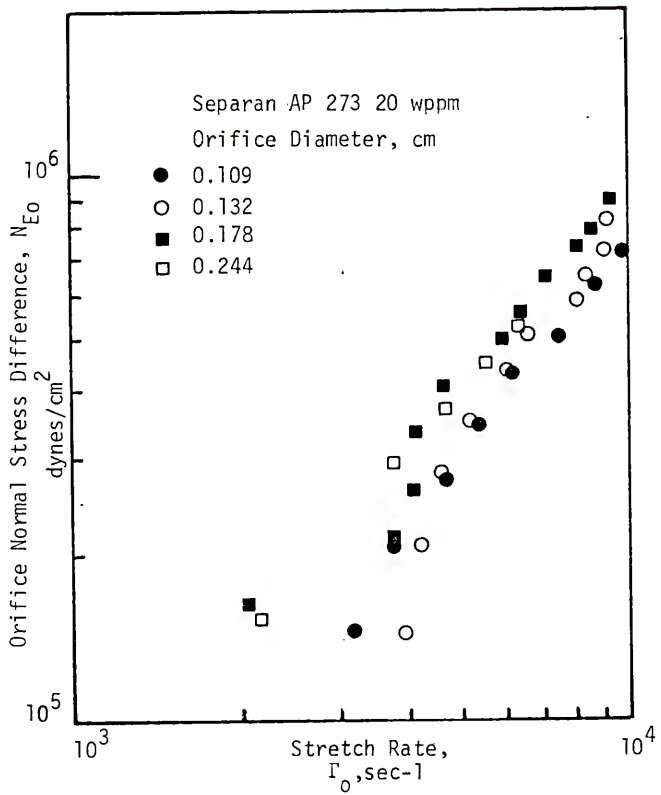

Figure 5-3. Dependence of Normal Stress on Stretch Rate

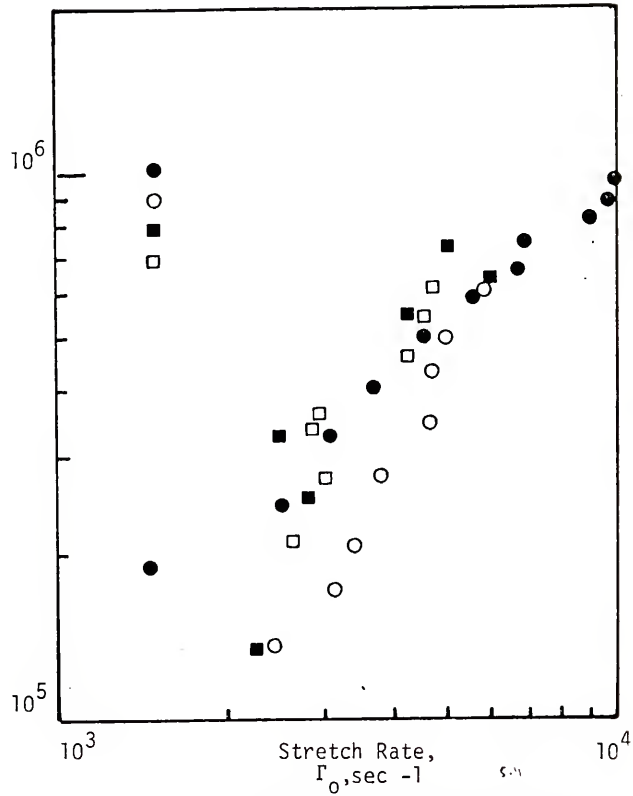

Figure 5-4. Dependence of Normal Stress Difference on Stretch Rate

For the flow field described by equation (2-11), the r and θ components of the equations of motion (in physical components) reduce to

$$\rho v^r \frac{dv^r}{dr} = \frac{d}{dr} T^{rr} + \frac{2N_E(r)}{r} \tag{5-6}$$

$$T^{\theta\theta} \neq T^{\theta\theta}(\theta) \tag{5-7}$$

In equation (5-6) $N_E(r) \equiv T^{rr} - T^{\theta\theta}$. In obtaining equation (5-7), it was assumed that the second normal stress difference $T^{\theta\theta} - T^{\phi\phi} = 0$. In spherical sink flow towards a point sink, the flow is uniform with respect to the θ and φ directions and therefore $T^{\theta\theta} = T^{\phi\phi}$. This is also rigorously predicted by Simple Fluid Theory (Coleman (1968), Murch (1970)).

Using equation (2-27) which describes the velocity field, we obtain

$$\frac{dT^{rr}}{dr} + \frac{2N_E(r)}{r} = \frac{-\rho Q^2}{2\pi^2(1 - \cos\theta)^2 r^5} \tag{5-8}$$

Equating $T^{\theta\theta}$ with $-p_R$ where p_R is the "isotropic" pressure in the recirculating region (see Section 2-6), equation (5-8) can be written as

$$\frac{d}{dr} T^{rr} + \frac{2T^{rr}}{r} + \frac{2p_R}{r} = \frac{-\rho Q^2}{2\pi^2(1-\cos\theta)^2 r^5} \tag{5-9}$$

Equation (5-9) can be integrated between $r = r_\infty$ and r to give

$$\left[\bar{r}^2\, T^{\bar{r}\bar{r}}\right]_{r_\infty}^{r} = \frac{-\rho Q^2}{2\pi^2(1-\cos\theta)^2}\left\{-\frac{1}{2r^2}\right\}_{r_\infty}^{r} - 2p_R\left\{\frac{r^2}{2}\right\}_{r_\infty}^{r} \qquad (5\text{-}10)$$

At $r = r_\infty$ (far away from the orifice, where WGS flow begins), $T^{rr} = -p_o$, the isotropic pressure. It has also been found from experiments that the pressure in the region upstream of the WGS flow is equal to the pressure in the recirculating region p_R. Equation (5-10) then reduces to

$$N_E(r) = T^{rr}(r) + p_R = \frac{\rho Q^2}{4\pi^2(1-\cos\theta)^2}\left[\bar{\frac{1}{r^4}} - \bar{\frac{1}{r^2 r_\infty^2}}\right] \qquad (5\text{-}11)$$

Equation (5-11) shows that $N_E = 0$ at $r = r_\infty$ and that it increases as the orifice is approached. The maximum value of N_E occurs at the orifice and is given by

$$N_{Eo} = \frac{\rho Q^2}{4\pi^2(1-\cos\theta)^2}\left[\bar{\frac{\sin^4\theta}{R_o^4}} - \bar{\frac{\sin^2\theta}{R_o^2\, r_\infty^2}}\right] \qquad (5\text{-}12)$$

When $r_\infty >>> R_o$ as is the case with the PAMs, equation (5-12) simplifies to

$$N_{Eo} = \frac{\rho v_o^2}{4}(1+\cos\theta)^2 \qquad (5\text{-}13)$$

where $v_o = \dfrac{Q}{\pi R_o^2}$

Murch (1970) obtained a similar result without assuming equality of p_o and p_R, or of $T^{\theta\theta}$ and $-p_A$

$$N_E(r) = \rho v^2(r) = \frac{\rho Q^2}{4\pi^2(1-\cos\theta)^2 r^4} \qquad (5\text{-}14)$$

At the orifice, $r = \frac{R_o}{\sin\theta}$ and substituting this value of r in equation (5-14) gives equation (5-13). This finding offers support for the assumptions made in deriving equation (5-13).

Figures 5-5 to 5-8 compare N_{Eo} obtained from experiments with those predicted by equation (5-13) for a few PAMs. Agreement between the two is found to be very close, suggesting the validity of the assumptions made in equating N_{Eo} with ΔP_e (equation 2-39).

It should be noted that equation (5-13) is applicable only for the cases in which WGS flow extends to a considerable distance into the reservoir and that the whole theoretical treatment applies only when a WGS flow is present.

5.3 Comparison with Previous Investigations

The extensional flow behavior of polymeric materials has been studied by several investigators. However, almost all these studies have been conducted with concentrated polymer solutions or polymer melts and, to the best of our knowledge, the present work is the first attempt to measure extensional viscosities at polymer concentrations as low as 10 wppm. In this section, the results of the present work (obtained with deionized water solutions) are compared with those of other investigations.

Referring to the results obtained with Separan AP 273 solutions at 10, 20, and 40 wppm, and plotting the data as N_{Eo} versus Γ_o (Figures 5-2 to 5-4), it is seen that the slopes of the lines are 1.26, 1.19,

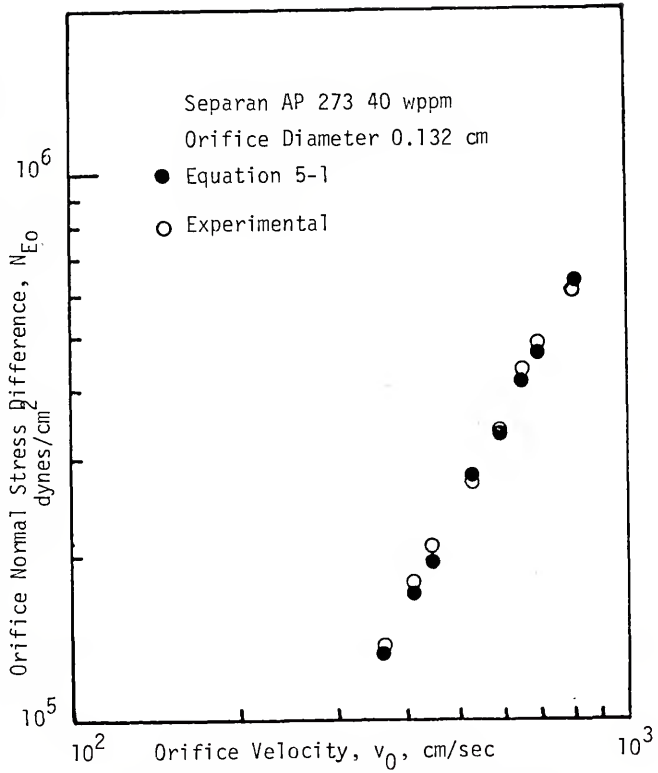

Figure 5-5. Comparison of Predictions of Equations of Motion with Experiment

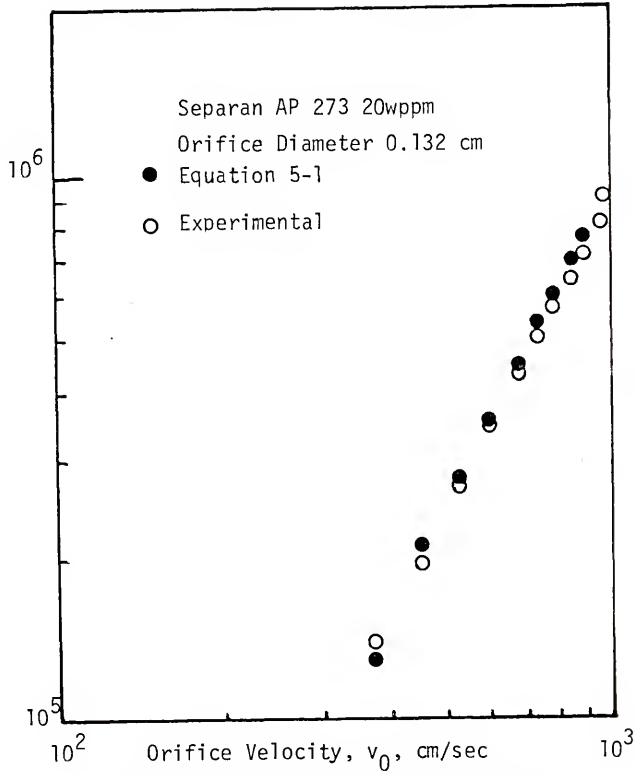

Figure 5-6. Comparison of Predictions of Equations of Motion with Experiment

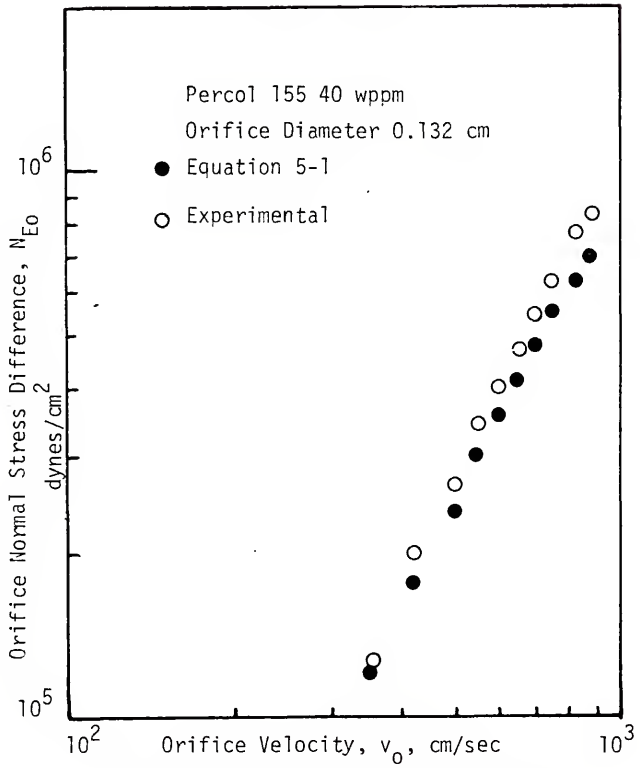

Figure 5-7. Comparison of Predictions of Equations of Motion with Experiment

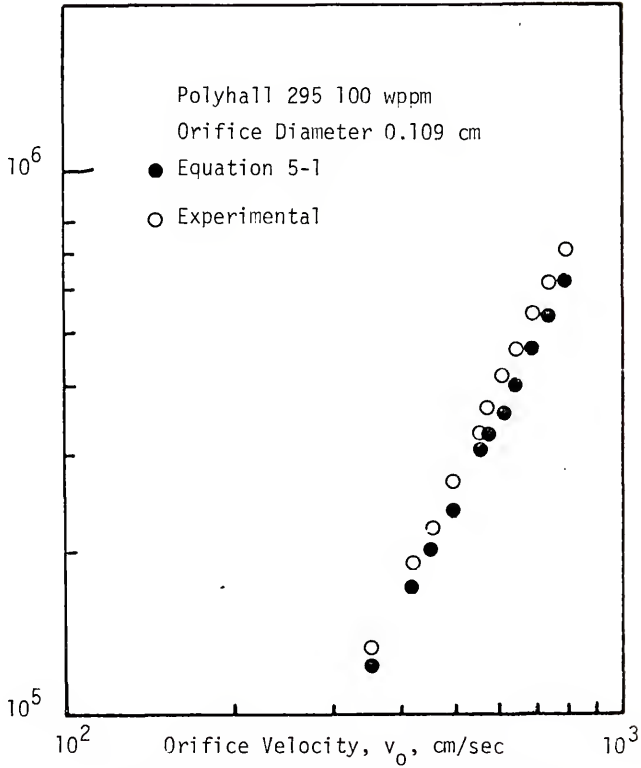

Figure 5-8. Comparison of Predictions of Equations of Motion with Experiment

and 1.25 respectively. Thus, the extensional viscosity defined by equation (5-4) is only a weak function of Γ, the stretch rate, and as mentioned in Section 5-1, the polymer solutions seem to exhibit power law (shear thickening) behavior in extension. For the lowest concentration studied (10 wppm), the shear viscosity of the solution (at shear rates comparable to those encountered in extensional flow experiments) was nearly equal to that of water and the extensional viscosity was about 30 poises. This gives a Trouton ratio of about 3000, nearly three orders of magnitude greater than that for the solvent.

Large Trouton ratios such as those measured here have been reported in other studies conducted with polymer melts and polymer solutions of concentrations higher than those used in the present work (Ballman (1965), Cogswell (1969,1972b), Han and Lamonte (1972), Hudson et al. (1974), Everage and Ballman (1975), Pickup (1970), Murch (1970), Metzner and Metzner (1969), and Oliver and Bragg (1973a)). Most of these studies were of the unsteady or steady state extension or of the fiber spinning type. The last four studies were carried out in apparatuses that were similar in configuration to the experimental setup used in the present work. It is then instructive to compare the results of these studies with those obtained here.

Pickup (1970) determined extensional viscosities from entrance pressure drop measurements in two dimensional converging flow (flow through a slit die), as well as from Fano flow experiments. The extensional viscosities measured from the entrance pressure drop experiments were extremely large and increased sharply with stretch rate. For a 0.3% solution of Separan AP 30, Pickup obtained a Trouton

ratio of 28 at a stretch rate of 30 sec^{-1}. This is an order of magnitude greater than what would be expected for a Newtonian fluid but much less than the value obtained in the present work.

Murch (1970) used a converging flow apparatus similar to that used in this work to measure extensional viscosities. As briefly mentioned in Chapter II, Murch combined measurements of $T^{\theta\theta}$ (as a function of r) with the r component equation of motion in spherical coordinates to obtain primary normal stress differences in spherical sink flow towards a point sink:

$$N_E(r) = \rho v^2(r) + \frac{1}{r^2}\int_r^\infty (\bar{r})^2 \frac{dT^{\theta\theta}}{d\bar{r}}\, d\bar{r} \qquad (2\text{-}24)$$

$T^{\theta\theta}$ profiles were obtained by introducing probes into the central region of the WGS flow, with the active surfaces of the probes tangential to the streamlines. Three types of probes were used--fluid filled, solid, and beveled tip. It has been pointed out by Astarita and Metzner (1967) that the use of probes to make point measurements of stresses gives inaccurate results in the case of viscoelastic fluids. This is due to the solid-like response of the fluid adjacent to the probe--a situation that occurs when the Deborah Number is large. In the case of probes with holes in them, one has to consider hole errors (Kaye et al. (1963)) arising from the bending of streamlines into the hole. In accounting for such errors (arising from boundary layer formation and hole errors), Murch used corrections obtained from centerline measurements in fully developed pipe flow, with the assumption that the corrections were independent of

the stress rate and stretch history of the fluid. This assumption is clearly unjustified because the stress response of a viscoelastic fluid depends on its stretch history (Section 2.1), and the flow in which the probes were calibrated for errors (fully developed pipe flow) is quite different from the flow in which they were used for stress measurements. The former is a flow of constant stretch history while the latter is not, and there is no reason to expect that the corrections will be the same in both flows. Moreover, the results Murch used in calculating the integral in equation (2-24) were obtained with fluid filled probes that had corrections as large as 150% of the corrected value! Thus, the normal stress differences calculated by Murch are ambiguous and subject to considerable error.

In calculating stretch rates, Murch extrapolated data obtained by Uebler (with a 3.76 cm dia orifice, twice as large as that used by Murch) with the assumption that the stretch rate in WGS flow was linearly dependent on the velocity.

$$\Gamma(r) = K\, v(r) \qquad (5\text{-}15)$$

Equation (5-15) implies constancy of the group $\sin\theta\ (1 + \cos\theta)/R_o$ which, in light of results obtained in the present work, is incorrect. Due to uncertainties in both normal stress difference and stretch rate measurements, the values of extensional viscosities obtained by Murch are likely to be erroneous. Even so, his results are still indicative of the large extensional viscosity of polymer solutions. For a 0.5% solution of Separan AP 30, Murch calculated a Trouton ratio of about 1000, which is considerably larger than that obtained by Pickup.

Both Metzner and Metzner and Oliver and Bragg measured extensional viscosities of Separan solutions at concentrations in the 100-1000 wppm range, higher than those used in this work. The experimental apparatus used by these two groups were of the jet thrust type. Oliver and Bragg used a thrust apparatus identical to that used here, and calculated N_{Eo} from the equation

$$N_{Eo} = \frac{T_W - T_M}{\pi R_o^2} \tag{5-16}$$

where T_W = thrust measured for water

T_M = thrust measured for polymer solution

R_o = orifice radius

The orifices used by these authors were square edged and had diameters of 0.032 cm and 0.06 cm. The polymer used was Separan ET 597 (now designated as AP 273) and the concentration ranged from 100 wppm to 1000 wppm. Stretch rates and N_{Eo} were not measured simultaneously in Oliver and Bragg's work and extensional viscosities were calculated from measured N_{Eo} (from thrust measurements and equation (5-16)) and stretch rates that were approximated by the equations

$$\Gamma_o = K_1 v_o \tag{5-17}$$

and

$$\Gamma_o = K_2 \frac{v_o}{R_o^n} \tag{5-18}$$

Equations (5-17) and (5-18) were obtained by Oliver and Bragg by the following reasoning: if the angle of convergence θ decreases with decreasing R_o, then

$$\Gamma_o \sim \frac{v_o}{R_o^n} \qquad 0 \leq n < 1 \qquad (5\text{-}19)$$

The condition n = 0 corresponds to the case where θ does not change with R_o. Equation (5-19) implies that for a fixed orifice radius, Γ_o is a linear function of v_o. As mentioned earlier, the results of the present work have shown this assumption to be incorrect.

Oliver and Bragg, using experimental data obtained with a 100 wppm solution of Separan ET 597, found K_1 = 2.61 (in equation (5-17)) and K_2 = 0.89 and n = 0.5 (in equation (5-18)). They calculated extensional viscosities of 128 poise at Γ_o = 3915 sec^{-1} (equation (5-17)) and 18.5 poise at Γ_o = 1780 sec^{-1} (equation (5-18)). Metzner and Metzner (1970) used a thrust apparatus of configuration slightly different from that used by Oliver and Bragg. Thrusts were measured by mounting the converging flow apparatus (which consisted of a small brass cube to which orifices could be fitted) on a set of leaf springs and measuring the jet thrust from deflection of the springs. A schematic of Metzner's thrust apparatus is given in Figure 5-9.

The equation used by Metzner and Metzner to calculate the normal stress difference at the orifice was similar to equation (5-16), with the term T_W replaced by $\rho v_o^2 \pi R_o^2$, the thrust that would be measured with water if there was no vena contracta formation. The total stress at the orifice in the direction of flow was given by

$$T_{11o} = \rho(Q/\pi R_o^2)^2 - \frac{T_M}{A_o} \qquad (5\text{-}20)$$

$$= N_{Eo}$$

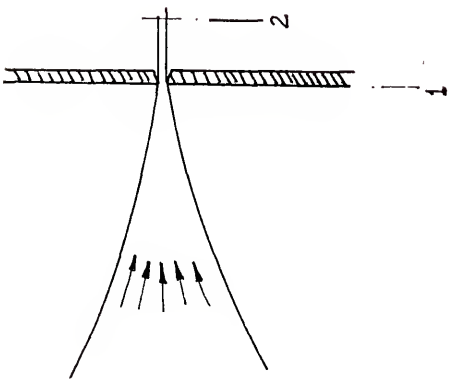

Figure 5-10. Momentum Balance: Control Surfaces

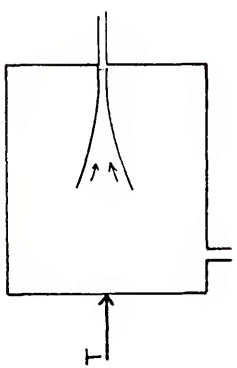

Figure 5-9. Metzner's Thrust Apparatus

In arriving at the relationship $T_{11o} = N_{Eo}$, both Oliver and Bragg and Metzner and Metzner made the assumption that T_{22} at the orifice was zero. That this assumption is incorrect can be shown by making a momentum balance across the orifice in WGS flow (Figure 5-10). For the sake of simplicity we assume that the angle of convergence of streamlines (2θ) is small and that there is no die swell.

$$\rho v_2^2 A_2 - \int_1 \rho v^2 dA = - \int_1 T_{11} dA \qquad (5\text{-}21)$$

Assuming a flat profile at 1 (valid for small values of θ), equation (5-21) becomes

$$- \rho v_2^2 A_2 + \rho v_1^2 A_1 = - T_{11}\Big|_1 A_1 \qquad (5\text{-}22)$$

In the limiting case where sections 1 and 2 coincide with the plane of the orifice, v_2 and v_1 become identical and equation (5-22) reduces to

$$T_{11o} = 0 \qquad (5\text{-}23)$$

If, following Metzner and Metzner, we set T_{22o} equal to zero, the normal stress difference at the orifice would also be equal to zero! This is clearly not the case and T_{22o} is therefore not equal to zero.

The thrust apparatus used in the present work was very similar to that used by Oliver and Bragg. N_{Eo} was related to the thrust measured in the apparatus by making a momentum balance. The control volume is shown in Figure 5-11. Section 0 coincides with the plane of the orifice

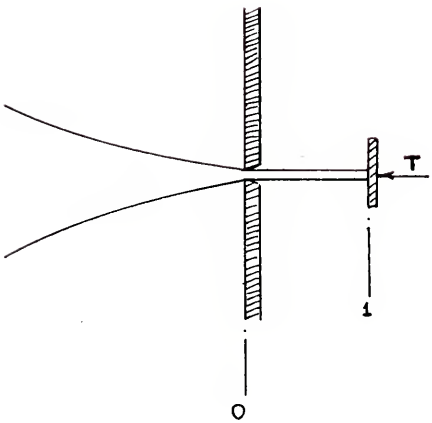

Figure 5-11. Momentum Balance: Control Surfaces

and section 1 with the Plexiglas plate (which is connected to the thrust measuring device) that the jet strikes. By making a balance between 0 and 1

$$- \int_0 \rho v^2 dA = - \int_0 T_{11}\, dA - T \qquad (5\text{-}24)$$

T is the thrust and T_{11} is the total stress and v the velocity in the direction of flow. For small values of θ, the angle at which the polymer solution converges into the orifice, the velocity v in the direction of flow can be replaced by v_0, the average velocity at the orifice. The integrals can then be removed and equation (5-24) rewritten as

$$- \rho v_0^2 A_0 = - T - T_{11o}\, A_0 \qquad (5\text{-}25)$$

T_{11o}, the total stress at the orifice in the direction of flow can be divided into isotropic and deviatoric terms to give

$$T_{11o} = (- p + \tau_{11})_o \qquad (2\text{-}32)$$

Also,
$$T_{22o} = (- p + \tau_{22})_o \qquad (2\text{-}33)$$

$$= - p_R$$

Eliminating the isotropic pressure term gives the result

$$T_{11o} = - p_R + N_{Eo} \qquad (5\text{-}26)$$

$$N_{Eo} = (\tau_{11} - \tau_{22})_o \tag{5-27}$$

Inserting this result in equation (5-25) gives an expression for N_{Eo} in terms of the measured thrust.

$$N_{Eo} = p_R + \frac{T}{A_o} - \rho v_o^2 \tag{5-28}$$

Since p_R is equal to ΔP_e, the entrance pressure drop,

$$N_{Eo} = \Delta P_e + \frac{T}{A_o} - \rho v_o^2 \tag{5-29}$$

Comparison of the above equation with equation (2-39) (which was derived for the case where die swell and vena contracta effects were neglected) shows that they are very similar:

$$N_{Eo} = \Delta P_e \tag{2-39}$$

No such assumptions were made in deriving equation (5-29) and the thrust measurements therefore correct equation (2-39) for die swell or vena contracta effects, and cannot, by themselves, give the value of N_{Eo}. For dilute polymer solutions (with small values of θ, the angle of convergence), both die swell and vena contracta effects would be expected to be negligible and the measured value of thrust should be simply equal to the rate of momentum leaving the orifice.

$$T = \rho v_1^2 A_1 = \rho v_o^2 A_o \tag{5-30}$$

Thrust measurements carried out in this work confirmed the absence of significant die swell or vena contracta formation. The results obtained with Separan AP 273 at 40 wppm with orifice diameters 0.178 cm and 0.132 cm are shown in Figure 4-27 along with data for water. The data for the Separan solution are seen to be indistinguishable from those for water, suggesting that die swell was negligible. Also, the coincidence of data for water and for Separan AP 273 at 40 wppm with the dark line corresponding to ρv_o^2 indicates the absence of vena contracta formation. The thrust data for the 200 wppm Separan AP 273 solution are found to be significantly below those for water, indicating the occurrence of die swell. It is seen that the inverted triangles, corresponding to thrust calculated from photographic measurements of die swell, are also well below the data for water. Agreement between thrust and photographic measurements of die swell is not very close, presumably due to the slightly different geometry in which the latter measurements were made.*

The momentum balance used in the present work is compared with those of Metzner and Metzner (and Oliver and Bragg), and Pickup in Table 5.2. The point of departure from similarity between columns 1 and 2 is found to be in estimating T_{22} at the orifice. Pickup's treatment is identical to that used here if die swell and losses due to friction in the die are neglected.

It is clear then that the measurements of Metzner and Metzner and Oliver and Bragg are not of N_{Eo} but of die swell. The latter is considerably smaller than the former as shown in Figure 5-14 in which N_{Eo}

*In order to photograph the jet as soon as it emerged from the orifice, the orifice plate was mounted backwards as shown in Figure 5-13. This is to be compared with the usual orifice arrangement (shown in Figure 5-12) in which the orifice was mounted flush with the converging flow apparatus.

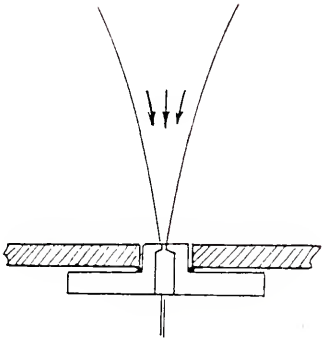

Figure 5-12. Orifice Arrangement During Normal Runs.

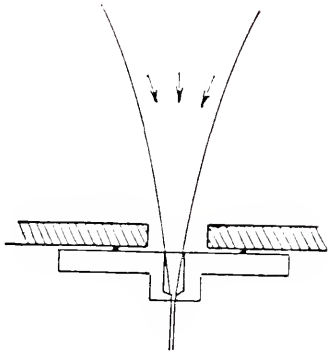

Figure 5-13. Orifice Arrangement During Die Swell Measurements.

Table 5.2. Comparison of Momentum Balances

	Present Work	Metzner & Metzner (Oliver & Bragg)	Pickup
Apparatus Used	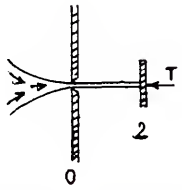	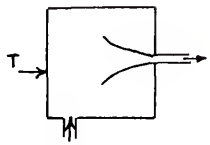	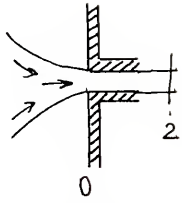
Solutions Used	Separan AP 273, 10-40 wppm	Separan AP 30, 50-1000 wppm	Separan AP 30 in Glycerine water systems. Highly viscous solutions
Momentum Balance	Between 0 and 2	Over the entire apparatus	0 and 2
Velocity Profile at 0	Flat topped	Flat topped	Flat topped
Equations	$\rho v_o^2 A_o = T + T_{11o} A_o$	$\rho v_o^2 = T + T_{11o} A_o$	$- T_{11} A_o = \Delta p_w A_w$ Δp_w = Pressure drop in die A_w = Wall area of die
Key Assumption	$T_{22o} = -p_R = (-p + \tau_{22})_o$ $T_{11o} = (\tau_{11} - \tau_{22})_o - p_R$	$T_{22o} = (-p + \tau_{22})_o = 0$ $T_{11o} = (\tau_{11} - \tau_{22})_o$	$T_{22o} = (-p + \tau_{22})_o = -p_R$ $T_{11o} = (\tau_{11} - \tau_{22})_o - p_R$
Expression for N_{Eo}	$N_{Eo} = p_R + \rho v_o^2 - \frac{T}{A_o}$	$N_{Eo} = \rho v_o^2 - \frac{T}{A_o}$	$N_{Eo} = p_R - \Delta p_w \frac{A_w}{A_o}$

calculated from entrance pressure measurements is compared with N_{Eo} calculated from thrust measurements using equation (5-20). It is therefore not surprising that both these groups of authors were not able to measure significant differences between thrust measurements for water and polymer solutions at concentrations below 100 wppm--the die swell shown by these solutions would be expected to be negligible at such low concentrations. In the present work, entrance pressure drop measurements with Separan AP 30 yielded large values of N_{Eo} at concentrations as low as 20 wppm (Figure 4-15). And as mentioned earlier, Separan AP 30 is an excellent drag reducer at these concentration levels (Figure 4-1).

To summarize, the results of the present work indicate that dilute polymer solutions, even at concentrations as low as 10 wppm, possess extremely large extensional viscosities. They also show that extensional viscosity is only a weak function of stretch rate in the WGS flow of dilute polymer solutions. Close examination of results obtained by Metzner and Metzner and Oliver and Bragg shows that the extensional viscosities calculated by these groups of authors are conservative due to their use of the thrust technique which measures die swell rather than N_{Eo}.

5.4 Correlation Between DR, VI, and Extensional Viscosity

In this section, the correlation between extensional viscosity, DR and VI is investigated. First, the drag reducing and vortex inhibiting abilities of deionized water solutions of the polymers used in this study are compared with their extensional viscosities.

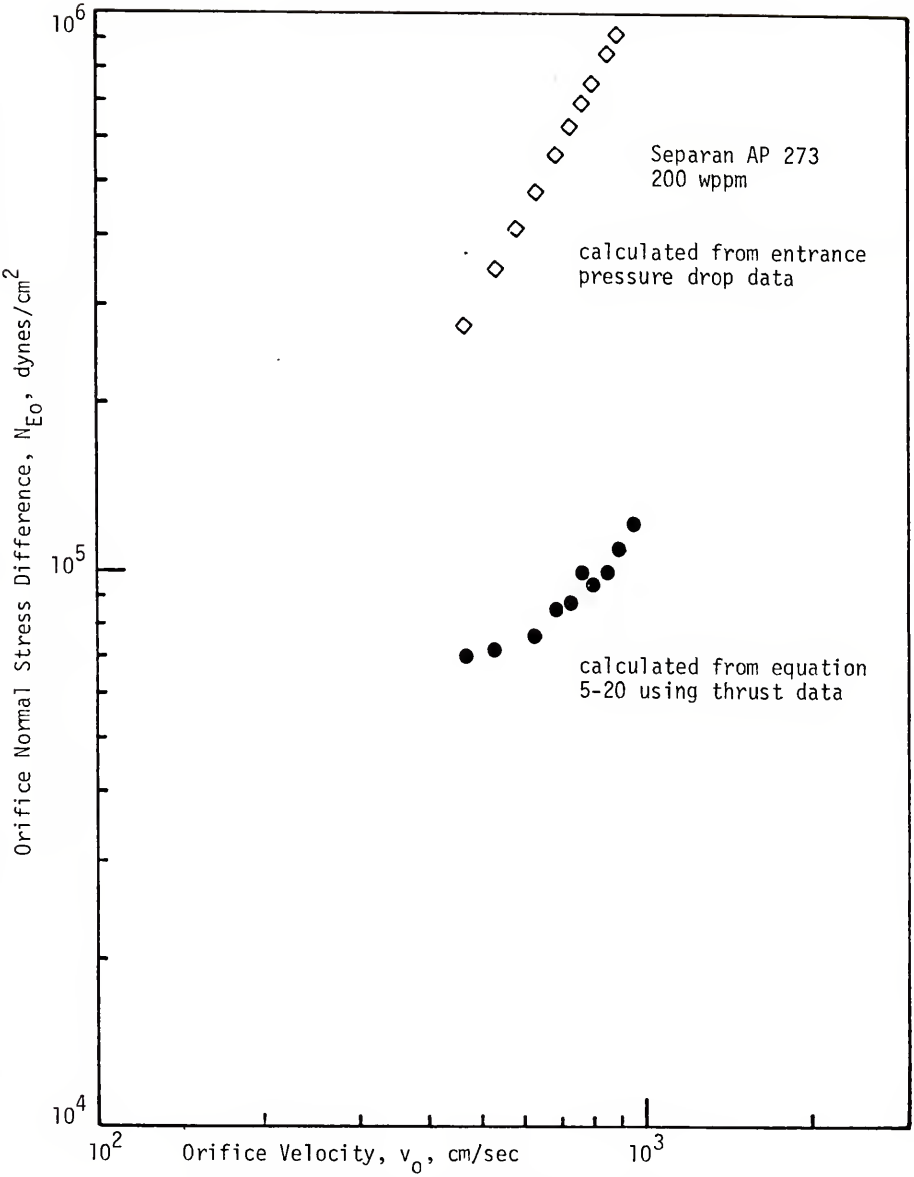

Figure 5-14. Comparison of Normal Stress Differences Calculated by Entrance Pressure Drop and Thrust Measurements

Following this, the dependence of DR, VI, and extensional viscosity on polymer conformation and polymer degradation is discussed.

5.4.1 Comparison of DR, VI, and extensional viscosity of deionized water solutions

Friction factor versus Reynolds Number curves for the polymers used in this work are shown in Figure 4-1. It is clear from the figure that there is a significant non-Newtonian viscosity effect at low N_{Re} with the polyacrylamide solutions. This can of course be corrected by using the generalized Reynolds Number (Metzner and Reed (1955)) but this would obscure the true drag reducing efficiency of the polymer solutions. Reynolds Numbers were therefore calculated using solvent viscosity.

Inspection of Figure 4-1 reveals that the polymers can be ordered, according to their drag reducing ability, as shown in Table 5.3.

Table 5.3

Ordering of Polymers According to Their Drag Reducing Ability

1. Separan AP 273
2. Percol 155
3. Polyox WSR 301
4. Separan AP 30
5. Polyhall 295
6. Versicol 525

Considering next the vortex inhibiting ability of these polymers as shown in Table 4.1, it is immediately apparent that there is excellent

correlation between the drag reducing and vortex inhibiting abilities of all the polymers except one--Versicol S25. Thus, Separan AP 273, Percol 155 and Polyox WSR 301, which are all excellent drag reducers, have C_{VI}'s of 2 wppm, 2 wppm and 3 wppm respectively. Polyhall 295 which, along with Versicol S25, is the least effective drag reducer, has C_{VI} = 15 wppm. Versicol S25 does not appear to follow the trend shown by the other polymers in the sense that it has an extremely small value of C_{VI} (3 wppm) even though it is a poor drag reducer compared to the first three polymers of Table 5.3.

Extensional viscosities of the polymers used in this study are compared in Table 5.4 at concentrations at which they could be measured. Comparisons were made at a stretch rate of 5000 sec^{-1}.

Table 5.4

Comparison of Extensional Viscosities in Deionized Water

Polymer	Concentration wppm	Stretch Rate sec^{-1}	η_{ex} poise
Separan AP 273	10	5000	35
	20		70
	40		110
Percol 155	40		100
Separan AP 30	20		50
Polyhall 295	100		75
Versicol S25	100		40

It is clear from the Separan AP 273 results in Table 5.4 that extensional viscosity does not exhibit a monotonic increase with concentration. Also, the similar values of extensional viscosity of Separan AP 273 and Percol 155 at 40 wppm suggest that the two polymers probably have similar values of extensional viscosity at 20 and 10 wppm as well.* With this observation in mind, comparison of results obtained with Separans AP 30 and AP 273 at 20 wppm shows that the former has a lower extensional viscosity than either the latter or Percol 155. Polyhall 295 has an extensional viscosity of about 75 poise at a concentration of 100 wppm, nearly equal to that of Separan AP 273 at 20 wppm. Versicol S25 seems to have the lowest extensional viscosity of all the polymers--40 poise at 100 wppm. The data presented in Table 5.4, compared with Table 5.3, show that the drag reducing abilities of the polymers seem to correlate with their extensional viscosities. Of particular extensional interest is the large extensional viscosities that were measured at concentrations as low as 10 wppm. To the best of our knowledge, there is no other rheological property (besides DR and VI) of polymer solutions that is so dramatically different from that of the solvent at such low polymer concentrations.

Extensional viscosities could not be calculated for Polyox WSR 301 due to reasons already mentioned in Chapter IV--the absence of WGS flow and of entrance pressure drops greater than those exhibited by water, at least with the orifices used in this study. This result does not imply that the extensional properties of Polyox solutions are <u>not</u>

*Unfortunately, extensional viscosities were not measured at 10 and 20 wppm for Percol 155.

different from those of water.* Instead, it points out the limitation of the technique used in this work to measure extensional viscosities--it is restricted to only those polymer solutions that exhibit WGS flow. This point is further discussed in subsequent sections.

5.4.2 Dependence of DR, VI, and extensional viscosity on polymer conformation

The dependence of DR on polymer conformation has been studied quite extensively by several investigators (Hand and Williams (1969, 1970), Parker and Hedley (1972), Kim et al. (1973), Banijamali et al. (1974), Balakrishnan and Gordon (1975), White and Gordon (1975)). As mentioned in Chapter I, the current opinion is that the drag reducing ability of a polymer is maximized when it is an extended state. Recent work conducted on VI has shown that it depends on polymer conformation much the same as DR does (Balakrishnan and Gordon (1975), White and Gordon (1975)). This observation lends further substance to the notion that both DR and VI are due to the same mechanism.

Results of conformational studies carried out in the present work are summarized in Section 4.5. Changes in polymer conformation were followed by viscosity measurements as shown in Figure 4-28 in which the viscosity of a 200 wppm solution of Separan AP 273 is plotted as a function of pH. The maximum viscosity occurs at a pH of about 9 and an increase or decrease of pH results in reduction of viscosity, the effect being more dramatic at low pH. In neutral medium (pH = 9.4), the ionized carboxyl groups along the length of the polymer chain repel each other.

*Large extensional viscosities have been measured for Polyox solutions by Oliver (1973) who employed the triple jet technique. Using a 1000 wppm solution of a coagulant grade Polyox, he obtained extensional viscosities that were as large as 1400 times the shear viscosity.

This leads to chain expansion and, therefore, large viscosity. The addition of NaOH to increase the pH results in an excess of Na^+ counterions which shield the ionized carboxyl groups and thereby cause a reduction in chain expansion. The polymer molecule would be expected to be more flexible at high pH than in neutral medium. At low pH, the mechanism by which viscosity reduction occurs is quite different--ionization of carboxyl groups is suppressed at low pH and there is evidence to suggest that intramolecular hydrogen bonding might occur at very low pH, making the polymer molecules compact and rigid (Mathieson and MacLaren (1965), White and Gordon (1975)).

The effect of polymer conformation on DR is shown in Figure 4-29a in which friction factor versus Reynolds Number curves are shown for a 10 wppm Separan AP 273 solution in deionized water, high pH and low pH solutions and in 0.5% NaCl solution. As mentioned earlier in Section 5.4.1, Reynolds Numbers were calculated using solvent viscosity in order to portray the true drag reducing ability of the polymer solutions.

Figure 4-29a clearly shows that of the four solutions, the low pH solution is the least effective drag reducer. The polymer in deionized water and at high pH shows equal DR at high N_{Re}. At low N_{Re}, the high pH solution is superior to the deionized water solution, due to the adverse effect that the large viscosity of the latter has on its drag reducing ability. Experiments performed with the gravity flow apparatus yielded similar results (Figure 4-29b).

Macromolecular conformation can also be changed by adding salts to polyelectrolyte solutions. Viscosity data obtained with Separan AP 273 in salt solution is shown in Figure 4-28 by the dark point. The shear viscosity of the 200 wppm polymer solution was about 2 cp

in 0.5% NaCl, comparable to the viscosity of the polymer solution at low pH; however, the DR behavior of the two solutions (salt solution and low pH solution) is quite different. The salt solution shows much better DR than the low pH solution, and at large N_{Re} it is almost as effective as the deionized water and high pH solutions. This observation seems to suggest that the dimensions of the polymer molecule in simple shearing flow, as indicated by solution viscosity, do not entirely determine its drag reducing ability. White and Gordon (1975) and White (1975) have discussed this in detail in terms of the potential extensibility of the polymer molecules and have suggested that the poor drag reducing ability of the low pH solution is due to the inability of the molecules in solution to fully extend in a turbulent flow field, perhaps due to intramolecular hydrogen bonding. Polymer molecules in the solutions at high pH and in salt solution are capable of achieving much greater extension than the low pH solution, particularly at large N_{Re} when the deforming forces would be greatest, and are therefore considerably superior to the low pH solution in reducing friction.

Results of VI measurements are given in Table 4.2. It is immediately clear from the table that Separan AP 273 shows much better VI at high pH than at low pH, and that changes in polymer conformation have the same effect on DR and VI.

With regard to the effect of polymer conformation on extensional viscosity, it was mentioned in Chapter IV that the 10 wppm solution of Separan AP 273 exhibited the same entrance pressure drop at high pH and 0.5% salt solution as it did in deionized water, while the low pH solution was indistinguishable

from water. It was also mentioned that N_{Eo}'s could not be calculated for all the solutions except that in deionized water because they did not exhibit WGS flow. When the flow field is Newtonian (i.e., the flow enters the orifice from a 180° solid angle), it is not possible to relate the entrance pressure drop to the normal stress difference at the orifice due to the complexity of the flow. Moreover, the stretch rate at the orifice can be determined only from detailed velocity profile measurements. As pointed out by Baid (1973), the shearing and extensional deformation rates in Newtonian converging flow are nearly equal in magnitude and extremely difficult to measure due to sharp increase in velocity close to the orifice. Thus it is not possible to calculate an extensional viscosity for polymer solutions that do not exhibit WGS flow. However, qualitative observations can be made on the extensional properties of these solutions based on the fact that the high pH and salt solutions exhibit entrance pressure drops greater than those exhibited by water while the low pH solution does not. The indistinguishability of the low pH solution from water implies that the solution possesses extensional properties similar to those of water, at least under the conditions at which the experiments were conducted. This does not however preclude exhibition of DR by the low pH solution. It is entirely possible that the extensional properties of the solution may become apparent if the orifice used were of smaller dimensions, as in the case of Polyox WSR 301 which (Sections 4.3 and 5.5) exhibited dependence of increment of entrance pressure drop (over water) on orifice diameter.

In the case of high pH and salt solutions large entrance pressure drops were measured. Since the shear viscosity of these solutions was nearly identical to that of water (as evidenced from the absence of non-Newtonian viscosity effect in their f versus N_{Re} curves), the large entrance pressure drops exhibited by these solutions is indicative of response of the solutions to stretching modes of deformation close to the orifice. This implies that these solutions possess large extensional viscosities as compared to water.

The findings of this study on the dependence of extensional viscosity on macromolecular conformation are consistent with the predictions of a recent theory of Batchelor (1971), where the elongational viscosity is calculated for a non-dilute suspension of elongated rigid particles. For a suspension of cylindrical particles, Batchelor calculated a Trouton ratio given by

$$\frac{\eta_{ex}}{\mu_{sh}} = \frac{12}{9} \frac{\ell^2/R_o^2}{\log (\pi/c)} \qquad (5\text{-}31)$$

c is the volume fraction of the particles, η_{ex} and μ_{sh} are the extensional and shear viscosities respectively, l is half the length of the particle and R_o the radius of the particle. Equation (5-31) was obtained by Batchelor for the case where

$$l >> h >> b$$

where b is the effective radius of the particle and h, the average distance between neighboring particles. Mewis and Metzner (1974)

have recently confirmed equation (5-31) for various suspensions of glass fibers in polybutene. Equation (5-31) is of interest to this work with regard to its prediction of dependence of extensional viscosity on the aspect ratio (l/R_o) of the particle.

Idealizing Separan molecules as rigid fibers in deionized water,* addition of NaOH or HCl to alter the conformation of the molecules would lower the extensional viscosity of the solution. Also, reduction in extensional viscosity would, according to equation (5-31), be expected to be greater at low pH due to the compactness of the molecule at low pH as compared to its conformation at high pH.

5.4.3 Effect of polymer degradation on DR, VI, and extensional viscosity

The dependence of rheological properties of polymeric systems on polymer molecular weight (MW) and molecular weight distribution (MWD) can be best studied by using fractionated samples. In the absence of such facilities indirect methods have to be used to obtain information on the effect of MW and MWD on rheological properties. In this investigation, experiments were performed with polymers belonging to a homologous series (Separans AP 273 and AP 30) to determine the dependence of DR, VI, and extensional viscosity on MW. Information on the effect of MWD on these properties was obtained by mechanically degrading polymer solutions and measuring their DR, VI, and extensional viscosity before and after degradation. Both DR and VI are known to depend predominantly on the high molecular weight

*Recent studies on the DR of Separan AP 273 in deionized water have shown the polymer to exhibit diameter independence in f versus N_{Re} plots--a feature of DR that has been observed with fibers (Lee et al. (1974)). This suggests that solutions of Separan AP 273 in deionized water may indeed be similar to fiber suspensions.

species (HMWS) of a polymer sample, and these HMWS are known to be extremely susceptible to shear degradation (Gordon and Balakrishnan (1972)).

The effect of polymer MW on DR, VI, and extensional viscosity is shown in Figure 4-1 and Tables 4.1 and 5.4. The drag reducing abilities of Separan AP 273 and Separan AP 30 are compared in Figure 4-1. The f versus N_{Re} plots in the figure clearly show that the former is a much better drag reducer than the latter. Results of VI experiments summarized in Table 4.1 reveal a similar trend in the dependence of VI on MW. C_{VI} for Separan AP 273 is only 2 wppm while that for Separan AP 30 is 10 wppm.

Considering next the dependence of extensional viscosity on MW, it is seen from Table 5.4 that Separan AP 273 at 20 wppm has a much larger viscosity than Separan AP 30 at the same concentration. As mentioned in Chapter III, the two Separans are believed to have similarly shaped MWD curves (with the AP 273 grade of a higher molecular weight than the AP 30 grade) and the results of this work therefore show that DR, VI, and extensional viscosity all increase with increasing MW. This result has been obtained for DR by several investigators (Paterson (1969), Morgan and Pike (1972), Gordon and Balakrishnan (1972)), and for VI by our group (Gordon and Balakrishnan (1972)). As far as extensional viscosity is concerned, the present work, to the best of our knowledge, is the first attempt to determine the effect of polymer MW on extensional viscosity in such dilute systems.

The results of polymer degradation experiments are summarized in Figures 4-32 to 4-35. The effect of shear degradation on DR is

shown in Figure 4-32 in which f versus N_{Re} plots are given for 10 wppm solutions of Separan AP 273 at different stages of degradation. The solution degraded at N_{Re} = 20,000 is seen to be nearly identical to the fresh solution, indicating high resistance to shear degradation by the polymer solution. Earlier studies conducted with the same polymer have yielded similar results (Balakrishnan (1972), White (1975)). The solution degraded at N_{Re} = 40,000 shows significantly less DR than the other two solutions.

Figure 4-33, in which the change in VI due to shear degradation is shown, reveals a similar trend. C_{VI} for the polymer solution degraded at N_{Re} = 20,000 is identical to that for the fresh solution, while there is a slight increase in C_{VI} for the solution degraded at N_{Re} = 40,000. This indicates that a loss in drag reducing ability is accompanied by a loss in vortex inhibiting ability.

Considering next the change in extensional viscosity with degradation, it is seen from Figure 4-35 that the entrance pressure drop characteristics of the three solutions--the fresh solution and the solutions degraded at N_{Re} = 20,000 and 40,000--are nearly identical. However, as mentioned in Section 4.6, the flow fields exhibited by the three solutions were remarkably different from one another. The fresh solution exhibited pronounced WGS flow and extensional viscosities could be calculated (Figure 5-2). The solution degraded at N_{Re} = 20,000 exhibited WGS flow at low flow rates and extensional viscosities could be calculated only under these conditions. At large flow rates, the flow did not resemble WGS flow--the flow entered the orifice from 180° close to the orifice, even though small recirculating regions were

clearly visible (Figure 4-34). In order to compare the extensional viscosities of the fresh solution with those of the solution degraded at N_{Re} = 20,000, N_{Eo} is plotted against Γ_o for the two solutions (Figure 5-15). It is seen that the degraded solution has smaller values of N_{Eo} than the fresh solution at equal values of Γ_o, particularly at larger values of Γ_o. This indicates a slight reduction in extensional viscosity due to shear degradation. In the case of the solution degraded at N_{Re} = 40,000, traces of WGS flow could be seen at very low flow rates. At moderate flow rates the flow field appeared as illustrated in Figure 4-34 and finally, at high flow rates, the flow field appeared almost Newtonian (Figure 4-34). Values of N_{Eo} and Γ_o could be obtained for this solution at only one flow rate and are shown in Figure 5-15 by a dark square. Comparison of this point with the data presented for the other two solutions shows that the solution degraded N_{Re} = 40,000 has considerably lower extensional viscosity than the solution degraded at N_{Re} = 20,000 or the fresh solution. Thus, shear degradation seems to have the same effect on extensional viscosity as it does on DR.

To summarize: Experiments performed in the present work to determine the correlation between DR, VI, and extensional viscosity yield the following results:

(i) There is excellent correlation between DR and VI in the case of all polymers except Versicol S25 which, as mentioned earlier, is a poor drag reducer but has an extremely low value of C_{VI}. This seemingly anomalous behavior of the polymer is currently being investigated by Chiou (1976).

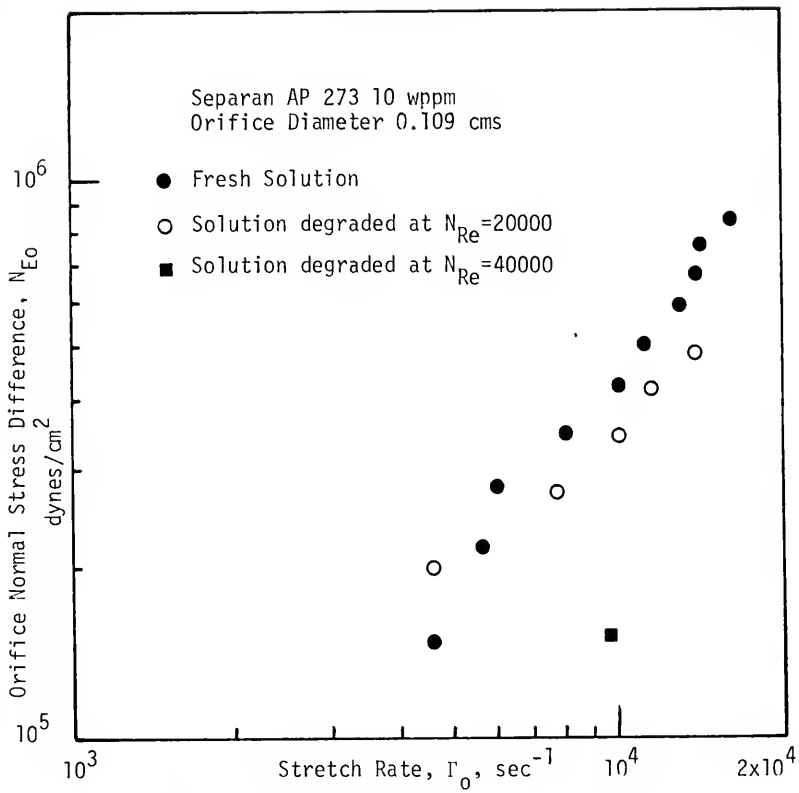

Figure 5-15. Effect of Shear Degradation on Extensional Viscosity

(ii) There appears to be excellent correlation between DR and extensional viscosity. Both properties of polymers seem to have similar dependence on macromolecular conformation and molecular weight and molecular weight distribution. At the polymer concentrations used in this study, extensional viscosity is the only rheological property that is dramatically different from solvent properties, and the correlation between DR and extensional viscosity observed in this work suggests that DR is indeed a manifestation of the large extensional viscosity of dilute polymer solutions.

(iii) The sink flow kinematics proposed by Uebler (1966) (Equations (2-11)) do not apply to the converging flow of all polymer solutions. The precise property or combination of properties of dilute polymer solutions that is responsible for the occurrence of WGS flow is not well known, and its determination was beyond the scope of this work.

5.5 Observations on the Converging Flow of Poly(ethylene oxide)

It was mentioned in Section 5.4 that Polyox WSR 301 and Separan AP 273 show nearly identical DR and VI behavior but quite different converging flow behavior. PEO was found to have much smaller entrance pressure drops than Separan AP 273 at equal concentrations and did not exhibit WGS flow except when extremely small orifices were used. In addition, PEO seemed to exhibit a diameter dependence of entrance pressure drop that was not present with SAP 273.

Perusal of literature reveals that experiments performed to study the orifice flow behavior of poly(ethylene oxide) polymers have yielded conflicting results. Bate (1967), using a 30 wppm solution of PEO found a reduction in pressure drop across a 0.355 cm sharp edged orifice mounted in a 1.25 cm diameter tube.* Giles (1969) used a coagulant grade of Polyox and obtained results that were contrary to those of Bate. Using both square and sharp edged orifices (of diameters similar to those used in the present work), and polymer concentrations ranging from 300 to 600 wppm, Gadd found large reductions in discharge coefficients due to polymer addition.

In a detailed study of the orifice flow of dilute poly(ethylene oxide) solutions, Bilgen (1973), using solutions of four different grades of Polyox of concentrations ranging from 5 to 200 wppm, obtained results similar to those of Gadd. The orifice used in his work was 0.01 cm in diameter, nearly an order of magnitude less than the orifice diameters used in this study. Bilgen also found that the entrance pressure drop exhibited by Polyox solutions increased with increasing molecular weight and concentration, the polymer did not exhibit entrance pressure drops in excess of those exhibited by water. Thus Polyox WSR 205 (molecular weight 10^6) was indistinguishable from water while the Polyox WSR 301 used by Bilgen (molecular weight 4×10^6) showed large values of entrance pressure drop.**

---

*This somewhat anomalous behavior reported by Bate might be a manifestation of vena contracta inhibition, a new viscoelastic phenomenon in which the addition of minute amounts of certain polymers to water suppresses vena contracta formation in orifice flow resulting in increased throughputs (Chiou and Gordon (1976)).

**Molecular weights were calculated from Bilgen's intrinsic viscosity data and the Mark-Houwink equation for poly(ethylene oxide) given by Paterson (1969).

It is clear from the results of this study and from Bilgen's work that poly(ethylene oxide) polymers behave quite differently from polyacrylamides. Unfortunately, the reasons for this difference in behavior between the two polymers are not very clear.

It should be emphasized that the onset of elevated entrance pressure drops in polymer solutions, in excess of those exhibited by water, does not require the formation of a WGS flow. The results presented in Section 5.4 on the entrance pressure drop characteristics of salt and high pH solutions have clearly shown that large entrance pressure drops can occur even in the absence of WGS flow.

5.6 Comparison of Experimental Results with Predictions of Constitutive Theories

Viscoelastic theories of polymeric materials have traditionally been formulated to accurately portray their behavior in steady or oscillatory laminar shearing flows. In recent years, the utility of these theories in predicting the extensional flow behavior of polymer systems has received considerable attention. This has been primarily due to the fact that extensional flows (such as WGS flow) are commonly encountered in polymer processing operations (Petrie (1975), Denson and Gallo (1971)).

In this section, the predictions of stresses in WGS flow by constitutive theories of dilute polymer solutions are discussed and compared with experimental results.

Since most constitutive theories are no more than special cases of the Simple Fluid Theory (SFT) (Noll (1958,1959)), we consider first the predictions for a simple fluid in WGS flow.

The SFT states that the stress in an isotropic, incompressible fluid is determined, to within an arbitrary isotropic pressure, by the functional of the history of the relative deformation gradient $\underset{\sim}{F}(s)$

$$\underline{T} = - p\underline{I} + \overset{\infty}{\underset{s=0}{F}} [\underline{F}(s)] \tag{5-32}$$

The relative deformation gradient relates the differential separation $\underline{dx}$ between two particles in a continuum at the present time t to the separation $\underline{dx}'$ at some reference time τ. Defining the history parameter $s = t - \tau$, the relative deformation gradient is given by

$$\underline{dx} = \underline{F}(s)\ \underline{dx}' \tag{5-33}$$

Marucci and Murch (1970), treating spherical sink flow (used here to describe WGS flow), as a special case of the expansion of a spherical shell (Coleman (1968)), obtained the following result for the physical components of $\underline{T}$

$$T^{r\theta} = T^{\theta\phi} = T^{r\phi} = 0 \tag{5-34}$$

$$T^{rr} - T^{\theta\theta} \equiv N_E = N_E(\Gamma) \tag{5-35}$$

$$T^{\theta\theta} - T^{\phi\phi} = 0 \tag{5-36}$$

Thus, the SFT predicts that the stress response of a material in spherical sink flow is determined by a single material function N_E that depends only on the local rate of stretching Γ, even

though the flow is not one of constant stretch history (Section 2.2).

As discussed in Section 5.1, the experimental results of this work are consistent with the predictions of the SFT.

The utility of the SFT lies in its ability to make general predictions that all continuum theories have to obey. However, it does not give the functional dependence of stresses on deformation rates. In order to obtain such predictions, more specific constitutive theories, such as the continuum modified dumbbell or bead spring theories (Chapter II) of Everage (1973) may be used. The use of such theories requires careful characterization of the viscometric functions of dilute polymer solutions. Unfortunately, such measurements could not be carried out in this work due to the lack of adequate facilities.

5.7 Conclusions and Recommendations

5.7.1 Conclusions

Dilute polymer solutions at concentrations as low as 10 wppm were found to have extensional viscosities as large as 3000 times the shear viscosity. These values were considerably larger than other previously published results. The experimentally measured extensional viscosities were found to be independent of stretch history, as predicted by the Simple Fluid Theory, and were found to increase with stretch rate.

It was shown that the thruster technique, in the absence of entrance pressure drop measurements, does not yield accurate values of extensional normal stress differences (N_E). Comparison of experimentally measured N_E with the predictions of the equations of motion

for spherical sink flow kinematics (used to describe WGS flow) showed that N_{Eo} is nearly equal to ρv_o^2, at least over the range of orifice stretch rates studied in this work.

The extensional viscosities measured in this work appeared to increase with increasing molecular weight (as indicated by results obtained with 20 wppm solutions of Separans AP 273 and AP 30). They were also found to be extremely sensitive to shear degradation, more so than either DR or VI. This finding suggests that extensional viscosity depends on the highest molecular weight species of a polydisperse polymer sample. Comparison of the DR behavior and extensional viscosity of deionized water solutions of the polymers used in this study showed excellent correlation. In the cases where they could be measured, drag reduction was found to increase with increasing extensional viscosity.

Experiments carried out to determine the dependence of extensional viscosity on polymer conformation did not yield conclusive results. However, it appeared that extensional viscosity was greater when the polymer molecules were extended and flexible than when they were rigid and compact. This dependence of extensional viscosity on polymer conformation is similar to that of DR and VI. The results of this work therefore suggest that both DR and VI are indeed manifestations of the large resistance to stretching motions exhibited by dilute polymer solutions.

The converging flow method was found to be useful as a means to determine the extensional viscosities of polymer solutions only when they exhibited WGS flow. Changes in polymer conformation and

molecular weight distribution (due to shear degradation) were found to have an adverse effect on the WGS flow pattern exhibited by dilute polymer solutions. The precise mechanism that is responsible for the occurrence and/or disappearance of WGS flow could not be determined.

5.7.2 Recommendations

The logical extension of this work would be in the areas of

(i) understanding of the mechanism by which WGS flow occurs. Results obtained in this work show that WGS flow occurs only with certain polymers (such as the partially hydrolyzed polyacrylamides used in this study) and that it disappears at high and low pH and in the presence of added salt. These results suggest that a possible requirement for the occurrence of WGS flow might be the presence of a three-dimensional network in the polymer solution, a situation that can occur in deionized water solutions of partially hydrolyzed polyacrylamides due to hydrogen bonding.* The addition of electrolyte acid or base would destroy the network and, therefore, WGS flow pattern.

An understanding of the mechanism of WGS flow might also help explain the converging flow behavior of poly(ethylene oxide) which is quite different from that of the polyacrylamides.

(ii) development of experimental techniques that can measure extensional viscosities of dilute polymer solutions that do not exhibit WGS flow. A possible method is the triple jet

*Both the amide and carboxyl groups in partially hydrolyzed polyacrylamides are potential hydrogen bond acceptors (Pimentel and McClellan (1960)).

technique described by Oliver (1973).

(iii) a detailed and careful study of instability in WGS flow. Information obtained by using dilute polymer solutions might prove useful in understanding melt flow instabilities and melt fracture.

(iv) development of techniques to accurately characterize the viscometric functions of dilute polymer solutions. This would enable the comparison of predictions of constitutive theories with experimental measurements of extensional viscosity.

APPENDIX A

ENTRANCE PRESSURE DROP DATA FOR WATER

TEMPERATURE : 23°C

ORIFICE DIAMETER: 0.040 cms

FLOW RATE ML/S	ENTRANCE PRESSURE DROP ΔP_e INS HG
1.400	23.35
1.333	21.05
1.283	18.90
1.230	17.05
1.180	15.10
1.110	13.00
1.005	10.65
0.848	8.75
0.784	6.90
0.667	5.00
0.507	2.90

ORIFICE DIAMETER: 0.051 cms

FLOW RATE ML/S	ENTRANCE PRESSURE DROP ΔP_e INS HG
2.300	23.4
2.200	21.25
2.067	19.10
1.940	17.05
1.817	15.10
1.700	12.95
1.550	10.60
1.433	8.85
1.233	6.70
1.033	4.60
0.833	2.95

TEMPERATURE : 23°C

ORIFICE DIAMETER: 0.109 cms

FLOW RATE ML/S	ENTRANCE PRESSURE DROP ΔP_e INS HG
3.80	2.87
4.85	4.90
5.70	6.70
4.05	3.50
5.16	6.10
5.86	8.10
6.86	11.00
7.77	14.15
8.38	16.90
9.08	19.15
9.53	21.60
10.40	25.70
3.05	1.85
4.80	5.35
5.90	7.40
6.50	9.80
7.30	12.05
7.80	13.50
8.20	15.90
9.00	18.10
9.30	19.10
10.2	22.5

TEMPERATURE : 23°C

ORIFICE DIAMETER: 0.132 cms

FLOW RATE ML/S	ENTRANCE PRESSURE DROP ΔP_e INS HG
4.60	1.70
6.10	3.50
7.50	5.90
9.00	8.80
10.90	13.00
12.00	15.90
13.20	18.85
15.00	23.80
13.40	19.60
8.70	8.60
6.00	3.75
6.40	3.90
8.30	6.50
9.70	9.30
11.00	12.55
11.98	15.50
12.71	17.95
14.11	21.35
15.16	25.00
16.08	27.60

TEMPERATURE : 23°C

ORIFICE DIAMETER: 0.178 cms

FLOW RATE ML/S	ENTRANCE PRESSURE DROP ΔP_e INS HG
10.265	3.300
12.925	5.700
14.980	7.900
16.490	9.900
18.175	11.900
19.550	14.150
20.720	16.200
22.140	18.150
23.230	20.300
24.400	22.200
25.380	24.450
7.900	2.100
9.000	2.550
10.350	3.600
12.000	5.100
12.800	5.900
13.800	6.900
15.000	8.200

ORIFICE DIAMETER: 0.244 cms

21.28	3.60
26.56	6.25
30.46	8.05
34.26	10.45
38.55	13.50
41.08	15.85
43.625	17.35
46.46	20.45
49.72	23.15

POLYMER : Separan AP 273
CONCENTRATION : 10 ppm
pH : Neutral
TEMPERATURE : 23°C
ORIFICE DIAMETER: 0.109 cms

FLOW RATE ML/S	ENTRANCE PRESSURE DROP, ΔP_e INS HG	ANGLE OF CONVERGENCE, 2θ, DEGREES
3.750	4.300	36.750
4.675	6.350	36.000
5.365	8.100	32.500
6.130	10.500	40.000
6.840	12.550	45.500
7.475	14.950	45.500
8.125	17.400	49.500
8.730	20.000	49.500
9.245	22.400	47.500
10.000	25.050	51.000

ORIFICE DIAMETER: 0.132 cms

FLOW RATE ML/S	ENTRANCE PRESSURE DROP, ΔP_e INS HG	ANGLE OF CONVERGENCE, 2θ, DEGREES
5.220	3.800	36.750
6.632	6.000	36.750
7.935	8.050	45.000
9.390	10.000	48.000
10.290	12.300	48.000
11.320	14.300	46.500
11.950	16.300	45.000

POLYMER : Separan AP 273
CONCENTRATION : 10 ppm
pH : Neutral
TEMPERATURE : 23°C
ORIFICE DIAMETER: 0.178 cms

FLOW RATE ML/S	ENTRANCE PRESSURE DROP, ΔP_e INS HG	ANGLE OF CONVERGENCE, 2θ, DEGREES
11.510	5.800	87.000
13.500	7.900	99.000
15.250	10.100	104.000
16.810	12.400	100.000
18.750	14.700	NO WGS FLOW
20.200	17.300	NO WGS FLOW
21.140	19.400	NO WGS FLOW

POLYMER : Separan AP 273
CONCENTRATION : 20 wppm
pH : Neutral
TEMPERATURE : 23°C
ORIFICE DIAMETER: 0.109 cms

FLOW RATE ML/S	ENTRANCE PRESSURE DROP, ΔP_e INS HG	ANGLE OF CONVERGENCE, 2θ, DEGREES
3.455	4.2	28
4.080	5.95	28
4.760	8.0	30
5.445	10.0	35
6.275	12.4	35
6.760	14.45	Not Clear
7.285	16.5	Not Clear
7.760	18.45	35
8.335	20.65	35
8.945	23.4	36
9.470	25.4	36

POLYMER : Separan AP 273
CONCENTRATION : 20 ppm
pH : Neutral
TEMPERATURE : 23°C
ORIFICE DIAMETER: 0.132 cms

FLOW RATE ML/S	ENTRANCE PRESSURE DROP, ΔP_e INS HG	ANGLE OF CONVERGENCE, 2θ, DEGREES
5.105	4.100	43.000
6.190	6.100	36.500
7.235	8.150	34.000
8.225	10.200	34.000
9.325	12.400	35.000
10.125	14.500	35.000
10.890	16.650	42.500
11.725	18.700	40.000
12.335	20.800	40.000
13.275	23.550	37.000
14.050	25.500	48.000

POLYMER : Separan AP 273
CONCENTRATION : 20 ppm
pH : Neutral
TEMPERATURE : 23°C
ORIFICE DIAMETER: 0.178 cms

FLOW RATE ML/S	ENTRANCE PRESSURE DROP, ΔP_e INS HG	ANGLE OF CONVERGENCE, 2θ, DEGREES
7.507	3.000	26.500
9.250	4.700	29.000
10.330	5.900	58.500
11.140	6.550	46.500
12.095	7.800	46.500
14.020	9.700	39.000
15.587	12.000	39.000
17.120	14.500	47.000
18.380	16.400	47.000
20.650	19.250	47.000
21.610	21.400	52.000
22.750	23.350	52.000
24.600	26.600	52.000

ORIFICE DIAMETER: 0.244 cms

FLOW RATE ML/S	ENTRANCE PRESSURE DROP, ΔP_e INS HG	ANGLE OF CONVERGENCE, 2θ, DEGREES
42.490	19.450	62.000
37.100	15.500	62.000
33.170	13.350	62.000
30.110	10.950	56.000
26.550	8.600	51.000
18.280	4.400	41.000

POLYMER : Separan AP 273
CONCENTRATION : 40 ppm
pH : Neutral
TEMPERATURE : 23°C
ORIFICE DIAMETER: 0.109 cms

FLOW RATE ML/S	ENTRANCE PRESSURE DROP, ΔP_e INS HG	ANGLE OF CONVERGENCE, 2θ, DEGREES
2.765	2.800	8.000
3.885	5.550	11.000
4.380	7.200	17.000
5.190	9.700	17.500
5.690	11.800	19.000
6.360	14.950	21.000
6.925	17.300	24.000
7.405	19.400	27.000
7.990	21.800	26.000
8.405	24.000	32.500
9.000	26.100	33.000
9.270	28.400	33.000

ORIFICE DIAMETER: 0.132 cms

FLOW RATE ML/S	ENTRANCE PRESSURE DROP, ΔP_e INS HG	ANGLE OF CONVERGENCE, 2θ, DEGREES
6.105	6.100	30.000
5.700	5.000	30.000
5.005	4.000	25.000
4.095	2.500	23.500
2.355	0.700	11.500
7.255	8.100	28.000
8.050	10.200	30.000
8.975	12.700	27.500
9.515	14.350	27.500
11.040	18.200	27.500

POLYMER : Separan AP 273
CONCENTRATION : 40 ppm
pH : Neutral
TEMPERATURE : 23°C
ORIFICE DIAMETER: 0.178 cms

FLOW RATE ML/S	ENTRANCE PRESSURE DROP, ΔP_e INS HG	ANGLE OF CONVERGENCE, 2θ, DEGREES
8.320	3.900	35.000
11.155	7.300	32.300
12.920	9.800	25.000
14.475	12.400	15.600
16.795	16.100	33.000
18.445	19.000	44.000
20.040	21.650	32.800
21.500	24.750	17.000

ORIFICE DIAMETER: 0.244 cms

FLOW RATE ML/S	ENTRANCE PRESSURE DROP, ΔP_e INS HG	ANGLE OF CONVERGENCE, 2θ, DEGREES
21.060	6.250	43.000
24.160	8.200	43.000
26.000	10.000	37.000
26.560	10.800	37.000
33.660	16.000	47.500
30.810	13.800	48.500
36.950	18.450	44.000
39.110	20.200	41.100

POLYMER : Separan AP 30
CONCENTRATION : 20 ppm
pH : Neutral
TEMPERATURE : 23°C
ORIFICE DIAMETER: 0.109 cms

FLOW RATE ML/S	ENTRANCE PRESSURE DROP, ΔP_e INS HG	ANGLE OF CONVERGENCE, 2θ, DEGREES
4.640	6.950	45.500
5.440	9.000	40.000
6.125	11.100	35.000
6.750	13.150	37.500
7.460	15.200	39.000
7.960	17.150	41.000
8.515	19.250	40.000
9.015	21.400	43.500
9.040	23.250	45.000

ORIFICE DIAMETER: 0.132 cms

FLOW RATE ML/S	ENTRANCE PRESSURE DROP, ΔP_e INS HG	ANGLE OF CONVERGENCE, 2θ, DEGREES
5.860	4.900	44.000
7.070	6.900	39.000
8.295	9.000	38.000
9.180	11.000	38.000
10.220	13.200	32.000
11.065	15.100	32.000
11.780	17.120	35.000
12.650	19.100	40.000
13.304	21.250	41.500
14.025	23.250	41.500

POLYMER : Percol 155
CONCENTRATION : 40 wppm
pH : Neutral
TEMPERATURE : 23°C
ORIFICE DIAMETER: 0.109 cms

FLOW RATE ML/S	ENTRANCE PRESSURE DROP, ΔP_e INS HG	ANGLE OF CONVERGENCE 2θ, DEGREES
3.39	4.8	14
3.82	6.0	17.5
6.17	14.9	Not Clear
6.56	17.05	"
6.905	18.7	20
7.445	21.5	20
7.835	23.7	20

ORIFICE DIAMETER: 0.132 cms

FLOW RATE ML/S	ENTRANCE PRESSURE DROP, ΔP_e INS HG	ANGLE OF CONVERGENCE 2θ, DEGREES
4.89	3.9	31
5.68	5.55	28
6.22	6.7	29.2
6.74	7.95	31.5
7.26	9.35	31.5
7.865	11.0	30.75
8.33	12.4	40
8.845	14.05	40
9.505	16.15	34.5
10.135	18.15	30
10.75	21.0	24.5

POLYMER : Percol 155
CONCENTRATION : 40 wppm
pH : Neutral
TEMPERATURE : 23°C
ORIFICE DIAMETER: 0.178 cms

FLOW RATE ML/S	ENTRANCE PRESSURE DROP, ΔP_e INS HG	ANGLE OF CONVERGENCE, 2θ, DEGREES
9.12	4.65	33.5
10.3	5.8	36
11.82	7.9	36
12.8	9.85	34.5
14.35	12.45	33
15.227	14.2	35.5
17.02	17.15	32
18.31	19.5	35
19.22	21.6	35
20.36	24.1	35

POLYMER : Polyhall 295
CONCENTRATION : 100 wppm
pH : Neutral
TEMPERATURE : 23°C
ORIFICE DIAMETER: 0.109 cms

FLOW RATE ML/S	ENTRANCE PRESSURE DROP, ΔP_e INS HG	ANGLE OF CONVERGENCE, 2θ, DEGREES
3.3	3.75	17
3.95	5.9	17
4.58	7.9	24
5.155	10.05	24
5.645	12.0	32
6.11	14.0	32
6.56	16.05	32
7.025	18.3	32.5
7.465	20.8	41
7.77	23.1	53
8.22	25.2	53

ORIFICE DIAMETER: 0.132 cms

FLOW RATE ML/S	ENTRANCE PRESSURE DROP, ΔP_e INS HG	ANGLE OF CONVERGENCE, 2θ, DEGREES
4.695	3.65	36.0
5.890	5.90	38.0
6.720	7.90	42.0
7.550	9.95	53.5
8.330	11.95	67.9
9.025	14.00	70
9.675	16.50	70
10.270	18.30	70
10.855	20.30	54
11.350	22.80	46.7

POLYMER : Versicol S25
CONCENTRATION : 40 wppm
pH : Neutral
TEMPERATURE : 23°C
ORIFICE DIAMETER: 0.109 cms

FLOW RATE ML/S	ENTRANCE PRESSURE DROP, ΔP_e INS HG	ANGLE OF CONVERGENCE, 2θ, DEGREES
3.400	4.15	Not Clear
4.200	5.85	"
5.100	8.10	"
5.785	10.10	"
6.545	12.40	"
7.160	14.65	"
7.950	17.40	"
8.445	19.30	"
9.03	21.80	"
9.54	23.75	"

CONCENTRATION : 80 wppm
ORIFICE DIAMETER: 0.109 cms

FLOW RATE ML/S	ENTRANCE PRESSURE DROP, ΔP_e INS HG	ANGLE OF CONVERGENCE, 2θ, DEGREES
3.027	3.90	Not Clear
3.670	5.75	"
4.615	7.95	"
5.100	10.20	"
5.740	12.20	"
6.345	14.20	"
6.940	16.30	"
7.400	18.30	"
7.950	20.40	"
8.600	23.30	"
9.050	25.30	"

POLYMER : Versicol S25
CONCENTRATION : 100 wppm
pH : Neutral
TEMPERATURE : 23°C
ORIFICE DIAMETER: 0.109 cms

FLOW RATE ML/S	ENTRANCE PRESSURE DROP, ΔP_e INS HG	ANGLE OF CONVERGENCE, 2θ, DEGREES
3.690	5.10	33
4.155	6.80	40
4.755	8.95	35
5.027	11.15	46
5.975	13.20	88
6.700	16.30	Not Clear
7.675	19.55	Not Clear
3.096	4.05	43
2.750	3.15	43

POLYMER : Polyox WSR 301
CONCENTRATION : 40 wppm
pH : Neutral
TEMPERATURE : 23°C
ORIFICE DIAMETER: 0.109 cms

FLOW RATE ML/S	ENTRANCE PRESSURE DROP, ΔP_e INS HG	ANGLE OF CONVERGENCE, 2θ, DEGREES
3.80	2.87	
4.85	4.90	
5.70	6.70	↑
6.30	7.85	
7.10	10.10	Newtonian Flow Field
7.75	12.20	
8.50	14.65	
9.10	17.00	↓
9.80	19.15	

ORIFICE DIAMETER: 0.051 cms

FLOW RATE ML/S	ENTRANCE PRESSURE DROP, ΔP_e INS HG	ANGLE OF CONVERGENCE, 2θ, DEGREES
0.810	3.00	
1.016	4.90	
1.185	6.95	↑
1.333	9.00	
1.463	10.90	Newtonian Flow Field
1.600	13.10	
1.733	15.30	
1.863	17.45	↓
1.987	19.05	
2.133	22.65	

POLYMER : Polyox WSR 301
CONCENTRATION : 40 wppm
pH : Neutral
TEMPERATURE : 23°C
ORIFICE DIAMETER: 0.040 cms

FLOW RATE ML/S	ENTRANCE PRESSURE DROP, ΔP_e INS HG	ANGLE OF CONVERGENCE, 2θ, DEGREES
0.4625	2.70	Not Clear
0.6200	4.95	"
0.7200	6.90	"
0.8240	8.80	"
0.9200	10.90	"
1.0600	13.15	"
1.1333	17.10	"
1.2000	19.05	"
1.2567	21.20	"
1.3333	23.00	"

POLYMER : Polyox WSR 301
CONCENTRATION : 100 wppm
pH : Neutral
TEMPERATURE : 23°C
ORIFICE DIAMETER: 0.109 cms

FLOW RATE ML/S	ENTRANCE PRESSURE DROP, ΔP_e INS HG	ANGLE OF CONVERGENCE, 2θ, DEGREES
4.130	4.30	
4.970	6.40	
5.755	8.65	
6.445	10.85	↑
6.895	12.65	
7.465	14.75	Newtonian Flow Field
8.030	17.00	
8.575	19.20	
9.370	23.15	↓
9.795	25.25	
10.205	27.25	

ORIFICE DIAMETER: 0.132 cms

FLOW RATE ML/S	ENTRANCE PRESSURE DROP, ΔP_e INS HG	ANGLE OF CONVERGENCE, 2θ, DEGREES
6.100	3.90	
7.495	6.30	
8.580	8.50	
9.520	10.40	↑
10.245	12.45	
11.075	14.65	Newtonian Flow Field
11.625	16.90	
12.685	18.85	
13.270	21.25	↓
14.165	23.70	
14.875	26.50	

POLYMER : Polyox WSR 301
CONCENTRATION : 100 wppm
pH : Neutral
TEMPERATURE : 23°C
ORIFICE DIAMETER: 0.178 cms

FLOW RATE ML/S	ENTRANCE PRESSURE DROP, ΔP_e INS HG	ANGLE OF CONVERGENCE, 2θ, DEGREES
11.020	4.40	
13.315	6.60	
14.905	8.70	
16.435	10.50	↑
18.205	13.00	
20.375	16.55	Newtonian Flow Field
22.060	19.05	
22.950	21.20	
24.060	23.40	↓
24.855	25.35	
26.270	28.40	

POLYMER : Separan AP 273

CONCENTRATION : 10 wppm

pH : Neutral

TEMPERATURE : 23°C

ORIFICE DIAMETER: 0.109 cms

SOLUTION DEGRADED AT N_{Re} = 20000

FLOW RATE ML/S	ENTRANCE PRESSURE DROP, ΔP_e INS HG	ANGLE OF CONVERGENCE, 2θ, DEGREES
4.68	5.90	29
5.52	8.10	43
6.34	10.15	50
7.13	12.30	50
7.73	14.35	57.5
8.57	16.90	--
8.94	18.85	--
9.31	20.60	--

SOLUTION DEGRADED AT N_{Re} = 40000

4.340	5.05	90
4.095	4.45	--
4.830	6.05	--
5.645	7.95	--
6.345	10.05	--
7.340	12.70	--
7.920	14.65	--

POLYMER : Separan AP 273
CONCENTRATION : 10 wppm
pH : 3.4
TEMPERATURE : 23°C
ORIFICE DIAMETER: 0.109 cms

FLOW RATE ML/S	ENTRANCE PRESSURE DROP, ΔP_e INS HG	ANGLE OF CONVERGENCE, 2θ, DEGREES
5.415	6.80	
6.250	9.00	
6.800	11.00	
7.525	13.35	↑
7.960	15.20	
8.520	17.25	Newtonian Flow
8.965	19.05	Field
9.525	21.10	
9.960	23.30	↓
10.385	25.30	
10.875	27.50	

pH : 12.0
ORIFICE DIAMETER: 0.109 cms

3.685	4.15	
4.530	6.00	
5.450	7.85	↑
6.025	9.95	
7.080	12.00	Newtonian Flow
7.360	14.15	Field
8.170	16.10	
8.690	18.40	↓
9.090	20.20	
9.320	20.20	

BIBLIOGRAPHY

Adams, E. B., J. C. Whitehead and D. C. Bogue, AIChE J., 11, 1026 (1965).

Agoston, G. A., Ind. Eng. Chem., 46, 1017 (1954).

Astarita, G. and L. Nicodemo, Chem. Eng. J., 1, 57 (1970).

Astarita, G. and A. B. Metzner, AIChE J., 13, 550 (1967).

Bagley, E. B., J. Appl. Phys., 28, 624 (1957).

Bagley, E. B., Trans. Soc. Rheol., 5, 355 (1961).

Bagley, E. B. and A. M. Birks, J. Appl. Phys., 31, 556 (1960).

Baid, K. M., Ph.D. Thesis, University of Delaware (1973).

Bakewell, H. P. and J. L. Lumley, Phys. of Fluids, 10, 1880 (1967).

Balakrishnan, C., M.S. Thesis, University of Florida (1972).

Balakrishnan, C. and R. J. Gordon, AIChE J., 21, 1225 (1975a).

Balakrishnan, C. and R. J. Gordon, J. Appl. Poly. Sci., 19, 909 (1975b).

Ballenger, T. F., I-Jen Chen, J. W. Crowder, G. E. Hagler, D. C. Bogue and J. L. White, Trans. Soc. Rheol., 15, 195 (1971).

Ballman, R. L., Rheologica Acta, 4, 137 (1965).

Banijamali, S., E. W. Merrill, K. A. Smith and L. H. Peebles, Jr., AIChE J., 20, 824 (1974).

Batchelor, G. K., J. Fluid Mech., 44, 873 (1971).

Bate, H. G., Nature, 215, 1100 (1967).

Bilgen, E., J. de Mecanique, 12, 375 (1973).

Brodkey, R. S., J. M. Wallace, H. Eckelmann, J. Fluid Mech., 63, 209 (1974).

Bryson, A. W., G. D. Fulford, Jr., and Vr. Arunachalam, J. Fluid Mech., 47, 209 (1971).

Burkholder, N. D., The Dow Chemical Company, Personal Communication, February 3, 1971.

Chiou, C. S. and R. J. Gordon, J. Appl. Poly. Sci., in press (1976).

Clegg, P. L., in "The Rheology of Elastomers," ed. P. Mason and N. Wookey, Pergamon Press, London (1957).

Cogswell, F. N., Rheol. Acta, 8, 187 (1969).

Cogswell, F. N., Polym. Eng. Sci., 12, 64 (1972a).

Cogswell, F. N., Trans. Soc. Rheol., 383 (1972b).

Coleman, B. D., Proc. Roy. Soc., A306, 449 (1968).

Coleman, B. D. and W. Noll, Phys. Fluids, 5, 840 (1962).

Collins, M. and W. R. Schowalter, AIChE J., 9, 804 (1963).

Corino, E. R. and R. S. Brodkey, J. Fluid Mech., 37, 1 (1969).

Denn, M. M. and E. Marucci, AIChE J., 17, 101 (1971).

Denson, C. D. and Gallo, R. J., Polym. Eng. Sci., 11, 174 (1971).

Donohue, G. L., Ph.D. Thesis, Oklahoma State University (1972).

Eckelmann, H., G. Fortuna and T. J. Hanratty, Nature Physical Science, 236, 94 (1972).

Everage, A. E., Jr., Ph.D. Thesis, University of Florida (1973).

Everage, A. E., Jr. and R. J. Gordon, AIChE J., 17, 1257 (1971).

Everage, A. E., Jr. and R. L. Ballman, J. Appl. Poly. Sci., in press (1975).

Fabula, A. G., Proc. 4th Congress on Rheology, 1963, part 3, editor E. M. Lee, Interscience Publishers, N.Y. (1965), p. 455.

Fabula, A. G., "An Experimental Study of Grid Turbulence in Dilute High-Polymer Solutions," Report to U.S. Bureau of Weapons via Office of Naval Research (June 1966).

Fortuna, G. and T. J. Hanratty, J. Fluid Mech., 53, 575 (1972).

Frommer, M. A., A. Feder-Lavy and M. A. Kraus, J. Colloid and Interface Sci., 48, 165 (1974).

Gadd, G. E., Nature, 206, 463 (1965).

Giesekus, H., Rheol. Acta, 7, 127 (1968).

Giesekus, H., Rheol. Acta, 8, 411 (1969).

Giles, W. B., Nature, 224, 584 (1969).

Gordon, R. J., J. Appl. Poly. Sci., 14, 2097 (1970).

Gordon, R. J. and C. Balakrishnan, J. Appl. Poly. Sci., 16, 1629 (1972).

Gordon, R. J., C. Balakrishnan and S. B. Pahwa, AIChE Symp. Ser., No. 130, 69, 33 (1973).

Gyr, A. and G. A. Mueller, Chem. Eng. Sci., 29, 1057 (1974).

Han, C. D. and R. R. Lamonte, Trans. Soc. Rheol., 16, 447 (1972).

Hand, J. M. and M. C. Williams, J. Appl. Poly. Sci., 13, 2499 (1969).

Hand, J. M. and M. C. Williams, Nature, 227, 369 (1970).

Hershey, H. C., Ph.D. Thesis, University of Missouri at Rolla (1965).

Hoyt, J. W., J. Basic Engg., 258 (June 1972).

Hudson, N. E., J. Ferguson and P. Mackid, Trans. Soc. Rheol., 18, 541 (1974).

Kanel, F. A., Ph.D. Thesis, University of Delaware (1972).

Katchalsky, A. and H. Eisenberg, J. Poly. Sci., 6, 145 (1951).

Katsibas, P. and R. J. Gordon, AIChE J., 20, 191 (1974).

Kaye, A., A. S. Lodge and D. G. Vale, Rheol. Acta, 7, 368 (1968).

Kim, O. K., R. C. Little and R. Y. Ting, AIChE Symp. Ser., No. 130, 69, 39 (1973).

Lee, T. S., Sc.D. Thesis, Massachusetts Institute of Technology, Cambridge, Mass. (1966).

Lee, W. K., R. C. Vaseleski and A. B. Metzner, AIChE J., 20, 128 (1974).

Little, R. C. and P. Peyser, J. Appl. Poly. Sci., 15, 2623 (1971).

Little, R. C., R. J. Hansen, D. L. Munston, O. K. Kim, R. L. Patterson and R. V. Ting, Ind. Eng. Chem. Fundam., 14, 283 (1975).

Liaw, G. C., Ph.D. Thesis, University of Missouri at Rolla (1971).

Lodge, A. W., "Elastic Liquids," Academic Press, New York, N.Y. (1964).

Lodge, A. S. and J. Meissner, Rheol. Acta, 12, 41 (1973).

Lumley, J. L., J. Poly. Sci.: Macromol. Revs., 7, 263 (1973).

Marucci, G. and R. E. Murch, Ind. Eng. Chem., 9, 498 (1970).

Mathieson, A. R. and J. V. MacLaren, J. Poly. Sci. A, 3, 2555 (1965).

Meissner, J., Rheol. Acta, 10, 230 (1971).

Meissner, J., Trans. Soc. Rheol., 16, 405 (1972).

Merrill, E. W., K. A. Smith, H. Shin and H. S. Mickley, Trans. Soc. Rheol., 10, 335 (1966).

Metzner, A. B. and J. C. Reed, AIChE J., 1, 434 (1955).

Metzner, A. B., E. A. Uebler and C. F. Chan Man Fong, AIChE J., 15, 750 (1969).

Metzner, A. B. and A. P. Metzner, Rheol. Acta, 9, 174 (1970).

Mewis, J. and A. B. Metzner, J. Fluid Mech., 62, 593 (1974).

Mitchell, J. E. and T. J. Hanratty, J. Fluid Mech., 26, 199 (1966).

Morgan, D.T.G., Nature Physical Science, 231, 62 (1971).

Morgan, D.T.G. and E. W. Pike, Rheol. Acta, 11, 179 (1972).

Murch, R. E., Ph.D. Thesis, University of Delaware (1970).

Nakano, A. and Minoura, Y., J. Appl. Poly. Sci., 15, 927 (1971).

Nakano, A. and Minoura, Y., J. Appl. Poly. Sci., 19, 2119 (1975).

Noll, W., Arch. Rat. Mech. Anal., 2, 197 (1958/1959).

Oldroyd, J. G., Proc. First Int. Congress on Rheology, North-Holland Publishing Co., Amsterdam (1949).

Oliver, D. R., Can. J. Chem. Eng., 44, 100 (1966).

Oliver, D. R., W. MacSporran and B. M. Hiorns, J. Appl. Poly. Sci., 14, 1277 (1970).

Oliver, D. R., Nature Physical Science, 241, 131 (1973).

Oliver, D. R. and R. Bragg, Chem. Eng. J., 5, 1 (1973a).

Oliver, D. R. and R. Bragg, Can. J. Chem. Eng., 51, 287 (1973b).

Parker, C. A. and A. M. Hedley, Nature Physical Science, 236, 61 (1972).

Paterson, R. W., Ph.D. Thesis, Harvard University (1969).

Patterson, G. K., J. L. Zakin and J. M. Rodriguez, Ind. Eng. Chem., 61, 22 (1969).

Penzenstadler, R. J., The Dow Chemical Company, Personal Communication, April 11, 1975.

Peterlin, A., Pure Appl. Chem., 12, 563 (1966).

Peterlin, A., Nature, 227, 598 (1970).

Petrie, C.J.S., AIChE J., 21, 275 (1975).

Pickup, T.J.F., Ph.D. Thesis, Cambridge University (1970).

Pimentel, G. C. and A. L. McClellan, The Hydrogen Bond, W. H. Freeman and Co., San Francisco, Ca. (1960).

Pruitt, G. T. and H. R. Crawford, "Effect of Molecular Weight and Segmental Constitution on the Drag Reduction of Water Soluble Polymers," Final Report, Contract No. 4306(00), David Taylor Model Basin, Washington, D.C. (1965).

Rama Murthy, A. V., Trans. Soc. Rheol., 18, 431 (1974).

Runstadler, P. W., S. J. Kline and W. C. Reynolds, Thermosci. Div. Mech. Engg. Dept., Stanford University, Report MD-8 (1963).

Seyer, F. A., Ph.D. Thesis, University of Delaware (1969).

Shaver, R. G. and E. W. Merrill, AIChE J., 5, 181 (1959).

Sirkar, K. K. and T. J. Hanratty, J. Fluid Mech., 44, 589 (1970a).

Sirkar, K. K. and T. J. Hanratty, J. Fluid Mech., 44, 605 (1970b).

Spearot, J. A. and A. B. Metzner, Trans. Soc. Rheol., 16, 495 (1972).

Stevenson, J. F., AIChE J., 18, 540 (1972).

Sylvester, N. D. and S. L. Rosen, AIChE J., 16, 964 (1970).

Technical Service Report, "Let Separan Settle Your Settling Problems," The Dow Chemical Company (1969).

Toms, B. A., Proc. First Int. Congress on Rheology, North-Holland Publishing Co., Amsterdam (1949).

Tordella, J. P., in "Rheology," F. R. Eirich, Ed., Vol. 5, Academic Press, New York, N.Y. (1969).

Townsend, A. A., in "The Structure of Turbulent Shear Flows," Cambridge University Press, Cambridge (1956).

Trouton, F. T., Proc. Roy. Soc., A77, 426 (1906).

Uebler, E. A., Ph.D. Thesis, University of Delaware (1966).

Virk, P. S., AIChE J., 21, 625 (1975).

Virk, P. S., E. W. Merrill, H. S. Mickley, K. A. Smith and E. L. Mollo-Christensen, J. Fluid Mech., 30, 305 (1967).

Walsh, M. A., Ph.D. Thesis, California Institute of Technology, Pasadena, Ca. (1967).

White, D. D., Jr., M.S. Thesis, University of Florida (1975).

White, D. D., Jr. and R. J. Gordon, AIChE J., 21, 1027 (1975).

BIOGRAPHICAL SKETCH

Chander Balakrishnan, son of Krishnaswamy and Kanthi Balakrishnan, was born on September 19, 1947, in Guntur, India. In June, 1964, he was graduated from Hindi High School, Calcutta. In July, 1969, he received the degree of Bachelor of Chemical Engineering from Jadavpur University, Calcutta. Following graduation, he worked for Jenson and Nicholson (India) Ltd., for a year before enrolling in the Graduate School of the University of Florida. From September, 1970, until the present time, he has been a graduate assistant in the Chemical Engineering Department, pursuing his work towards the degree of Doctor of Philosophy in Engineering.

Chander Balakrishnan is a member of the Indian Institute of Chemical Engineers and the American Institute of Chemical Engineers.

I certify that I have read this study and that in my opinion it conforms to acceptable standards of scholarly presentation and is fully adequate, in scope and quality, as a dissertation for the degree of Doctor of Philosophy.

Ronald J. Gordon

Ronald J. Gordon, Chairman
Associate Professor of Chemical Engineering

I certify that I have read this study and that in my opinion it conforms to acceptable standards of scholarly presentation and is fully adequate, in scope and quality, as a dissertation for the degree of Doctor of Philosophy.

John C. Biery

John C. Biery
Professor of Chemical Engineering

I certify that I have read this study and that in my opinion it conforms to acceptable standards of scholarly presentation and is fully adequate, in scope and quality, as a dissertation for the degree of Doctor of Philosophy.

Robert D. Walker, Jr.

Robert D. Walker, Jr.
Professor of Chemical Engineering

I certify that I have read this study and that in my opinion it conforms to acceptable standards of scholarly presentation and is fully adequate, in scope and quality, as a dissertation for the degree of Doctor of Philosophy.

Herbert E. Schweyer

Herbert E. Schweyer
Professor of Chemical Engineering

I certify that I have read this study and that in my opinion it conforms to acceptable standards of scholarly presentation and is fully adequate, in scope and quality, as a dissertation for the degree of Doctor of Philosophy.

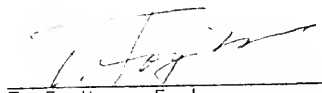

T. E. Hogen Esch
Associate Professor of Chemistry

This dissertation was submitted to the Graduate Faculty of the College of Engineering and to the Graduate Council, and was accepted as partial fulfillment of the requirements for the degree of Doctor of Philosophy.

March, 1976

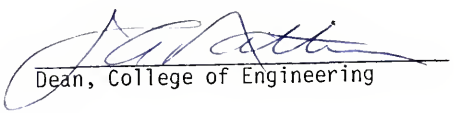

Dean, College of Engineering

Dean, Graduate School